University of Alberta

Enhancing mine haul truck KPIs via payload balance

by

Ali Chamanara

A thesis submitted to the Faculty of Graduate Studies and Research
in partial fulfillment of the requirements for the degree of

Doctor of Philosophy
in
Mining Engineering

Department of Civil and Environmental Engineering

Fall 2013
Edmonton, Alberta

Abstract

This research is a field, laboratory and numerical experimental study of a mining haul truck payload balance and its effect on the truck productivity and performance.

One of the most widely used ultra-class haul trucks in the world is Caterpillar 797, which can carry more than 360 metric tonnes of material per cycle. The large payload of today's haul trucks amplifies the importance of payload balance since a small difference between the designed centroid location of the payload and the actual centroid would subject the truck structure to excessive stresses that may breach the design limit of the truck reducing the truck availability affecting productivity, efficiency, life span and safety.

Key performance indicators (KPIs) have been defined to study the effect of varying truck payload balance. A field test was completed in an oil sand mine to study the adverse effects of an unbalanced payload on those KPIs. A laboratory scale truck body was built and the shovel loading sequence modeled to study the shovel load pass interaction with the truck body and also by the successive pass placed into the truck body.

An algorithm has been developed to model the cumulative shovel load passes within the truck body and to suggest an appropriate location for successive placed shovel load passes to achieve a balanced payload before the truck leaves the digging face.

Acknowledgment

I would like to first acknowledge my supervisor, Dr. Tim Joseph, for his continuous support and guidance. His straightforwardness and unique sense of humour as well as his great technical and practical engineering skills have been a benefit to me and his many, many students.

I wish to express my sincere gratitude to my co-supervisor, Dr. Jozef Szymanski, for his support and help during my study and also to complete the field test at Muskeg River Mine in 2011.

Shell Canada has also supported me since 2010 when I joined the company and provided me with the opportunity to complete my field study at Muskeg River Mine.

My dearest friend, Vahid Mesgarzadeh, has provided me with his unconditional support since we met in the elementary school.

Further, I wish to thank my beloved parents, Mohammad and Akram, and my sister, Shabnam, for their encouragement and support in my life and through my studies.

Finally, I would like to thank my fiancé, Sarah, for her inspiration, patience and love.

Table of Contents

1. Introduction 1

1.1 Problem statement 1

1.2 Research objectives 2

1.3 Hypothesis 3

1.4 Thesis layout 3

1.5 Significance of work 4

2. Literature review 5

2.1 Truck payload and speed 5

2.1.1 Truck payload 5

2.1.2 Speed impact 18

2.2 Cable versus hydraulic shovel loading sequence 18

2.3 Mine haul truck KPIs 20

2.3.1 Truck onboard information systems 20

2.3.2 Truck key performance indicators 20

2.4 Haul truck premature structural failure 27

2.4.1 Fatigue 27

2.4.2 Rack, truck payload balance and structural fatigue 29

2.4.3 Caterpillar 797B premature failures 31

3. Field investigation and verification of theory 36

3.1 Test objectives 36

3.2 Muskeg River Mine 36

3.3 Test procedure 37

3.4 Field data analysis 40

3.4.1 Truck cycle 1 41

3.4.2 Truck cycle 2 47

3.4.3 Truck cycle 3 50

3.5 Conclusion 52

4. Laboratory test and theory verification 53

4.1 Scale truck body and data acquisition system 53

4.2 Stiffness 59

4.3 Material types 59

4.4 PhotoModeller Scanner 62

4.5 Density 63

4.6 Calibration 65

4.6.1 Calibration of load cells and the scale truck body 65

4.6.2 Calibration of the load cell readings 65

4.7 Analyzing the laboratory data 67

4.8 Loading the scale truck body 69

4.8.1 Sand 69

4.8.2 Gravel 74

4.8.3 Oil sand 78

4.9 Conclusions 82

5. Mathematical and numerical models 84

5.1 Mathematical theory 84

5.2 Numerical analysis 88

5.2.1 Objectives 88

5.2.2 Procedure 88

5.2.3 Algorithm 91

5.2.4 Test scenario 93

5.3 Shovel operator payload balance assist system 97

6. Discussions and Conclusions 99

6.1 Conclusions 99

6.2 Contributions of the research 101

6.3 Errors 102

6.4 Future work 102

7. References 104

8. Appendices 108

8.1 Laboratory test 108

8.1.1 Test 1 108

8.1.2 Test 2 110

8.1.3 Test 3 112

8.1.4 Test 4 114

8.1.5 Test 5 116

8.1.1 Test 6 118

8.1.1 Test 7 120

8.2 Field Study 122

8.2.1 136 truck 122

8.2.2 137 Truck 128

8.3 Numerical Algorithm 132

8.3.1 Matlab program 132

8.3.2 Matlab Test 145

List of Tables

Table 2.1 Three Cat 797B truck frame failures at an oil sand mine (Amarra & El-Sayed, 2010) 32
Table 3.1 Caterpillar 797B haul truck tire air pressure 39
Table 3.2 Material Properties 40
Table 4.1 Density of gravel, oil sand and sand 64
Table 4.2 load distribution chart 66
Table 4.3 load cell reading calibration 67
Table 4.4 Laboratory data sample 68

List of Figures

Figure 1.1 Caterpillar 797B haul truck under an unbalanced load 2
Figure 2.1 Average productivity for 785B with a nominal load of 136 tonnes (Schexnayder et al., 1999)..... 6
Figure 2.2 Structural fatigue damage per round trip as a function of payload (Deslandes & Marshall, 1986) 7
Figure 2.3 Comparison of on-board to calculated payload under various operating conditions (Joseph, 2003) 8
Figure 2.4 Cat 797 Specifications (Caterpillar, 2010) 9
Figure 2.5 Truncated conical payload (Hagenbuch, 2002)..... 10
Figure 2.6 two cones common intersecting volume 11
Figure 2.7 Two intersecting cones (Beyer, Fawcett, Mauldin, & Swartz, 1987) . 12
Figure 2.8 The geometrical representation of the two intersecting cones (Balogun et al., 2000). 13
Figure 2.9 Location of the stereo camera and a close-up photo of the camera in its protective mount on the right (Brothwick, 2009) 15
Figure 2.10 A haul truck before and after load profiling with a volume of 108 cubic meters (Brothwick, 2009)..... 16
Figure 2.11 Plan view of robotic excavator sensor configuration (Anthony Stentz et al., 1999) 17
Figure 2.12 Working ranges of a Hitachi EX8000 hydraulic excavator (Hitachi, 2013) 19
Figure 2.13 Working ranges of a Cat 7495 HF electric rope shovel (Caterpillar, 2013) 19
Figure 2.14 Truck suspensions configuration for rack calculation..... 21
Figure 2.15 Truck suspensions configuration for pitch calculation..... 22
Figure 2.16 Truck suspensions configuration for roll calculation 23
Figure 2.17 Conventional TKPH comparison to real-time TKPH values for a truck with an unbalanced payload (Joseph & Chamanara, 2012)..... 25
Figure 2.18 Conventional TKPH comparison to real-time TKPH values for a truck with an balanced payload (Joseph & Chamanara, 2012)..... 26

Figure 2.19 Change in rack and acceleration equivalent (Berezan et al., 2004)... 27
Figure 2.20 Best-fit S-N curves for unnotched 300M alloy forging with an ultimate tensile strenght of 1930 MPa (Boardman, 1990) 29
Figure 2.21 Distribution of rack events incurred by a haul truck under an unbalanced payload (Joseph & Chamanara, 2012) 30
Figure 2.22 Distribution of rack events incurred by a haul truck under a balanced payload (Joseph & Chamanara, 2012) 31
Figure 2.23 General location of the cracks (Amarra & El-Sayed, 2010)..... 32
Figure 2.24 Frame crack (Truck A on the left and C on the right) (Amarra & El-Sayed, 2010) 33
Figure 2.25 Truck A total rack, pitch and bias alarms (Amarra & El-Sayed, 2010) 34
Figure 2.26 Truck B total rack, pitch and bias alarms (Amarra & El-Sayed, 2010) 34
Figure 2.27 RHF spindle failure on a 797B (Front view) (Finning, 2010)..... 35
Figure 2.28 RHF spindle failure on a 797B truck (Rear view) (Finning, 2010)... 35
Figure 3.1 A satellite map of Muskeg River and Jackpine mines taken in July 2013..... 37
Figure 3.2 Truck A, cycle 1, fully loaded 42
Figure 3.3 Strut suspended mass, truck A, cycle 1 43
Figure 3.4 Rack, roll and pitch for cycle 1 from Dispatch..... 46
Figure 3.5 Rack, roll and pitch for cycle 1 from data logger 46
Figure 3.6 Truck A, cycle 2, first shovel bucket load and final payload 47
Figure 3.7 Strut suspended mass, truck A, cycle 2 48
Figure 3.8 Rack, roll and pitch for cycle 2 49
Figure 3.9 Truck A, Cycle 3, fully loaded 50
Figure 3.10 Strut suspended mass, truck A, cycle 3 51
Figure 3.11 Rack, roll and pitch for cycle 3 52
Figure 4.1 Caterpillar 797B standard body – Rear view..... 55
Figure 4.2 Caterpillar 797B standard body – Side view 55
Figure 4.3 Caterpillar 797B 1:25 scale body – Rear view 56

Figure 4.4 Caterpillar 797B 1:25 scale body – Side view 57
Figure 4.5 3-D design of the 1:25 scale truck body 58
Figure 4.6 Load cell installation, power sources, eDaq software 58
Figure 4.7 Susan Lake screened sand sieve analysis 60
Figure 4.8 Oil sand sample sieve analysis 60
Figure 4.9 Limestone sample sieve analysis 61
Figure 4.10 Loading tool (Left), Material types (Right) 61
Figure 4.11 Digital Camera calibration in Photomodeller Scanner 62
Figure 4.12 An example of the payload model created by PhotoModeller 63
Figure 4.13 Digital scale and container 64
Figure 4.14 Cansel hand held level 65
Figure 4.15 Five pass loaded scale truck body with sand 70
Figure 4.16 Strut load distribution for sand test 71
Figure 4.17 Scaled-up strut mass for sand test 72
Figure 4.18 Rack, roll and pitch for sand test 73
Figure 4.19 Scaled-up rack, roll and pitch for sand test 74
Figure 4.20 Loaded scale truck body with gravel 75
Figure 4.21 Strut load distribution for gravel test 76
Figure 4.22 Rack, roll and pitch for gravel test 77
Figure 4.23 Scaled-up strut mass for gravel test 77
Figure 4.24 Scaled-up rack, roll and pitch for gravel 78
Figure 4.25 Loaded scale truck body with oil sand 79
Figure 4.26 Strut load distribution for oil sand test 80
Figure 4.27 Rack, roll and pitch for oil sand test 81
Figure 4.28 Scaled-up strut mass for oil sand test 81
Figure 4.29 Scaled-up rack, roll and pitch for oil sand test 82
Figure 5.1 Three piles of sand interacting with one another on the left and three cones interaction analyses on the right 85
Figure 5.2 Two intersecting cones 86
Figure 5.3 Numerical analysis flow chart 90

Figure 5.4 Trcuk floor planes and the 3D spacial configuration of the mesh network 91
Figure 5.5 a right cone of height h and radious r 92
Figure 5.6 First load pass shape within the truck body..... 94
Figure 5.7 Suggested location for the second load pass within the truck body 95
Figure 5.8 Payload after the second shovel load pass is performed 96
Figure 5.9 The truck payload shape after the third pass following the software instructions 97
Figure 5.10 Schematic of an excavator and hauler communication system (Joseph & Chamanara, 2012). 98
Figure 5.11 Data acquisition, wireless transmitter and touch screeen processor (Joseph & Chamanara, 2012)..... 98

Nomenclature

$\sigma_{xy}(t)$	Stress time history about every node
$P_i(t)$	Dynamic load time history of i
P_{ist}	The peak load of i
σ_{ixyst}	Stress of a the single I load
m	Whole load numbers
M_i	Suspended mass under 1g loading
a_i	Strut acceleration when the hauler is in motion
P_i	Strut pressure
A	Cross-sectional oleo-pneumatic bearing area in the strut
g	Gravitational acceleration (9.81 m/s^2)
E	Young's modulus
J	Job rate in TKPH
H	Total time in hours for the day
T_L	Tire load in metric tonne on the loaded machine
T_E	Tire load in metric tonne on the empty machine
K_L	Length of loaded haul in kilometer
K_E	Length of empty haul in kilometer
N_L	Number of the loaded trips for the time (H) period
N_E	Number of the empty trips for the time (H) period

Acronyms and Abbreviations

Aeq	Acceleration Equivalent
ASA	Application Severity Analysis
Cat	Caterpillar
DSM	Dense Surface Modelling
ERCB	The Energy Resources Conversation Board
FPC	Fleet Production and Cost Analysis
KPI	Key Performance Indicator
LF	Left Front Strut
LR	Left Rear Strut
LRI	Left Rear Inside Tire
LRO	Left Rear Outside Tire
MRM	Muskeg River Mine
OEM	Original Equipment Manufacturer
RF	Right Front Strut
RR	Right Rear Strut
RRI	Right Rear Inside Tire
RRO	Right Rear Outside Tire
SAE	Society of Automotive Engineers
TKPH	Tonne Kilometer Per Hour
TPMS	Truck Production Management System
USCS	Unified Soil Classification System
VIMS	Vital Information Management System
WBV	Whole Body Vibration

1. Introduction

1.1 Problem statement

Economies of scale have driven the bulk mining industry into an era of ultra-class mining haul trucks where the Gross Vehicle Weight (GVW) of these units exceeds 600 metric tonnes (mt). In rigid body trucks, 600 mt in motion can generate up to four times the corresponding forces on the truck struts, structure and tires (Joseph, 2003).

As an example, the Caterpillar 797 ultra-class hauler, including payload, weighs 625 mt, of which in the static case, one third is carried by the front tires, and two thirds by the rear tires (Caterpillar, 2010). Even though this weight generates high stresses on the truck structure, the Original Equipment Manufacturers (OEM) design equipment to be specifically capable of taking these forces during an effective equipment life span of approximately ten years without encountering major adverse fatigue.

As the hauler moves, it is subjected to dynamic loading, which can generate large forces exceeding the equipment design limit. For example, Prem (1998) simulated a 218 mt haul truck showing that the forces during a simple lane change are approximately 60 to 70 percent higher than static forces; these are further increased when the truck is moving over rough terrain compounded under an unbalanced load (Prem, 1998).

Studies revealed that not only do these high dynamic forces contribute in premature equipment failure, but also, an uneven load distribution on the struts, generating twisting forces on the truck frame. It has been shown by Whalen (2003) that the frame torsion is the key limiting factor in truck life (Whalen, 2003).

Figure 1.1 shows a Caterpillar 797B haul truck which has been loaded favoring the left side of the body closest to the shovel operator. The load balance results in roll events which increase the stress on the left side suspension and tires.

Figure 1.1 Caterpillar 797B haul truck under an unbalanced load

1.2 Research objectives

Given that uneven load distribution may be one of the root causes of truck structural premature failure, lower tire life, lower productivity and higher maintenance cost, all of which lead to lower availability; this research targets the following objectives:

a. To study the relation between incremental load placement and the final payload distribution and show the payload location effects on selected and defined truck Key Performance Indicator (KPI) values.
b. To develop a mathematical and numerical model of incremental load placement.
c. To conduct laboratory physical simulation for a scale Caterpillar 797 truck body, under incremental loading to verify the numerical

model and to develop an algorithm to enhance payload placement on a truck by the shovel operator.

d. To suggest a visual shovel operator assist system, communicating from the truck on-board system to shovel cab which will help the shovel operator to balance the load on the truck before it moves away.

1.3 Hypothesis

Suspension measured loads provide sufficient information to allow an accurate determination of the load position in the truck body to determine and influence the load balance.

1.4 Thesis layout

As outlined in this chapter, an unbalanced payload may negatively influence the truck KPIs and ultimately truck productivity and life span; therefore, in chapter 2, previous works are reviewed to determine any correlation between the truck KPIs and truck productivity, efficiency, life span and safety.

In chapter 3, the relationship between the unbalanced truck payloads and the truck KPIs are studied through a full scale field investigation. In addition, the shovel bucket load passes interaction in the truck body and the shovel loading sequence are studied.

In chapter 4, the conical shape of the shovel bucket load pass is studied as well as the relationship between the unbalanced payloads with the truck KPIs. In addition, the truck balance algorithm that is explained in chapter 5 is tested and verified.

Chapter 5 introduces the mathematical and numerical truck payload models. The truck payload balance algorithm is explained and a shovel operator loading assist system is introduced.

Chapter 6 outlines the conclusions, the thesis contributions, the possible errors in the research process and the future works.

Chapter 7 and 8 are allocated to the references and the appendices.

1.5 Significance of work

Despite the fact that various methods have been developed to assist the shovel operators in properly loading mining haul trucks, the effect of unbalance truck payload on the truck KPIs has not been independently verified. However, in this research, the influence of unbalanced truck payloads on the truck KPIs are identified through a full scale field investigation and a scale model in the laboratory.

In addition, the behaviour of the incremental shovel bucket load passes in the truck body to shape the final truck payload has not been previously studied; as a result, in this research a new approach, a conical shape approach, is introduced to model the shovel bucket load passes in the truck body shaping the final payload.

Also, using only the data collected from the truck onboard systems to develop a truck load balance algorithm is genuine that has potentials to be commercially developed which is very reliable, and it requires minimum maintenance and capital cost to be developed.

Finally, a new approach is introduced to develop a shovel operator loading assist system to improve the payload balance which would improve the truck KPIs and consequently the truck fleet productivity, safety and life span; as a result, a significant contribution is made to industry.

2. Literature review

2.1 Truck payload and speed

Two main contributing factors in haul truck productivity are speed and payload (Mills, 2002; Schexnayder, Weber, & Brooks, 1999): (I) the truck body space is not properly utilized when an unbalanced final payload is formed resulting in an under-load event; and (II) when the payload is not balanced a rougher ride is expected that would force the operators to slow down to enhance their comfort. As a result, having an unbalanced payload could lead to a lower payload and speed and as such, lower productivity.

2.1.1 Truck payload

The carrying capacity of a truck comprises the weight and volumetric carrying capacity. The Original Equipment Manufacturers (OEMs) usually design the equipment components based on the nominal weight capacity of the truck and the volumetric capacity is determined according to the SAE J1363 standard. Consequently, the nominal payload of the truck is set by the OEM to achieve the longest lifespan. Therefore, it is important to maintain the nominal truck payload during its operational life span.

It is the shovel operator's responsibility to appropriately load the haul truck relying on sight to judge the volumetric load and to fully utilize the truck body space and to determine the load shape with respect to the truck body (Schexnayder et al., 1999).

Schexnayder (1999) completed a productivity study to determine the effect of payload on production employing Caterpillar 785B trucks. Caterpillar Vital Information Management System (VIMS) and Truck Production Management System (TPMS) were tools employed to collect the production data for their analyses. It was revealed that production increases rapidly as the payload increases; however, when the payload exceeds the nominal payload the slope of

the production curve decreases by 20 to 65% as shown in figure 2.1 (Schexnayder et al., 1999).

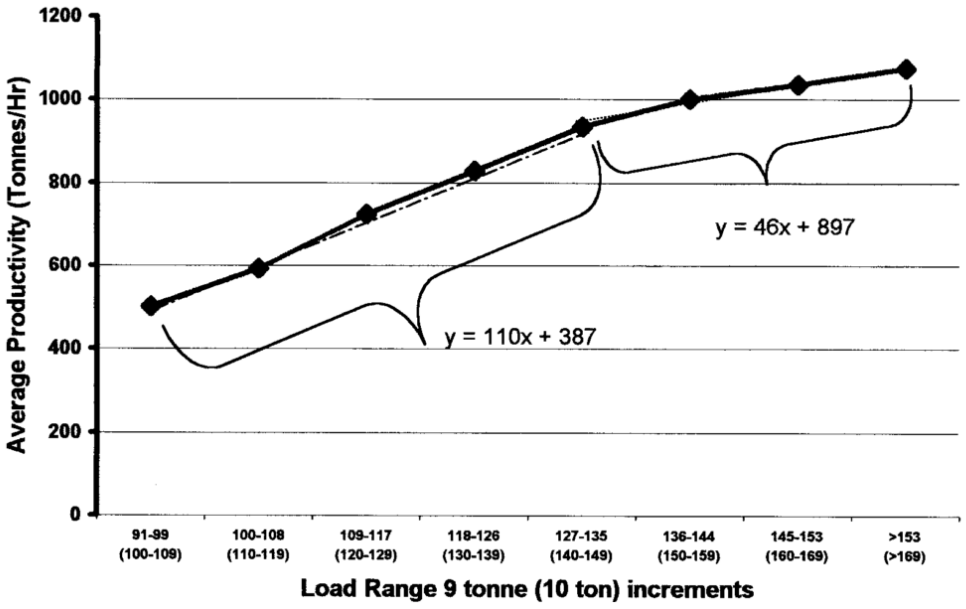

Figure 2.1 Average productivity for 785B with a nominal load of 136 tonnes (Schexnayder et al., 1999)

In addition, payload is one of the main contributing factors in the structural fatigue damage of the mining haul trucks. Figure 2.2 illustrates the influence of the payload on the structural fatigue damage on three type of haul trucks where the payload varies between 70% and 130% of the nominal payload (Deslandes & Marshall, 1986).

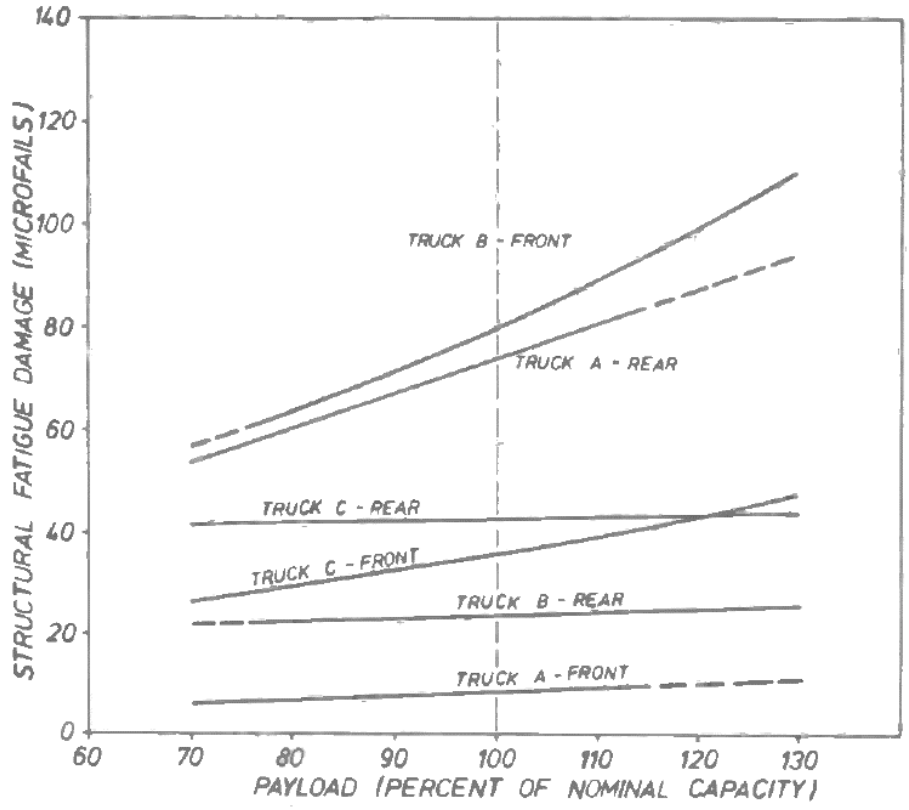

Figure 2.2 Structural fatigue damage per round trip as a function of payload (Deslandes & Marshall, 1986)

Joseph (2003) compared the second gear payload readings with the calculated payload using the strut pressures to prove that in soft ground conditions, especially in oil sand, the second gear payload values can be overestimated as shown in figure 2.3.

When the truck is in motion vertical accelerations are experienced that cause the dynamic weights to differ from the static determinations considered via Newton's 2nd law. When the truck is in motion, there are variations in acceleration (a_i) that is an increment or decrement of the gravitational acceleration (g); therefore, dynamic force is calculated using equation 1, which will differ from the static force if "a" is not equal to zero (Joseph, 2003).

$$F_{Dynamic} = \sum_{i=1}^{4} M_i(g + a_i) \qquad [1]$$

In soft undulated ground conditions, the truck struts will frequently extend or compress. Consequently, payloads will vary that may not give the actual values recalled by the onboard system at the transition from 1st to 2nd gear (Joseph, 2003).

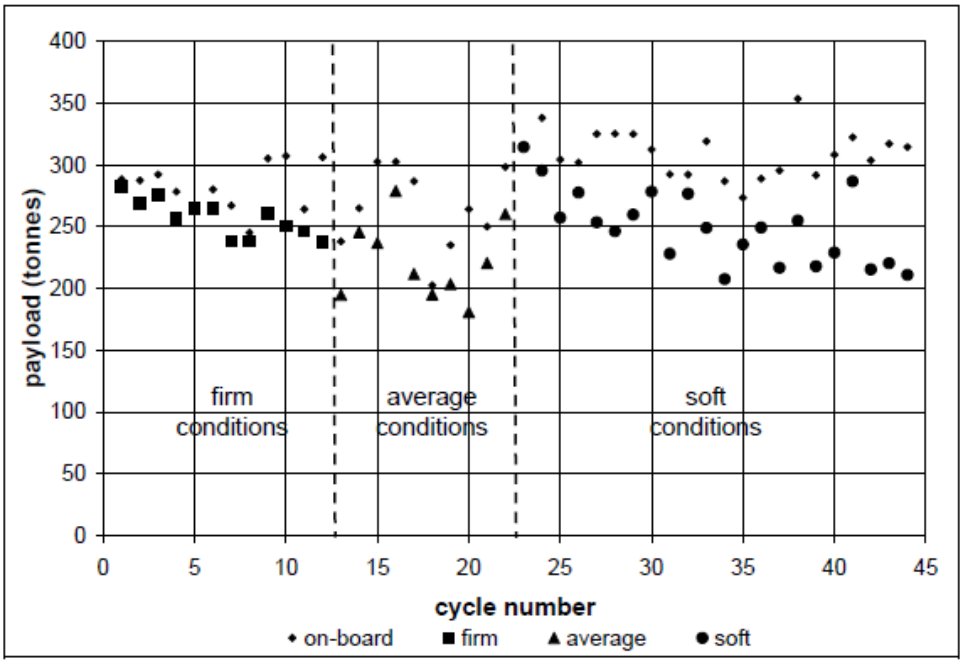

Figure 2.3 Comparison of on-board to calculated payload under various operating conditions (Joseph, 2003)

Volumetric capacity of haul trucks are rated by the manufacturer according to the SAE J1363 standard. For instance, as shown in figure 2.4, it is stated on the 797 specification sheet that the volumetric capacity of the truck is 240-267 m^3. However, Hagenbuch (2000, 2002) believed that the effective volumetric capacity of the truck is overrated by 15 to 20%. He also mentioned that certain South American countries factor the SAE 2:1 heaped volumetric rating of trucks by 0.85 to develop their own volumetric capacity standard (Caterpillar, 2010; Hagenbuch, 2002).

Operating Specifications		
Nominal Payload Capacity	363 tonnes	400 tons
Heaped SAE (2:1) Capacity	240-267 m^3	314-350 yd^3
Top Speed – Loaded	67.6 km/h	42 mph
Machine Clearance Turning Diameter	42 m	138 ft
Capacity – MSD II – 100% fill factor		
Struck	188-213 m^3	246-290 yd^3
Heaped (SAE 2:1)	240-267 m^3	314-350 yd^3

Figure 2.4 Cat 797 Specifications (Caterpillar, 2010)

If the volumetric and load carrying capacity of trucks define their carrying capacity, they both need to be synchronized to the actual load placed.

There are problems with the SAE J1363 standard. First of all, it assumes a 2:1 angle of repose for heaped material, however in the real world few materials have an angle of repose of 26.6 degrees in a static condition. In addition, the SAE J1363 standard calculates the material heaped at a 2:1 angle of repose sitting on a 1:1 heap at the rear of the body that is too steep and unrealistic.

Hagenbuch (2000, 2002) believed that the loose material placed on a flat surface would define a cone, or if a front end loader dumps, it may shape an elongated cone (Hagenbuch, 2000, 2002).

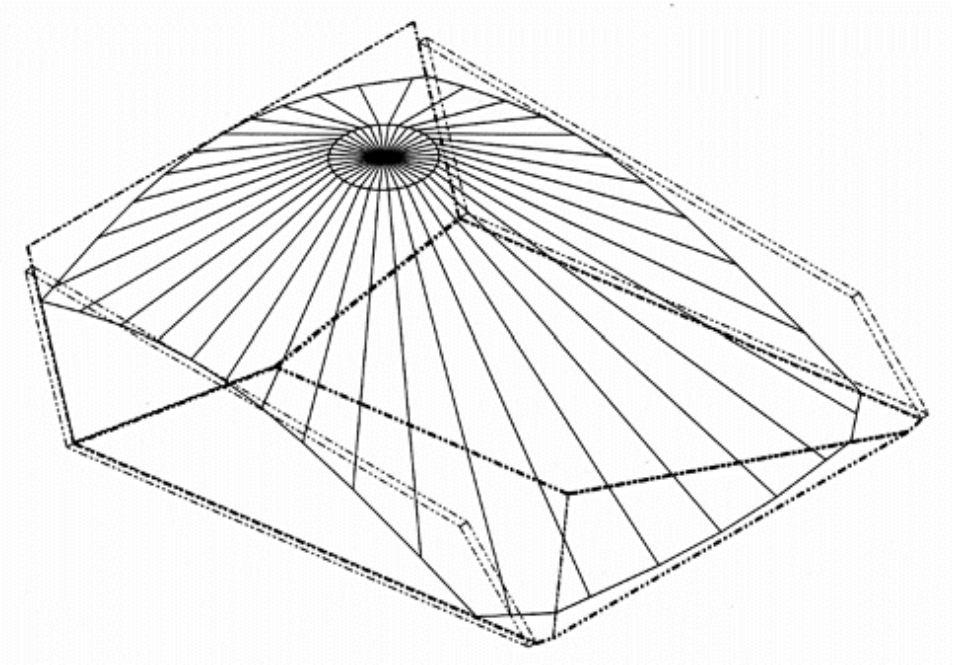

Figure 2.5 Truncated conical payload (Hagenbuch, 2002)

Simplistically, the actual 2:1 volumetric capacity of a truck body is calculated by dividing the oblong or round plateau shown in figure 2.5 into segments in 10º increments. Each segment line is drawn downwards at a 2:1 slope until it intersects with the truck body to form a point of contact. The same step is taken for all 36 segments to form the payload profile in the truck body. Consequently, the volumetric capacity of the truck, can be determined using the new load profile (Hagenbuch, 2000, 2002, 2011).

In reality, the volume content in a haul truck is a series of intersecting cones formed by the number of shovel load passes loading the truck body (Joseph & Chamanara, 2012). Therefore, identifying the volume of the cones and also their common intersection volume is the first step in determining the actual truck volumetric carrying capacity.

Figure 2.6 illustrates two intersecting cones with their common space. If the two cones common volume is calculated, the combined volume of both cones can be determined. Research has previously been done to calculate the common

volume of two intersecting cones; however, if the cone vertices do not cross and are parallel to one another, the cones common volume is infinite and requires to be limited with a plane.

As a result, the common volume is encompassed by two cones and a plane. When estimating the truck payload volume, the plane represents the truck body floor, and also payload's interaction with the truck body walls.

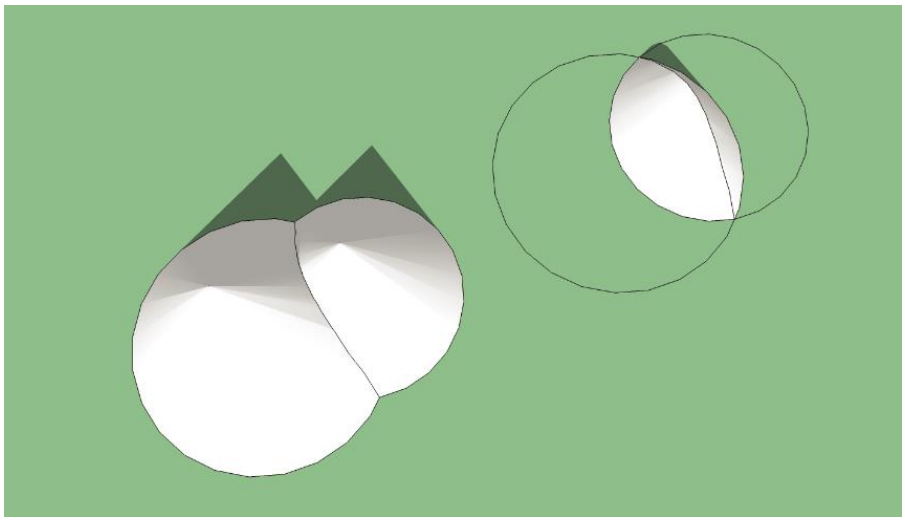

Figure 2.6 two cones common intersecting volume

2.1.1.1 Two cones common volume

If two circular cone axes cross at a common point P with the vertices of the cones being at an equal distance from P and α being the angle that one cones axis makes with the cone's generator and also d being the distance from the intersection of the cones' axes to either vertex as shown in figure 2.7.

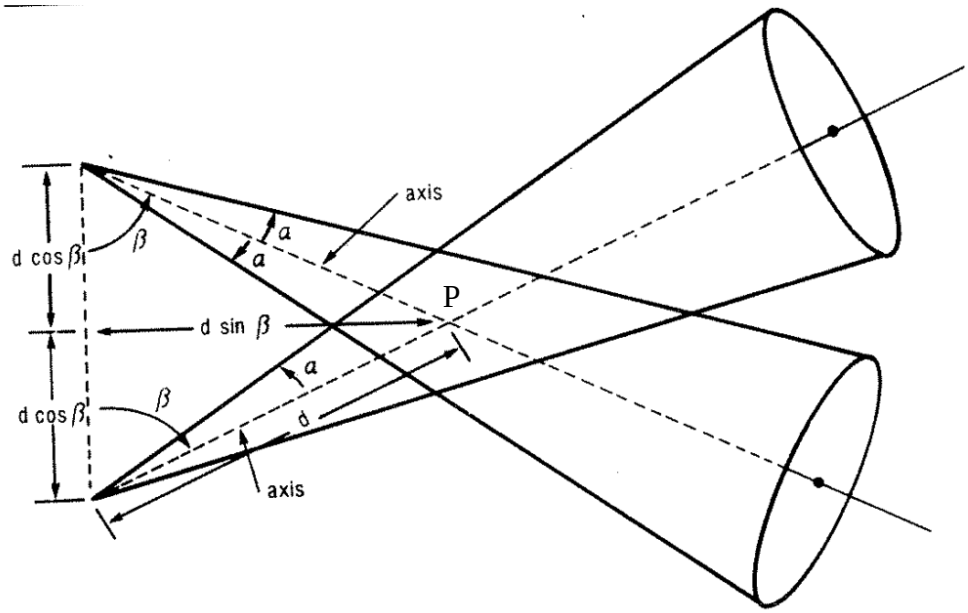

Figure 2.7 Two intersecting cones (Beyer, Fawcett, Mauldin, & Swartz, 1987)

Assuming that α+β is less than $\frac{\pi}{2}$, the volume of the intersection of the cones is given by,

$$V_{cones} = \frac{4}{3}\frac{d^3a^2}{1-a^2b^2}\left[\frac{a(1+b^2)\sqrt{b^2-a^2}}{b^2(1+a^2)^2} + \frac{1}{\sqrt{1-a^2b^2}}\tan^{-1}\left(\frac{a(1+b^2)}{\sqrt{(b^2-a^2)(1-a^2b^2)}}\right)\right] \quad [2]$$

"a" and "b" are defined, where ($a = tan\alpha, and\ b = tan\beta$)

In the radiation industry, cross beam measurements are often made; therefore, determining the geometrical target volume is important. The overlap of collimated source and detector's fields of view, are represented by a two cone common space (Balogun, Brunetti, & Cesareo, 2000).

Balogun (2000) has developed a numerical algorithm to determine two cones common volume. In this algorithm, a small elemental volume is scanned through the first cone and the center of the element position relative to the second cone is identified to determine whether the element is positioned inside the second cone or not (Balogun et al., 2000).

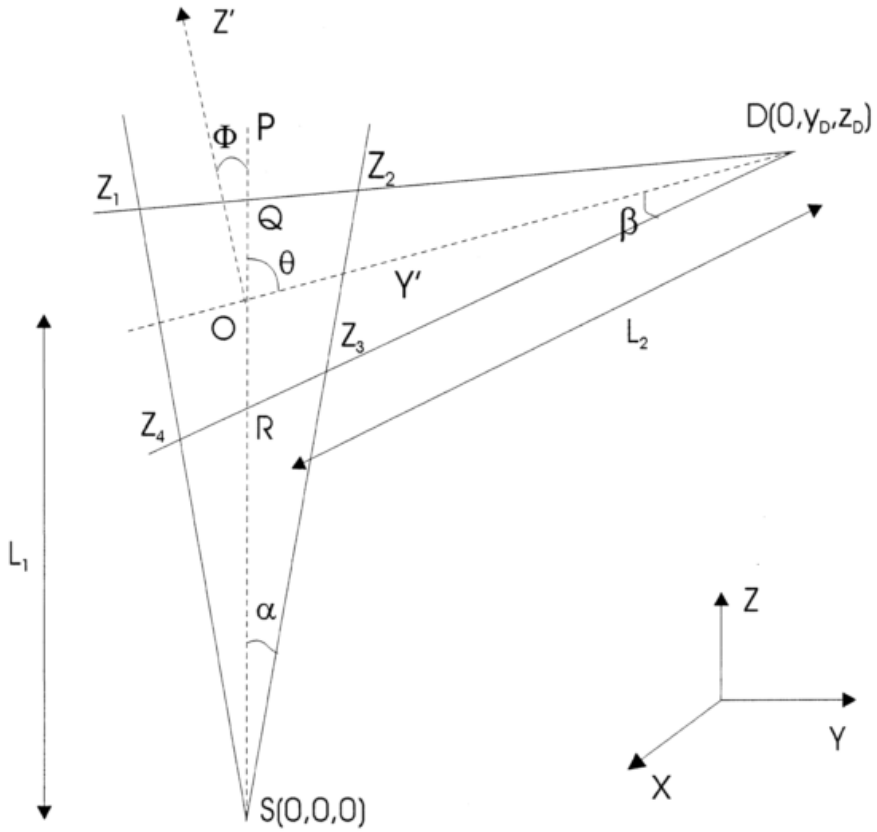

Figure 2.8 The geometrical representation of the two intersecting cones (Balogun et al., 2000).

As shown in figure 2.8, the scanning area along the Z axis is limited by four points given by the following expressions, equations 3a through 3d.

$$Z_1 = \frac{(ZP\tan(\theta+\beta)-YP)}{(\tan(\theta+\beta)-\tan\beta)} \qquad [3a]$$

$$Z_2 = \frac{(ZP\tan(\theta+\beta)-YP)}{(\tan(\theta+\beta)+\tan\alpha)} \qquad [3b]$$

$$Z_3 = \frac{(ZP\tan(\theta-\beta)-YP)}{(\tan(\theta-\beta)-\tan\alpha)} \qquad [3c]$$

$$Z_4 = \frac{(ZP\tan(\theta-\beta)-YP)}{(\tan(\theta-\beta)+\tan\alpha)} \qquad [3d]$$

And the volume of intersection is given by the following triple integral (Balogun et al., 2000).

$$\Delta V = \int_{Z_{min}}^{Z_{max}} dz \int_{-z\tan\alpha}^{z\tan\alpha} dy \int_{-\sqrt{(z\tan\alpha)^2-y^2}}^{\sqrt{(z\tan\alpha)^2-y^2}} dx \qquad [4]$$

Z_{min} and Z_{max} are the limit of the scan that are chosen from the four values calculated in equations 3a through 3d (Balogun et al., 2000).

2.1.1.2 Haul truck payload profiling and volume estimation

Various systems have been developed to profile the haul truck payload and to estimate the haul truck volume using laser scanners and stereo cameras.

One technology developed uses two scanning lasers mounted on a structure over a section of the haul road to scan the truck payload while the truck is passing under the scanners to estimate the volume of material contained within the haul truck body. This system can be beneficial to the industry for truck utilization and monthly production reconciliation. However, this system will not help to improve the truck payload balance since the measurements are taken after the truck is fully loaded and has left the shovel digging face (Duff, 2000).

In addition, a haul truck pose estimation system has been developed using stereo cameras that have the capability of payload profiling (Borthwick, Lawrence, & Hall, 2009; Brothwick, 2009). Figure 2.9 illustrate the location of a stereo camera installed on the shovel boom and a close-up picture of the camera in its protection mount.

Figure 2.9 Location of the stereo camera and a close-up photo of the camera in its protective mount on the right (Brothwick, 2009)

Using the stereo cameras a scene point cloud of the truck is generated and the truck position is estimated by positioning a second model point cloud, the haul truck representation model, into the scene point cloud. This system can be used to determine the position of the haul truck with respect to the shovel in developing a shovel operator loading assist system (Borthwick et al., 2009; Brothwick, 2009).

In addition, this system can be used to profile the truck payload. This system is not very reliable since parts of the payload are not in the camera view field; therefore, only the middle 90 percent of the truck body content is measured and the unavailable data is interpolated from the observed surface. Another challenge is maintaining the stereo cameras in their optimum operating condition in the dusty and harsh mining environment, and operating in severe weather conditions is also challenging that makes the system very unreliable. In addition, as it is shown in figure 2.10, the payload of the haul truck is profiled and the mass center line of the payload is shown in dotted line comparing to the ideal solid center line. This is one step towards developing a shovel operator loading assist system, however, the shovel bucket loads interaction within the truck body needs to be studied and an algorithm needs to be developed to simulate and predict the ideal succeeding shovel bucket load pass locations within the truck body (Brothwick, 2009).

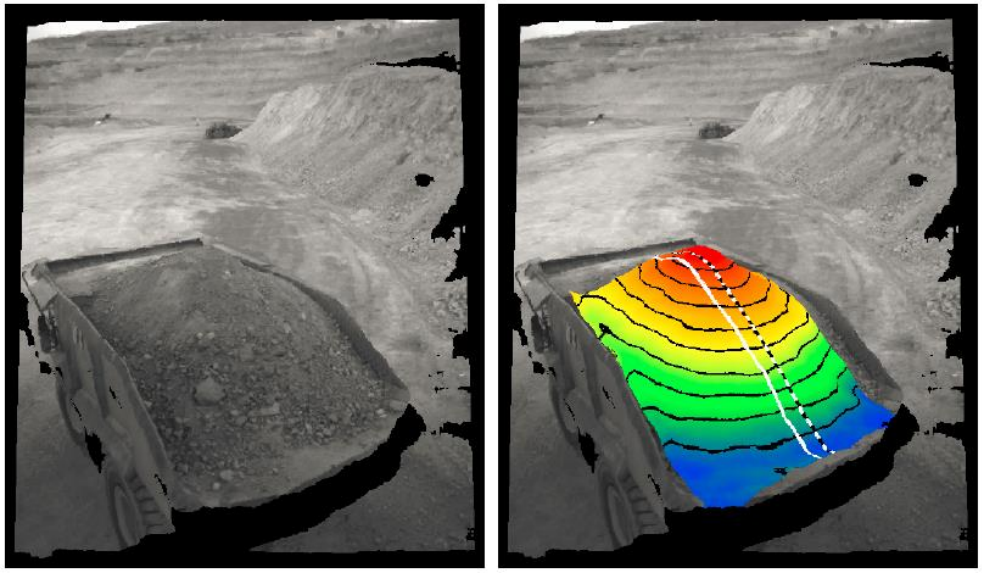

Figure 2.10 A haul truck before and after load profiling with a volume of 108 cubic meters (Brothwick, 2009)

Stentz et al. (1998) introduced a robotic excavator for autonomous truck loading. In this system, two scanning laser rangefinders are mounted on each side of the excavator boom to recognize and localize the truck, map the road surface and to detect obstacles. Figure 2.11 is a top view of the sensor configuration (Cannon, 1999; Stentz, Bares, Singh, & Rowe, 1998; A. Stentz, J. Bares, S. Singh, & P. Rowe, 1999).

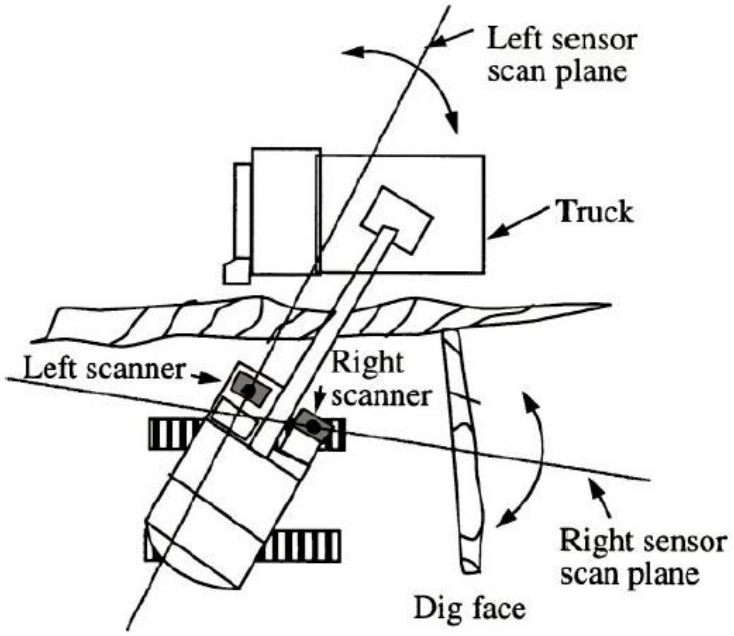

Figure 2.11 Plan view of robotic excavator sensor configuration (Anthony Stentz et al., 1999)

In this system multiple algorithms are used such as truck recognition, coarse-to-fine dig point planning, template-based dump planning, script based motion planning and obstacle detection algorithm. The template-based dump planning looks for the low region in the truck bed for the successive shovel bucket loads to be placed to form the final payload. This method does not investigate the shovel bucket loads interaction with one another and the truck body, and it does not necessarily build a balanced final payload. This system only looks for the low regions to fill the truck body. In addition, laser base scanners have the problems of dust penetration or a partially dirty exit window that would reduce the reliability of the system (Stentz et al., 1998).

US patent number 6157889 introduces the concept of identifying the center of gravity of the truck payload after each shovel bucket pass using weight sensors installed on the truck struts and introducing a visual aid system to the shovel operator to shift the payload center of gravity with the successive shovel

bucket loads to an ideal location to maintain the truck nominal load distribution on all the struts (Baker, 2000).

However, it does not verify the adverse effect of an unbalanced payload on the truck productivity, longevity as well as the operator wellbeing. It does not introduce an algorithm to simulate the shovel bucket load interactions with one another and the truck body in order to suggest a location for subsequent shovel bucket load passes to build a balanced payload in the truck body.

2.1.2 Speed impact

In a case study completed by Caterpillar of Australia using the Caterpillar software Fleet Production and Cost Analysis (FPC), it was determined that the actual truck productivity was reduced because of the speed reductions initiated by the operators to reduce their discomfort due to high rack events generated by the poor ground condition. The mine could have achieved the same production with three to four trucks that they were recording with five trucks (Mills, 2002).

2.2 Cable versus hydraulic shovel loading sequence

Caterpillar 797B and F haul trucks are commonly matched with Caterpillar 7495HF electric shovels and Hitachi EX8000 or Komatsu PC8000 hydraulic excavators.

There are slight differences in the loading sequence of the hydraulic and electric cable shovels mainly due to difference in their size and also the mechanical difference in their components. There are more side loadings observed from the hydraulic shovels than the electric shovels and also more front loading over the canopy from the electric shovels than the hydraulics. As it is shown in figure 2.12, the eye level of the hydraulic shovel operator is approximately 8.5m above the ground whereas it is 10.5m for the electric shovels. As a result, the cable shovel operators have a better sight of the truck body; on the other hand, the hydraulic shovel operators are not able to see the bottom of the truck body.

Since the excavator operators rely on sight to load the trucks, better visibility would improve the loading process leading to a better balanced final payload.

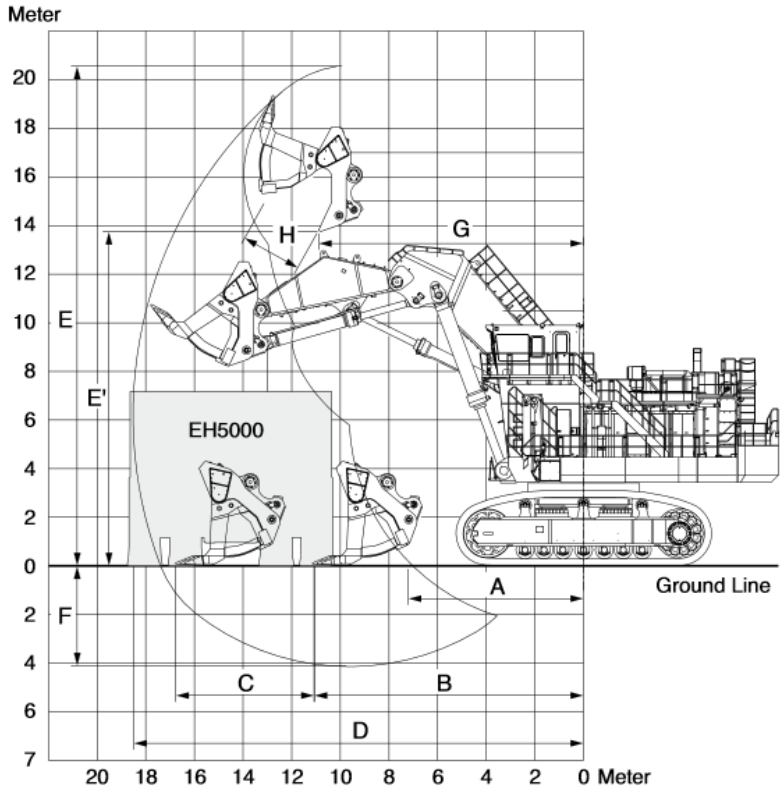

Figure 2.12 Working ranges of a Hitachi EX8000 hydraulic excavator (Hitachi, 2013)

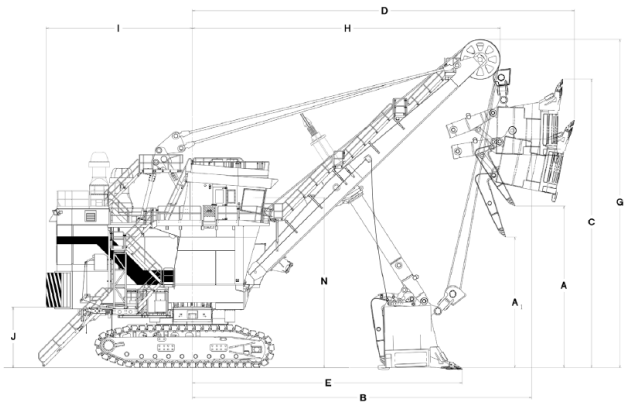

Optimal Working Ranges		
A	Dumping height	10.06 m (33 ft)
A_1	Dumping height at maximum electric crowd limit	8.61 m (28 ft 3 in)
B	Dumping radius (maximum)	21.64 m (71 ft)
C	Cutting height (maximum)	17.8 m (58 ft 5 in)
D	Cutting radius (maximum)	25.2 m (82 ft 8 in)
E	Radius of level floor	17.47 m (57 ft 4 in)
G	Clearance height (boom point sheaves)	20.87 m (68 ft 6 in)
H	Clearance radius (boom point sheaves)	19.65 m (64 ft 5 in)
I	Clearance radius (revolving frame)	max: 9.34 m (30 ft 8 in)
J	Clearance under frame (to ground)	3.76 m (12 ft 4 in)
K	Height of A-frame	14 m (46 ft)
L	Overall width	13.96 m (46 ft 1 in)
M	Clearance under lowest point in truck frame/propel gearcase	0.90 m (2 ft 11.5 in)
N	Operator's eye level	10.61 m (34 ft 10 in)

Figure 2.13 Working ranges of a Cat 7495 HF electric rope shovel (Caterpillar, 2013)

2.3 Mine haul truck KPIs

Truck performance KPIs have been developed using the critical data collected by the on board monitoring systems on the trucks. Some KPIs, such as rack, roll, pitch and Tonne Kilometer Per Hour (TKPH) are calculated using the truck speed, strut pressures and payload that are recorded by the truck on board systems. It will later be determined that the truck payload balance has a correlation with the truck KPIs and subsequently productivity.

2.3.1 Truck onboard information systems

Caterpillar Vital Information Management System (VIMS) is a tool that provide a wide range of information on the vehicle vital functions. Several hundred sensors are installed on haul trucks to monitor the functionality of many important components of the trucks and VIMS is the onboard microprocessor that collects the readings from the sensors which enables the technicians, engineers, managers and Caterpillar to monitor the vehicle condition and also to conduct intelligence analysis to improve production efficiency and to lower cost. The truck strut pressure sensors are four critical sensors on the truck that VIMS uses to calculate the payload of the truck.

A similar tool has been developed by Komatsu for the same purpose and is called Komtrax. It works wirelessly with a secure, web-based, application to record and communicate the equipment's vital information (Komatsu, 2013).

2.3.2 Truck key performance indicators

Rack, Roll, Pitch, TKPH and Whole Body Vibration (WBV) are KPIs used to monitor the truck fleet.

Using the input from VIMS and TPMS, Caterpillar of Australia have developed a concept, Application Severity Analysis (ASA), to analyze haulage performance for early detection of the poor performance areas and for assessment of the cost associated with these areas if they are not remedied (Mills, 2002).

The three concepts developed by Caterpillar of Australia used to assess the ASA are machine rack, pitch and bias (or roll).

2.3.2.1 Rack

Rack is the twisting (torsional) motion in a structure and it is defined as the twisting or tensile forces within the truck frame which will eventually transfer to other components. A strong correlation exists between the rack values and the stress and strain experienced by the machine structure (Mills, 2002).

Whalen (2003) showed that frame torsion is the main adverse motion contributing to truck dump body cracking. Consequently, the life of the truck frame could be predicted by the number of the recorded high "fatigue" rack values (Mills, 2002; Whalen, 2003).

If the right front, left front, right rear, and left rear struts are denoted RF, LF, RR, and LR respectively shown in figure 2.14 then rack can be calculated by the following expression in pressure units.

$$\text{Rack} = (LF + RR) - (RF + LR) \qquad [5]$$

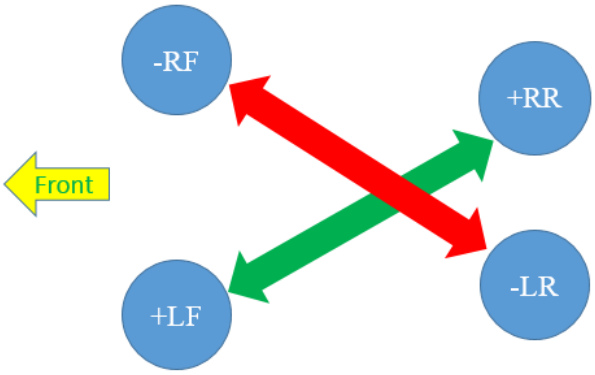

Figure 2.14 Truck suspensions configuration for rack calculation

Joseph (2003) offered a new unit for rack calculation, which gives a better understanding of the severity of the forces. He suggested calculating rack motion

on a g level scale which gives a clear understanding of the twisting force magnitudes that the truck structure is undergoing. He converted strut pressures to strut forces knowing the strut contact area and then defined the ratio of dynamic forces over the static forces as g values for each reading (Joseph, 2003).

$$\text{Rack} = \frac{1}{g}(a_{LF} + a_{RR}) - (a_{RF} + a_{LR}) \qquad [6]$$

Where a_{LF}, a_{RR}, a_{RF} and a_{LR} are the dynamic forces on the left front, right rear, right front and left rear struts respectively.

In equation 6, the datum value of g is cancelled. The same method can be applied to calculate the pitch and roll values.

2.3.2.2 Pitch

Pitch is the longitudinal motion of the truck and is calculated by the following formula.

$$\text{Pitch} = (LF + RF) - (LR + RR) \qquad [7]$$

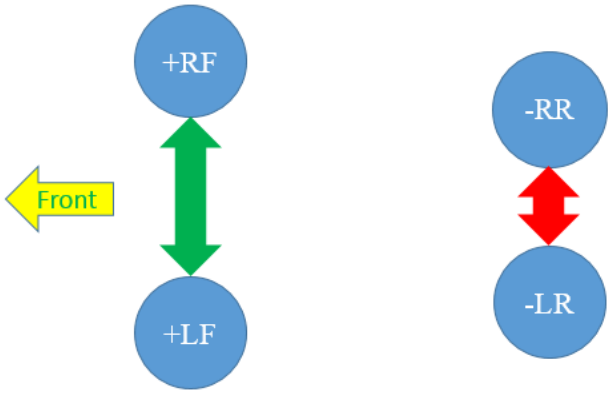

Figure 2.15 Truck suspensions configuration for pitch calculation

In order to maintain an even load distribution on all tires ($\frac{1}{6}$load/tire), one third of the total suspended load is divided to the front axle and two third to the

rear axle; therefore, the preferred pitch values are negative one third of the total nominal suspended load according to equation 7.

This proportion could change if the payload is not balanced. Front over loading occurs more often than rear loading as the canopy at the front of the body is in error used to bear additional payload, and the material to the rear often falls off of the truck body in motion.

The life of the tires, rims, front wheel bearings, steering components, front suspension cylinders, seals and mounting are significantly shortened by excessive front loading (Mills, 2002).

2.3.2.3 Roll (bias)

Roll is the lateral movement of the truck and it is defined by the equation 8 and shown in figure 2.16.

$$\text{Roll} = (LF + LR) - (RF + RR) \qquad [8]$$

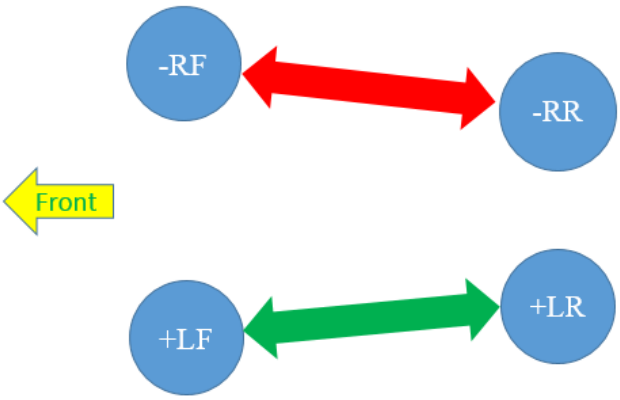

Figure 2.16 Truck suspensions configuration for roll calculation

High roll events reduce the life of final drives and wheel bearings and increase the probability of the strut gas charge being lost on the side that the load is bias to. Moreover, side bias and excessive front or rear loading could create tire

TKPH problems. The tires under the wheel positions that are affected could experience excessive temperature and tire wear problems (Mills, 2002).

In addition, a new KPI can be developed combining the individual strut pressure values with speed to produce dynamic tonne kilometer per hour to be used for the mine tire management (Mills, 2002).

2.3.2.4 Tonne kilometer per hour

Tonne kilometer per hour (TKPH) is a KPI used to select the appropriate tire type for a mine site and also to monitor the operational environment that the tires are subjected to. The tire manufacturers classify their products according to TKPH.

SAE J1098 outlines equation 9 to calculate the TKPH job rate of an individual tire based on work cycle analysis (SAE, 2012).

$$J = \frac{T_L K_L N_L + T_E K_E N_E}{2H} \quad [9]$$

Where J is job rate in TKPH, H is the total time in hours for the day from the beginning of the first shift to the end of the last shift, T_L and T_E are the tire load in metric tonne on the loaded and empty machine respectively, K_L and K_E are the length of the loaded and empty haul in kilometer, N_L and N_E are the number of the loaded and empty trips for the time (H) period.

However, as a result of unbalanced payload along with the uneven haul road profile, the actual TKPH values are usually higher than the nominal allowable tire TKPH which is proportional to the reduction in the life of the tires. The actual TKPH can be calculated from field data via the real time speed and strut pressure readings. Where the strut pressures are converted via cross sectional area to equivalent loads in times. The conventional TKPH evaluation process misses the load level variation and the frequency of the events which is a main

contributor to the tire life reduction. Figure 2.17 and 2.18 illustrate the real-time to conventional TKPH comparisons for two truck cycles. Figure 2.17 shows that about 15% of the events exceed 2000 TKPH and 1.3 gs and figure 2.18 shows that for a truck with a better balanced payload on the same running surface the tires are subject to lower levels of TKPH causing the data cloud to be more clustered and shifted to the left and only 1.5% of the readings are greater than 2000 TKPH and above 1.3 gs (Joseph & Chamanara, 2012).

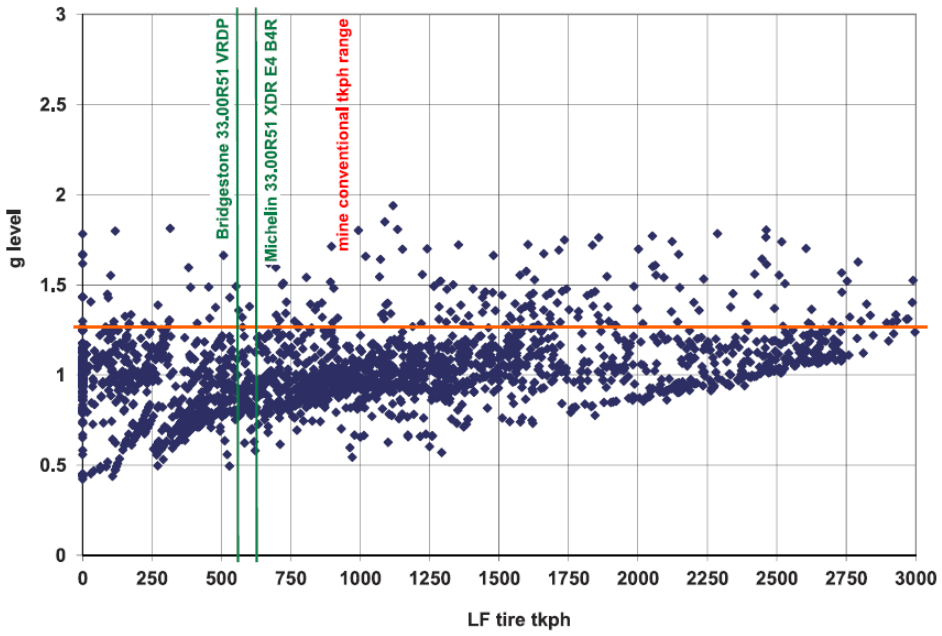

Figure 2.17 Conventional TKPH comparison to real-time TKPH values for a truck with an unbalanced payload (Joseph & Chamanara, 2012)

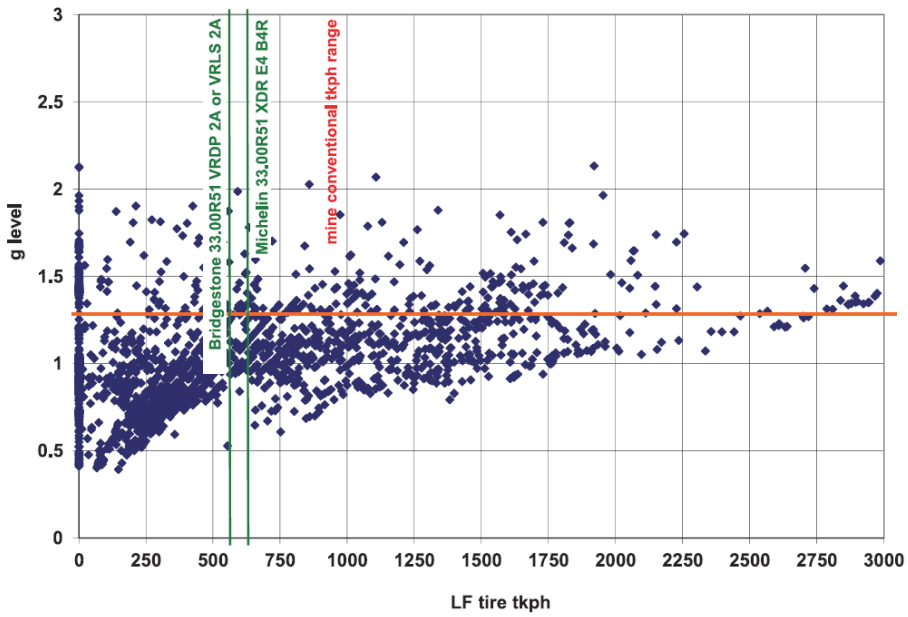

Figure 2.18 Conventional TKPH comparison to real-time TKPH values for a truck with an balanced payload (Joseph & Chamanara, 2012)

2.3.2.5 WBV

Whole body vibration (WBV) can cause psychological and physiological health problems to the operator. ISO 2631 standard exists for vibration exposure that defines a "caution to dangerous" health guideline zone for the operator (Berezan, Joseph, & Valle, 2004).

Berezan at al. (2004) stated that there are three ways to control the mobile equipment vibration through component change, road conditions or operational practices. Their paper presented a strong correlation between rack and acceleration equivalent (Aeq) for a given operating period as shown in figure 2.19.

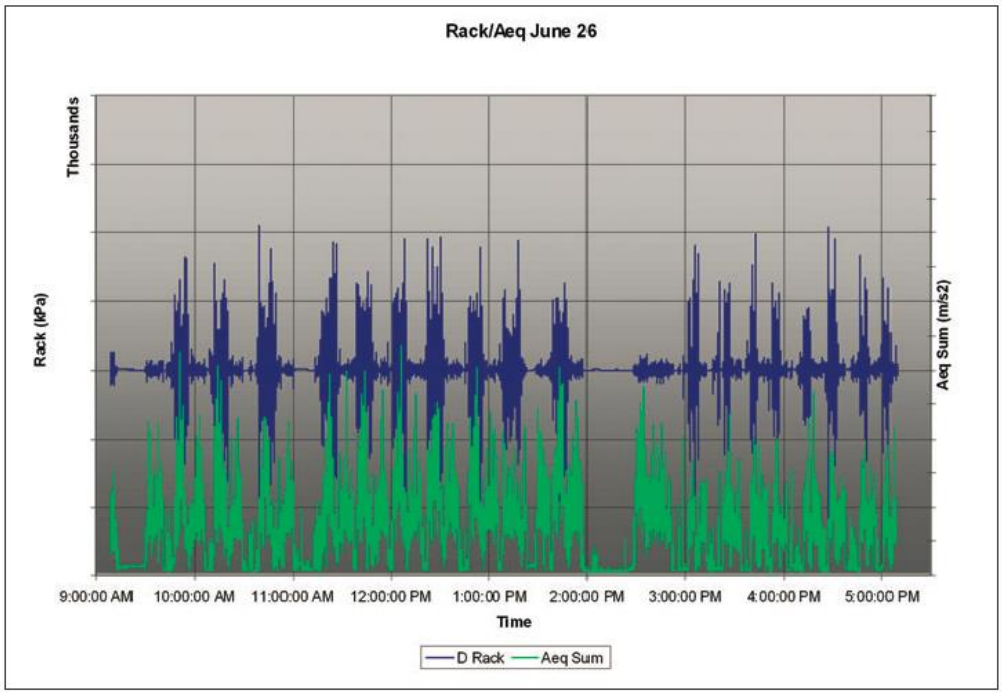

Figure 2.19 Change in rack and acceleration equivalent (Berezan et al., 2004)

If there is a correlation between rack and WBV, the vibration level of mining haul trucks could be reduced by enhancing the truck payload balance, if the payload balance shows a strong correlation to truck rack levels (Berezan et al., 2004).

2.4 Haul truck premature structural failure

One of the main contributing factor to haul truck structural failure is the cyclic loading on the structure due to dynamic forces on the structure while the truck is in motion. It is estimated that 85% to 90% of all structural failures are due to fatigue (Abd. Rahman, Nasir Tamin, & Kurdi, 2008; Mi, Gu, Yang, & Nie, 2012).

2.4.1 Fatigue

Fatigue is defined as the progressive, localized and permanent structural change occurring in a material that is subject to repeated or fluctuating strains at nominal stresses with maximum values of less than the tensile strength of the

material. Fatigue process consists of initial fatigue damage leading to crack initiation, crack progression to a state that the structure is incapable of carrying the impose load, and the final sudden fracture of the remaining cross section. In addition, the simultaneous action of cyclic stress, tensile stress and plastic strain cause fatigue damage (Boardman, 1990).

2.4.1.1 Frame fatigue life

It is possible to predict frame fatigue life through multibody dynamic analysis and finite element analysis of the frame. The dynamic stress time history of the frame can be estimated by expression 10 (Gu, Mi, Wang, & Jiang, 2012; Mi et al., 2012).

$$\sigma_{xy}(t) = \sum_{i=1}^{m} P_i(t) \cdot \frac{\sigma_{ixyst}}{P_{ist}} \quad [10]$$

Where $\sigma_{xy}(t)$ is stress time history about every node, $P_i(t)$ is the dynamic load time history of i, P_{ist} is the peak load of i, σ_{ixyst} is the stress of a single i load, and m is whole load numbers.

After obtaining the dynamic stress of frame from simulation, fatigue failure of frame can be predicted applying normal stress method (S-N curve) and Palmgren Miner Rule. The whole damage D can be defined by equation 11 if there are k stress levels, suffering each m_i cycles (Gu et al., 2012; Mi et al., 2012).

$$D = \sum_1^k D_i = \sum_1^k {m_i}/{N_i} \quad [11]$$

Finally, according to the S-N curve theory, the fatigue life can be calculated by expression 12.

$$S = 10^c N^b \quad [12]$$

Where c and b are the material parameters (Gu et al., 2012; Mi et al., 2012).

2.4.1.2 S-N curves

The fatigue data test results are commonly plotted as the stress amplitude or the maximum stress versus the number of cycle, N, to fracture in a logarithmic scale for the number of cycles. An S-N curve is the resulting curve of the data points. For a material tested at different stress ratios, a family of S-N curves is depicted in figure 2.20. Usually, an S-N curve represents the median, B_{50}, life which correlate to the number of cycles at which half of the specimens fail under a given stress level (Boardman, 1990).

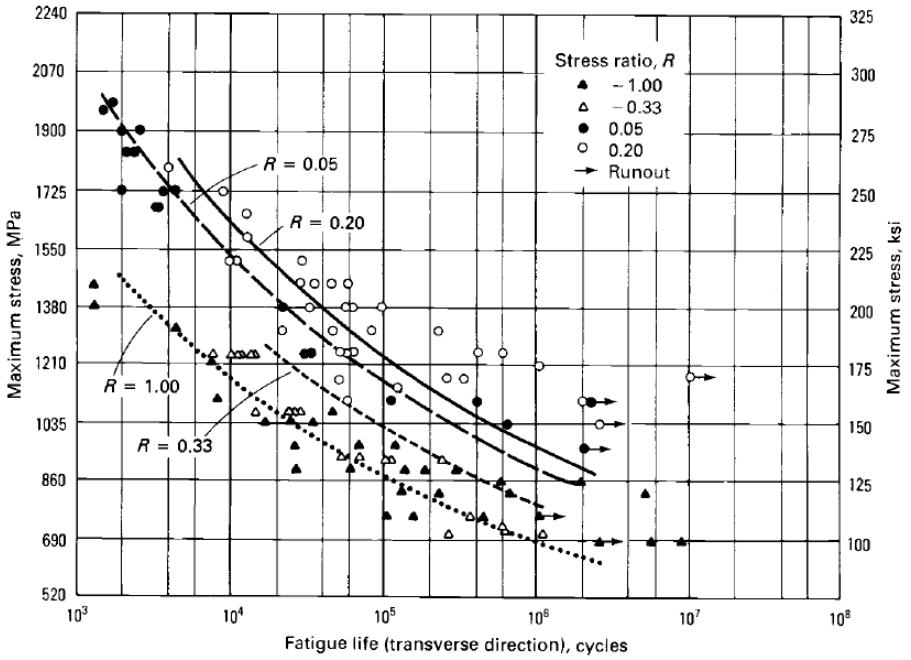

Figure 2.20 Best-fit S-N curves for unnotched 300M alloy forging with an ultimate tensile strenght of 1930 MPa (Boardman, 1990)

2.4.2 Rack, truck payload balance and structural fatigue

The frequency of the adverse loading cycles exceeding a given loading magnitude may define the haul truck structural fatigue. If a truck structure is experiencing higher magnitude of loading, a fewer number of adverse loading cycles are required to initiate the structural fatigue. Rack, twisting, motions subject truck structure to adverse motions that could result in truck structure

premature failure. In a study, it is suggested that one million rack events exceeding 1.5g in magnitude may cause structural fatigue (Joseph, 2003; Joseph & Chamanara, 2012).

Haul trucks experience a range of rack events during any given duty cycle; therefore, the rack events may be presented as a distribution curve as the ones shown in figures 2.21 and 2.22. In figure 2.21, the truck is under an unbalanced payload and the majority of rack event distribution is centered around the pre-set rack value due to the unbalanced payload shown by a solid red line in the figure. When a structure is under rack stress, it tries to release the rack stress to achieve a balance state by flexing out of the stressed condition causing reaction rack events in the opposite direction. This phenomenon can be seen as a rack event distribution in the opposite direction around +500 kN in figure 2.21. These reaction rack events are shorter-lived; therefore, the distribution is tighter but manifests as a larger event frequency at the peaks. As a result, both rack actions and reactions are of the concern when the truck is under an unbalanced payload (Joseph & Chamanara, 2012).

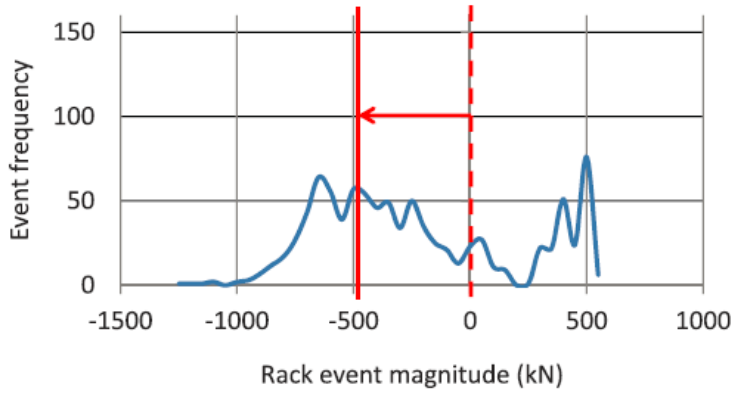

Figure 2.21 Distribution of rack events incurred by a haul truck under an unbalanced payload (Joseph & Chamanara, 2012)

Figure 2.22 illustrates a rack event distribution for a hauler duty cycle on the same running surface as the one shown in figure 2.21 but under a balanced

payload. As shown in the distribution curve, a relatively balance payload subjects the haul truck to a smoother ride with no twist reactions and much lower frequency of high magnitude rack events. Some events at the -500 kN rack level are most likely due to the poor haul road condition in certain sections of the haul road (Joseph & Chamanara, 2012).

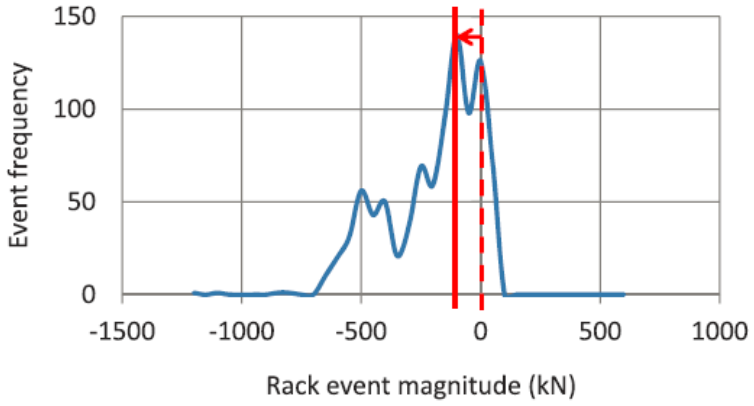

Figure 2.22 Distribution of rack events incurred by a haul truck under a balanced payload (Joseph & Chamanara, 2012)

2.4.3 Caterpillar 797B premature failures

Many frame premature failures are due to fatigue associated with high rack, roll and pitch events during the life of mining haul trucks. In a root cause analyses report at an oil sand mine after frame failures on three Caterpillar 797B trucks in two months, it was estimated that the life of a 797B truck at that site should be 96,000 operating hours. However, in three incidents the truck frames failed after approximately 52,000 operating hours as shown in table 2.1. On the other hand, the cost associated with replacing the failed truck frame with a new one was estimated to be equal and even higher than the cost of a brand new truck. Therefore, the life of the truck is reduced by 45%. This is a significant cost (Amarra & El-Sayed, 2010).

Table 2.1 Three Cat 797B truck frame failures at an oil sand mine (Amarra & El-Sayed, 2010)

TRUCK	FRAME HOURS WHEN CRACK WAS FOUND	CRACK LENGTH	CRACK LOCATION
A	52,130	70"	Left side behind coolers
B	52,555	20"	Left side behind coolers
C	51,993	7"	Left side behind coolers
C	51,993	14"	Right side behind coolers

Figure 2.23 illustrates the general location of the cracks within the frame and also figure 2.24 shows the actual cracks in the frames of unit A and C. The length of the crack on unit A was 70 inches which represented almost the entire circumference of the frame in this section. If the frame was separated on the opposite side, a catastrophic failure was imminent that could have hurt the operator if the truck was loaded and operating at a high speed.

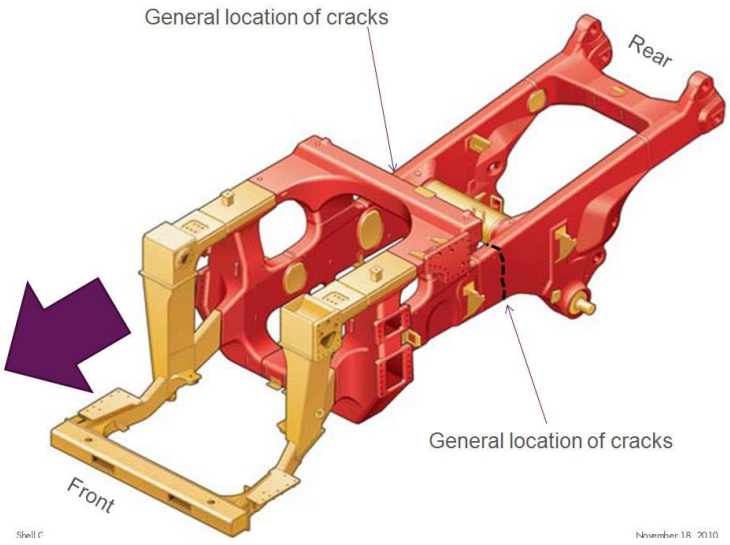

Figure 2.23 General location of the cracks (Amarra & El-Sayed, 2010)

Figure 2.24 Frame crack (Truck A on the left and C on the right) (Amarra & El-Sayed, 2010)

The number of rack, roll and bias (pitch) alarms prior to the frame failure were studied. Figures 2.25 and 2.26 illustrate the number of alarms for all three KPIs per month up to three years prior to the failures. These alarms are generated when the rack, pitch and bias values are greater than the maximum values set by the OEMs deemed to be normal. In both graphs, an increasing trend can be observed indicating that the truck frames were experiencing higher stresses. As a result, they failed approximately after six years being in service rather than the expected 10 years.

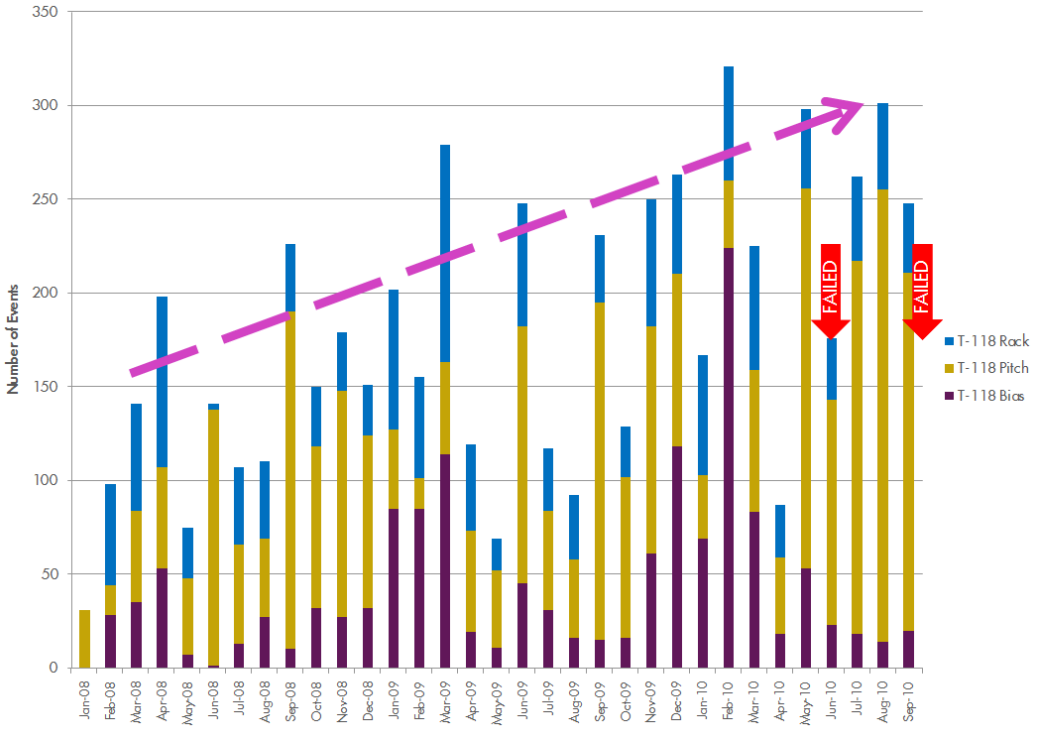

Figure 2.25 Truck A total rack, pitch and bias alarms (Amarra & El-Sayed, 2010)

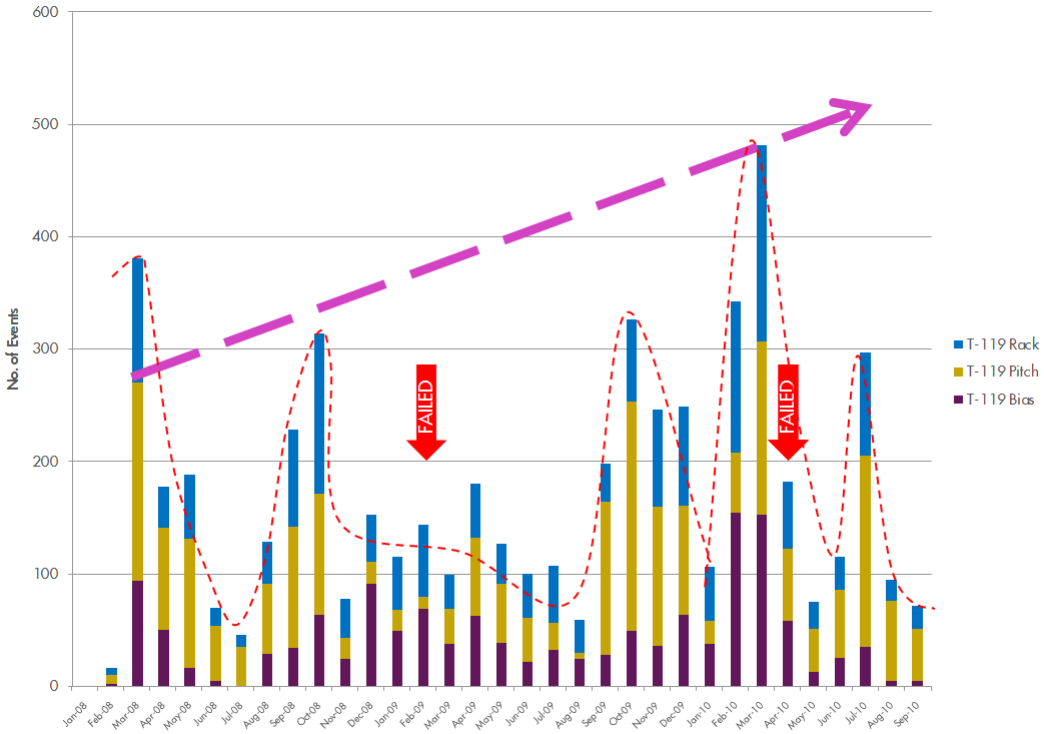

Figure 2.26 Truck B total rack, pitch and bias alarms (Amarra & El-Sayed, 2010)

Frame cracking is not the only failure that the ultra-class haulers experience. Figures 2.27 and 2.28 show a 797B truck with the right front wheel being separated under the load. In this incident, faulty component combined with high rack, roll and pitch events experienced by the truck caused the catastrophic failure.

Figure 2.27 RHF spindle failure on a 797B (Front view) (Finning, 2010)

Figure 2.28 RHF spindle failure on a 797B truck (Rear view) (Finning, 2010)

3. Field investigation and verification of theory

Field tests were conducted to study shovel loading pass interactions in a haul truck body to form the final payload, including correlations between the final payload balance and the haul truck KPIs at the Shell Canada Muskeg River Mine north of Fort McMurray.

3.1 Test objectives

The field tests were designed to study shovel loading passes required to nominally load trucks and to investigate the resulting truck motion KPIs during the ensuing duty cycle period. This was targeted to better understand how individually placed shovel bucket loads interact with one another as well as the truck body walls and floor to form the shape of the encompassed final payload.

Moreover, the tests were conducted to study any correlation between individual shovel load pass shape and location within the truck body allowing the formation of the final payload shape within the truck body, and also to better discern how the shovel bucket load locations affect the load distribution on the truck axles and suspension struts.

This test also illustrated the correlation between the truck payload balance and motion KPIs (rack, roll, pitch) and conversely the adverse effects of unbalanced payloads on KPIs. It also served as an illustration of the severity of truck working conditions (road surface) under unbalanced payloads.

Moreover, the field test was used to further verify the thesis hypothesis and theory, also illustrated by the controlled scale laboratory tests conducted in chapter 4.

3.2 Muskeg River Mine

The Shell Canada Muskeg River Mine (MRM) is an open pit oil sands mine operated by Shell Canada Ltd. located approximately 70 km north of Fort McMurray. The MRM loading and hauling fleet consists of Caterpillar 797B,

797F and 785C trucks, Caterpillar 7495HF electric shovels, Hitachi 8000 hydraulic excavators and also a few PC3000 and PC2500 backhoes.

More than 300,000 tonnes of ore is delivered to the crushers and more than 250,000 tonnes of waste is moved at MRM every day. In production at this scale, any small improvement in productivity and availability will save a significant amount of money attributed to operational costs and will significantly reduce the operational losses due to the potential loss of fleet availability and reliability.

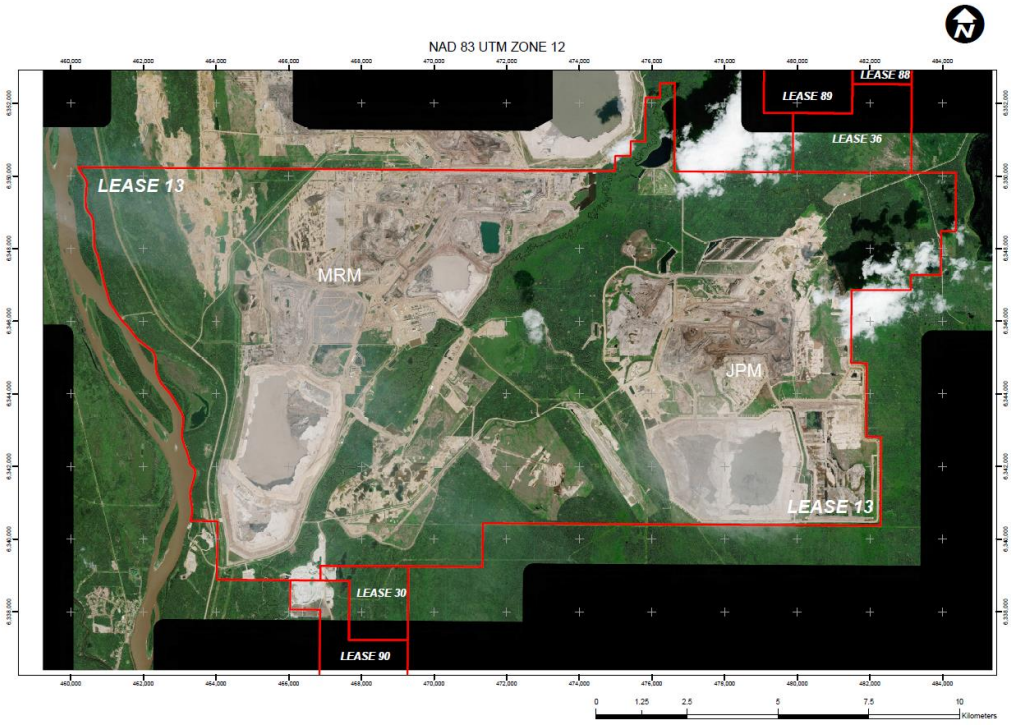

Figure 3.1 A satellite map of Muskeg River and Jackpine mines taken in July 2013

3.3 Test procedure

In preparation for the field tests, the following arrangements were made: After submitting a proposal to the mine manager, an approval was obtained in April 2011. The maintenance department was contacted and the test objectives and procedures were explained. The maintenance department identified two

Caterpillar 797B trucks that were recently released from the maintenance shop, where their suspension systems were recently re-charged and verified as operating at normal conditions. The truck body model on both haulers was identified as CAT MSD II model. The maintenance department also provided two technicians to install two data-loggers on the trucks and collect the required data during the test.

The Dispatch team was also contacted to set up a "trend track" in Dispatch to collect the same readings during the test remotely, so that two sets of data were recorded for redundancy and also to compare real time (on-board) versus dispatched viewed information. The Kal Tire on-site service group were also contacted to measure and verify the tire pressures during the test. As such, activities were conducted to best ensure a nominal known set of conditions for the tests.

The mine planning team identified a waste shovel that could be used for the test in order to have the least negative impact on site production during the tests. The geology department also provided a field geologist during the test to set up a Lidar scanner to scan the trucks' in-body payloads and also to collect a sample from the face and to send it to the lab for analysis.

The operations team at the mine was also involved to build a safe pad above the shovel face for the camera, scanner and observers.

On the day of the test, truck A and B were called to go to the in-pit fuelling and lube station during the operators' break at approximately 10 a.m. to install the data loggers. The data loggers were installed and the trucks were released to travel to the active shovel digging face by 10:30 a.m.

Prior to the trucks' arrival at the shovel, a video camera and Lidar scanner were mounted above the shovel face and operations dispatch was informed that the test was about to take place. The loading unit was identified as a Caterpillar 7495HF electric shovel. The first truck, A, arrived at the face at 10:45 a.m. and

the loading sequence was recorded by the video camera, Lidar scanner and through digital still photographs. Simultaneously, two maintenance personnel on the trucks collected the VIMS data which included the four strut pressures, the ground speed, the second gear payload recognition and the truck position via GPS northing and easting coordinates.

Five truck cycles were recorded in the morning. Truck A was loaded at 10:40 a.m., 11:12 a.m. and 12:05 p.m. and truck B was at the face at 11:15 a.m. and 11:53 a.m. The test continued until 12:30 p.m. when the trucks went back to the refuelling station during the scheduled lunch break, at which point the collected data was transferred onto a memory card. The data loggers were left unattended but activated to collect data for the afternoon. The Kal Tire service personnel measured the tire air pressures again prior to the second period of testing. The tire inflation status is illustrated below in table 3.1.

Table 3.1 Caterpillar 797B haul truck tire air pressure

	Unit A	Unit B
Position	Actual PSI	Actual PSI
LF	109	109
LRO	105	100
LRI	103	103
RRI	100	105
RRO	101	107
RF	107	107

The site geologist also collected a sample from the active digging face and sent it to the laboratory on site for analysis. The result from laboratory is given in table 3.2.

Table 3.2 Material Properties

Property	D_{10}	D_{50}	D_{90}	% BITUMEN	% SOLID	% H_20	% TOTAL	MOISTURE
Value	3.4	40.4	173.1	4.3	88.32	7.27	99.89	7.52

D_{10}, D_{50} and D_{90} numbers are the particle size diameter at 10^{th}, 50^{th}, 90^{th} percentile indicating the particle size distribution of the material. In this sample, 10 percent of the material particles have less than 3.4 μm diameter, 50 percent less than 40.4 μm and 90 percent less than 173.1 μm.

The Energy Resources Conservation Board (ERCB) of Alberta classifies any material that content less than seven weight percent bitumen as waste (ERCB, 2013). The waste material characteristics are slightly different from ore especially rich ore with bitumen content of greater than nine percent. The waste materials flow better than ore materials because they have less adhesive properties and they don't "chunk" together, which is typical of higher grade oil sand material which can also stick to truck body walls and floor as lumps.

3.4 Field data analysis

Fifteen truck cycles were investigated, which may be seen in appendix 8.2. However, three samples are used here to illustrate the field test outcomes for this research work. The raw data collected from the on-board Caterpillar vital information management system via data loggers and through the mine dispatch control centre were used to plot and verify the strut forces for each truck cycle and also to calculate and plot the rack, roll and pitch KPI values in tonnes for all cycles. Figures 3.4 and 3.5 provide examples of the KPI plots comparing the values sourced from dispatch data and the raw data loggers. Since the data acquisition frequency was set at 0.2 Hz at dispatch control (due to the magnitude

of data management for the entire hauler fleet) versus 1 Hz for the data loggers, it is evident that a large number of peak events are missed from the dispatch control viewpoint. As a result, the dispatch data was used solely as verification of the data logger acquired data, with reliance on the plots generated from the latter source. This gives us a much better view of the critical events experienced by a hauler compared to the information viewed by dispatch control for the truck cycles monitored.

3.4.1 Truck cycle 1

In cycle 1, the truck body was loaded to the satisfaction of the shovel operator in five full shovel bucket loads and one half bucket load. Figure 4.2 shows that within the truck final placed payload, a few large more intact pieces (chunky) material are evident in the truck body. The more intact nature (chunkier) the material, the less homogeneous the load in balance across the four suspension points becomes. The truck payload scale recorded the following payloads after each shovel load pass; 64, 131, 199, 266, 338, 370 tonnes and later 365 tonnes as the hauler achieved an instantaneous second gear re-weigh calculation auto-function within the VIMS system. Although the truck payload contained few large intact chuck-like lumps, it appears visually to an observer, from the picture, that the payload within the body still forms the shape of a truncated cone.

Figure 3.2 Truck A, cycle 1, fully loaded

3.4.1.1 Strut forces

In this first sample cycle, during the fifth and a half pass shovel loading sequence of the body, the right rear strut shows consistently higher forces than the left rear strut. However, after the truck proceeds to move away from the shovel under the payload state, the left rear strut shows slightly higher forces than the right strut. This is likely, and confirmed through visual inspection of the active face toe, due to the proximity of the toe to the rear dual wheel sets of the hauler while positioned parallel to the shovel and taking payload. Effectively, the right dual wheel set was elevated on lump material at the toe, relative to the left set. This is a common occurrence in truck - shovel mining operations, but only affects the relative tare weight condition on each suspension cylinder prior to the shovel loading the body. Increments of load, generating suspension forces relative to the position of the load in the body of the hauler are still proportional. This is confirmed as the suspended loads on the suspension in tare condition, although sitting on uneven ground are proportionate to the maximum available stroke of the oleo-pneumatic suspension, where the nitrogen (gas) spring is at its most sensitive and reflective of the loads accumulated above.

The total suspended load measured in the first sample was 520 tonnes (payload + tare weight). According to the manufacturer, to maintain a balanced load distribution on all six tires (1/6 GVW per tire), such that the front axle takes one third and the rear two thirds of the suspended load, 175 tonnes should be on each of the two rear struts and 87 tonnes on each of the front struts. This would be the expected state of the load before the truck commences its duty cycle motion.

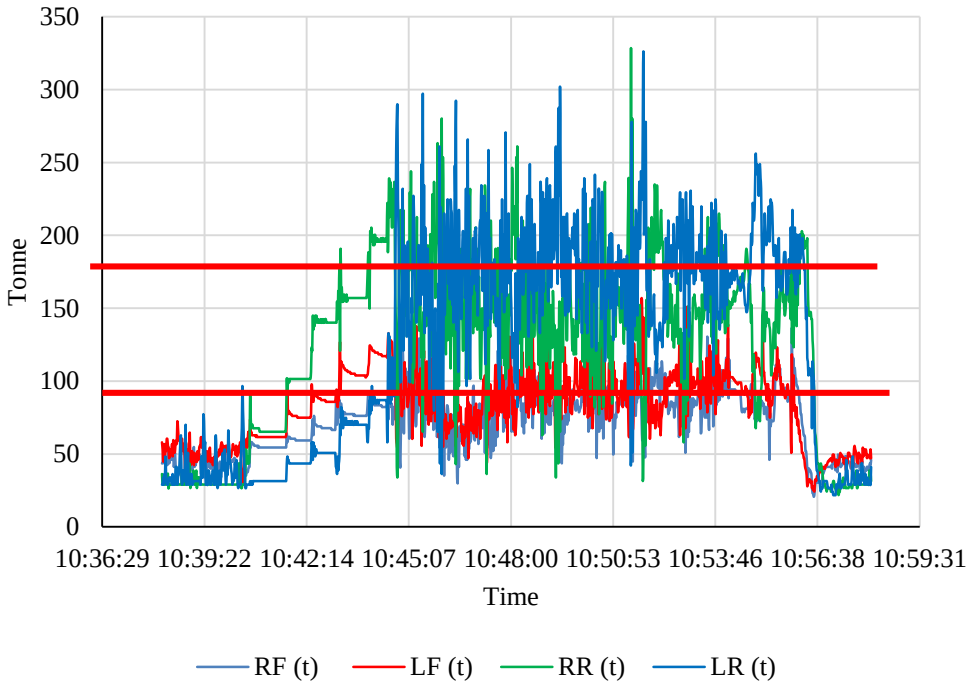

Figure 3.3 Strut suspended mass, truck A, cycle 1

Figure 3.3 illustrates that once the truck moves, the loaded suspension cylinders and the tire sets below are then subjected to much higher loads due to the motions of the truck, both relative to the load balance on the truck body above and the running surface quality below. The spikes in the left and right rear suspension strut suspended masses (LR and RR) in this case consistently approach and occasionally exceed 300 tonnes, double that above the desired 33% to 67% load distribution for the front and rear axles. The front suspension masses (LF and RF), although with variation, are much closer to the desired balance point.

3.4.1.2 Rack, roll and pitch

After each test run or sequence of runs were completed, the data was analyzed and the truck motion KPIs calculated in metric tonnes as a more familiar unit for communicating to mine operations personnel. As such tonnes here are considered as tonnes force. Having determined from the individual strut diameters, the effective bearing area in the front and rear struts as 0.126 m^2 and 0.114 m^2 respectively, the recorded strut pressures were converted to metric tonne units via

$$Mi = \left(\frac{F}{g+a_i}\right) = \frac{Pi\,A}{g} \quad [13]$$

Where M_i is the suspended mass under 1g loading when the hauler is stationary and the effective mass due to the changing increment or decrement of g; a_i when the hauler is in motion; P_i is the strut pressure at any time instant measured; A is the cross-sectional oleo-pneumatic bearing area in the strut and g is the acceleration due to 1 gravity (9.81 m/s^2).

The front struts are slightly larger than the rear struts to provide a larger bearing area of action for the oleo-pneumatic system, permitting any excess loads to be better controlled and thus enhancing the steering control of trucks (Joseph, 2003).

Figures 3.4 and 3.5 illustrate the rack, roll and pitch values for cycle 1 using the data collected from dispatch control and the installed data loggers respectively. The dispatch data was used to verify the accuracy of the data logger readings and it is clear from comparing figures 3.4 and 3.5, that the readings are in fact the same but at different acquisition speeds. The dispatch reading frequency was 0.2 Hz whereas the data loggers reading frequency were 1 Hz. There are some missing peak events, few of them are shown in circles in figure 3.5, in the dispatch data suggested that the mine has a limited understanding of the motion frequency of the haulers and the acquisition frequency needed to reflect that. For example, the data logger data shows roll events above 300 tonnes that

don’t appear in the dispatch data. As a result, the data for the test was much better represented by that recorded as raw sourced data directly from the VIMS on the truck. It has been previously documented by Joseph (2003) that the VIMS system does in fact take the direct data from the 0 – 20 mA strut pressure transducers that have a linear and reliable proportional range of 0 to 100 MPa. Instrument verification was performed by comparing VIMS data to direct data drawn from the pressure transducers by the researcher.

In this cycle, the payload appears to be at balance; evaluated as the mean suspension indicated values over the entire duty cycle; however the roll events approaching and exceeding 300 tonnes are of concern. One peak event exceeding 200 tonnes was attributed through field observations as due to the truck running over a berm at an intersection curve.

Negative pitch spikes, such as those in figure 3.4 greater than 300 tonnes subject the rear tires to higher than normal stresses. These high spikes are due to overloading the rear of the truck body, excessive ramp activity compounded with high pitching road undulations.

The high roll spikes, as roll is a function of rack motions (roll = -3rack) cause high whole body vibration (WBV) events (rack = f(WBV)) and high stresses on the tires (Berezan et al., 2004; Joseph, 2003).

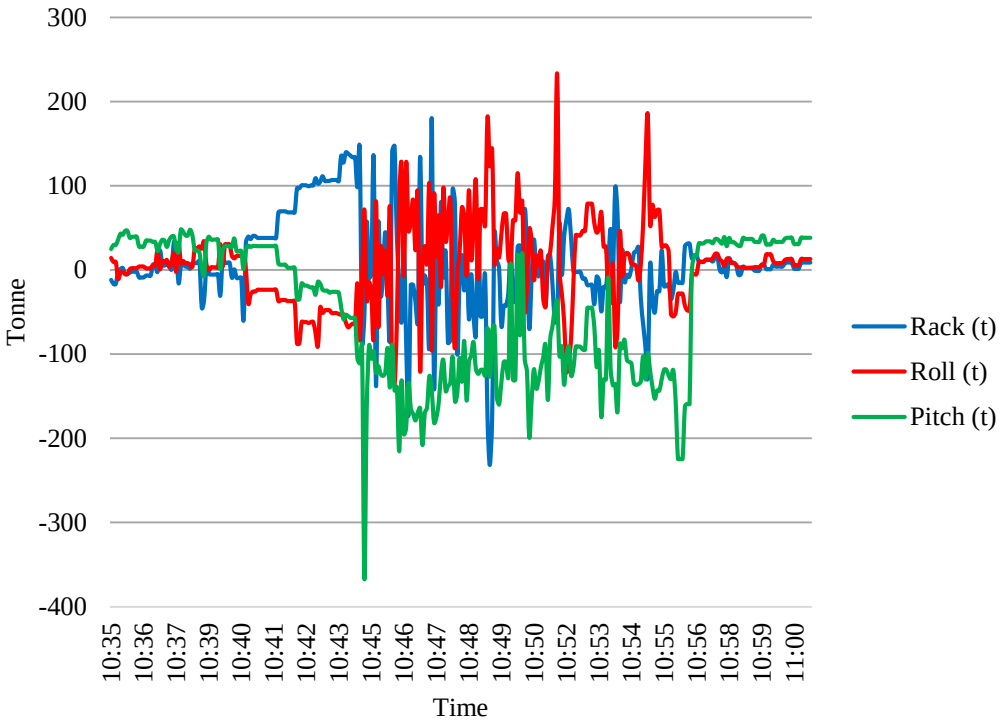

Figure 3.4 Rack, roll and pitch for cycle 1 from Dispatch

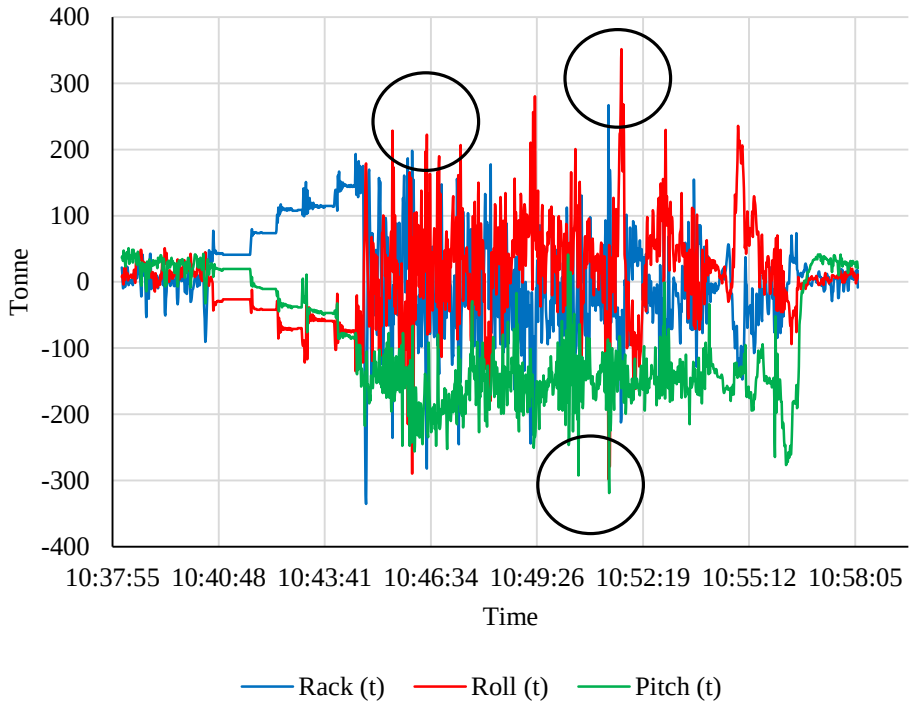

Figure 3.5 Rack, roll and pitch for cycle 1 from data logger

There are numerous excessive rack events illustrated in figure 3.5, indicating twisting (rack) forces greater than 200 tonnes and directly proportional to fatigue loading events on the truck structure that give rise to premature structural failure. These high spikes can be magnified by an unbalanced payload that will be illustrated in the next cycle evaluated.

3.4.2 Truck cycle 2

Figure 3.6 shows the placed truck payload for cycle 2 after the first and last shovel load passes, the latter when the truck is fully loaded. In this case, the truck was loaded with six shovel load passes with accumulative incremental recorded payloads of 52, 124, 210, 269, 346 and 372 tonnes, followed by a recorded second gear payload re-weigh of 364 tonnes. As illustrated in figure 3.6, the first shovel bucket load was placed slightly to the right that correlates with a spike in the right rear strut forces marked with a circle on the graph in figure 3.7.

Figure 3.6 Truck A, cycle 2, first shovel bucket load and final payload

3.4.2.1 Strut forces

The front and rear strut forces before the truck was loaded were representative of the proportionate share of the tare condition, noted at 11:03 a.m. and similarly after the truck dumped its load at 11:45 a.m.. During loading, the right rear and right front strut forces are higher indicating that the payload has been placed slightly to the right of the truck body balance centreline creating an unbalanced payload situation, which set a trend for all other loads placed into the

truck body. Shovel operators commonly use the first load pass as a target for subsequent load passes, resulting in an overall unbalanced payload by the time the truck moves away from the shovel. This highlights the importance of the first placed load pass in a truck body.

This particular case could have been alleviated after the first shovel load pass was completed with well-chosen placement of subsequent bucket loads; however, since the shovel operator could not discern an initial problem, the subsequent bucket loads were placed on top of the first load, resulting in an unbalanced final payload.

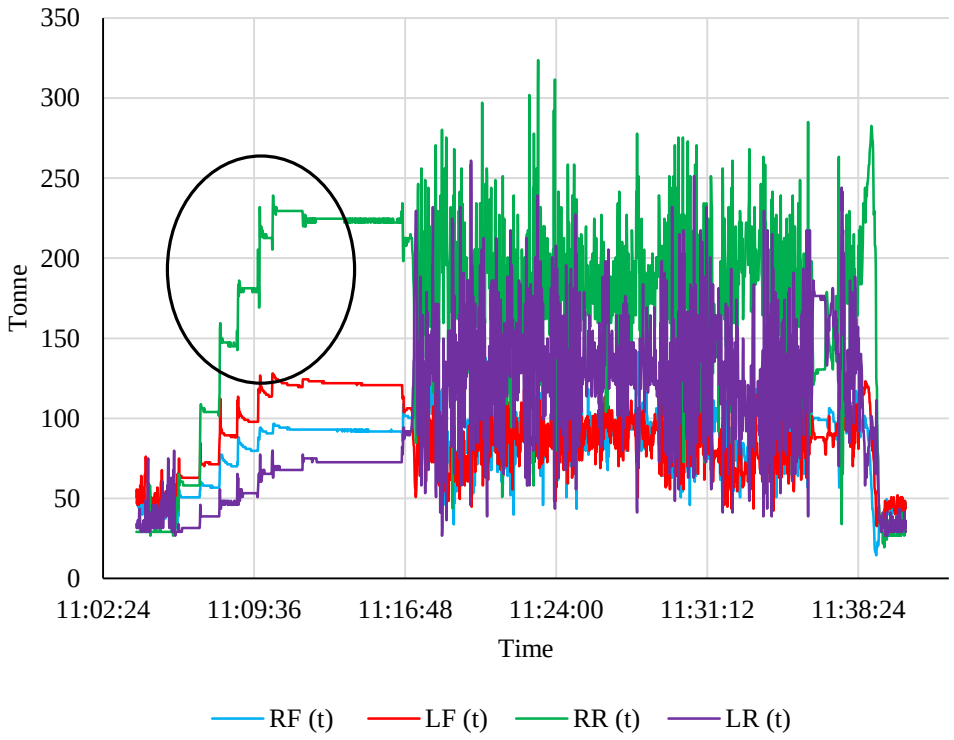

Figure 3.7 Strut suspended mass, truck A, cycle 2

As a result, there are spikes exceeding 250 tonnes showing much higher forces on the right rear strut than the left one resulting in high twisting forces on the frame. The second gear payload recorded at 364 tonnes is in this instance very close to the confirmed value from the suspension pressures.

3.4.2.2 Rack, roll and pitch

In cycle 2, the truck moved from the loading face after it was loaded and stopped to allow the geologist to scan the payload and then recommenced moving at around 11:16 a.m.

Since the payload was not balanced and was positioned to the right side of the truck body, the rack values are consistently above zero with events exceeding 200 tonnes. There are many roll and pitch events as well. Such an unbalanced payload has expected significant negative impacts on the truck KPIs.

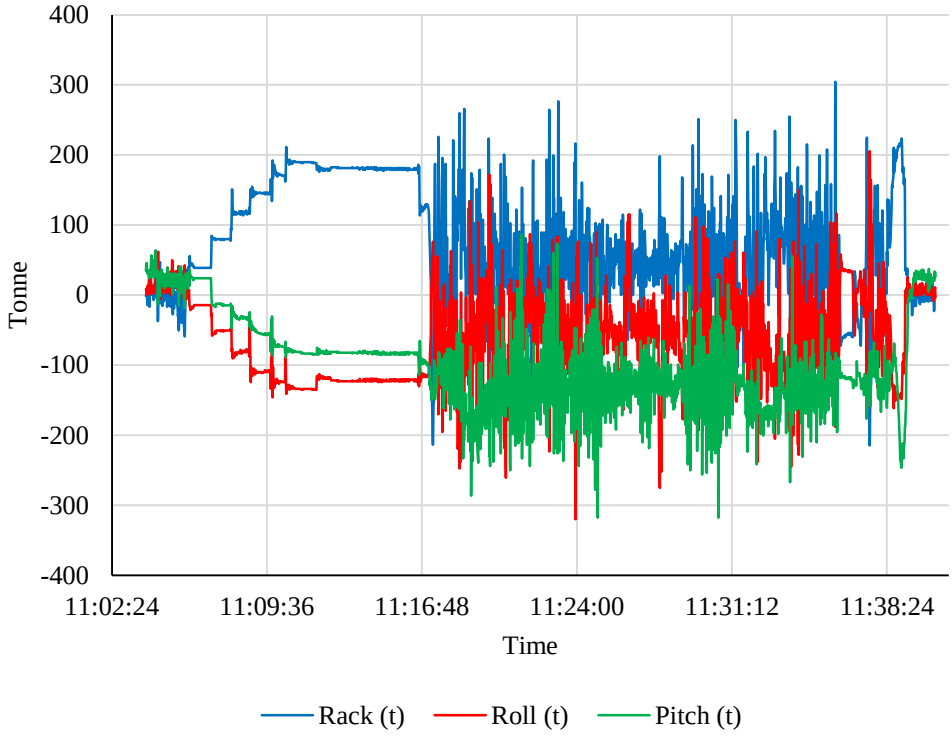

Figure 3.8 Rack, roll and pitch for cycle 2

The incremental offset forces cause higher whole body vibration impacts on the operator, and force the truck operator to slow down to reduce the vibration impacts on the operator's body, which in turn reduces production. Moreover, high rack even frequency will increase operational, maintenance and specifically tire costs.

3.4.3 Truck cycle 3

In cycle 3, shovel load passes were placed to the left of the truck body which is reflected in the force plot shown in figure 3.10. The photograph of the payload, figure 3.9, visually corresponds to the strut readings reported in figure 4.10. The magnitude of the five shovel load passes that form the final payload are 76, 151, 216, 272 and 323 tonnes with a second gear payload re-weigh of 307 tonnes. In this cycle, to see the effect of side loading, the truck was loaded in 5 load passes. The trucks are usually fully loaded in 6 passes; therefore, the production was effectively reduced with such an occurrence, but one that does occur within operations.

Figure 3.9 Truck A, Cycle 3, fully loaded

In figure 3.9, although the truck payload was not perfectly balanced, the truncated cone shape of the material is still recognizable.

3.4.3.1 Strut forces

The left rear and front struts show much higher readings than the right rear and front struts. Even though the truck payload in this cycle is significantly less than the truck payloads in cycles 1 and 2, there are many spikes in the truck strut

forces higher than 300 tonnes. These high strut forces amplify high twisting forces on the truck structure that reduce the life of the truck. Moreover, because of the unbalanced load, the space in the truck box was not well utilized. As a result, the final payload was less than the nominal payload leading to a reduction in production and the truck efficiency. Consequently, the overall operation cost would be effectively increased with such a practice.

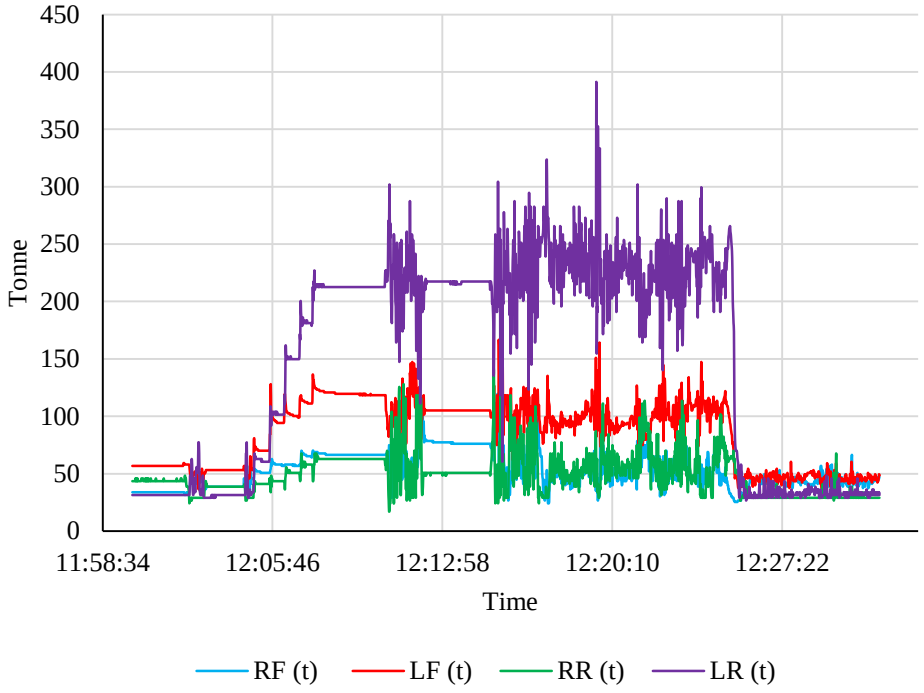

Figure 3.10 Strut suspended mass, truck A, cycle 3

3.4.3.2 Rack, Roll and Pitch

The roll values clearly indicates that the payload is not balanced and is sitting on the left side of the truck body. It also shows that the left struts are constantly under 200 tonnes more force than the right struts with spikes exceeding 300 tonnes. In addition, the rack values constantly approach negative 200 tonnes indicating that the truck body is twisted due to the unbalanced payload amplified by a poor road profile when the truck is in motion. These excessive static stresses on the truck structure make the truck more vulnerable and susceptive to premature structure failure. The negative values in rack, pitch or roll nearly indicate that

such motions are in the opposite directions that displayed by the “left-first” positive calculation.

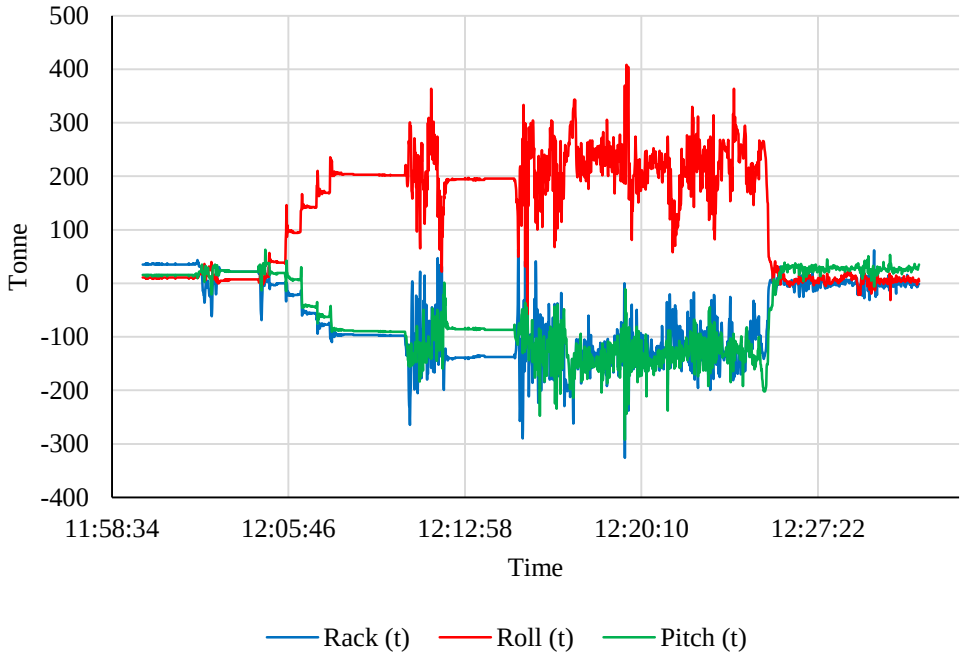

Figure 3.11 Rack, roll and pitch for cycle 3

3.5 Conclusion

The field test revealed that individual shovel pass load locations within the truck box are clearly reflected by the strut pressure readings, which provide a predictable base for simulation.

It is clear in all cases that the truck payload balance has a significant impact on the strut forces while the truck is in motion. The more the truck payload is out of balance, the greater the number of rack events are evident. As a result, the truck goes through higher twisting forces. In an extreme case such as cycle 3, a significant reduction in the truck payload is inevitable that will lead to a decrease in truck efficiency and production and an increase in operational cost.

The shovel bucket load passes, placed within the truck body, shape well defined truncated cones, even in the case of lean oil sand material.

4. Laboratory test and theory verification

The laboratory test was designed and conducted in two parts first objectives being to:

a. Simulate shovel bucket load shape placed in a truck body
b. Study shovel bucket load interactions in a truck body and how they intersect each other
c. Determine the relationship between the shovel load pass location and the final truck payload shape and location
d. Investigate the relationship between the strut readings and the shovel bucket load location within the truck box
e. Determine the adverse effects of an unbalanced payload on truck KPIs

And then to:

f. Validate the accuracy of the truck load balance algorithm, introduced in chapter 5, in predicting the shovel bucket load location to balance a truck body final payload

The controlled laboratory test procedure and steps will be explained in detail in this chapter.

4.1 Scale truck body and data acquisition system

Scientific study of scaling laws and scaling effect first presented by Galileo Galilei in his *Two New Sciences* book in 1638. Square-Cube law was also presented describing when an object's size increases proportionally, the new volume of the object is proportional to the cube of the multiplier and the object's new surface area is proportional to the square of the multiplier as shown in the mathematical expression 14 and 15 (Chakraborty, 2011; Wikipedia, 2013).

$$v_2 = v_1 \left(\frac{l_2}{l_1}\right)^3 \quad [14]$$

Where v_1 and l_1 are the original volume and length respectively and v_2 and l_2 are the new volume and length respectively.

$$A_2 = A_1 \left(\frac{l_2}{l_1}\right)^2 \text{ [15]}$$

Where A_1 and l_1 are the original surface area and length respectively and A_2 and l_2 are the new surface area and length respectively.

Building a 25th scale truck body is an "isomorphic" or "isometric" scaling rather than "allometric" scaling since the geometric integrity of the device is maintained with size. Isomorphic scaling law relate to the scaling of physical size of objects whereas the "allometric" scaling laws are related to a phenomenological behavior of an object or machine (Chakraborty, 2011)

In order to build a scale model of a Caterpillar 797 haul truck body, the actual dimensions for a 797 standard truck body were extracted from the 797B Caterpillar specification sheet (Caterpillar, 2010) and the truck body and strut locations were drawn in AutoCAD (figures 4.1 and 4.2).

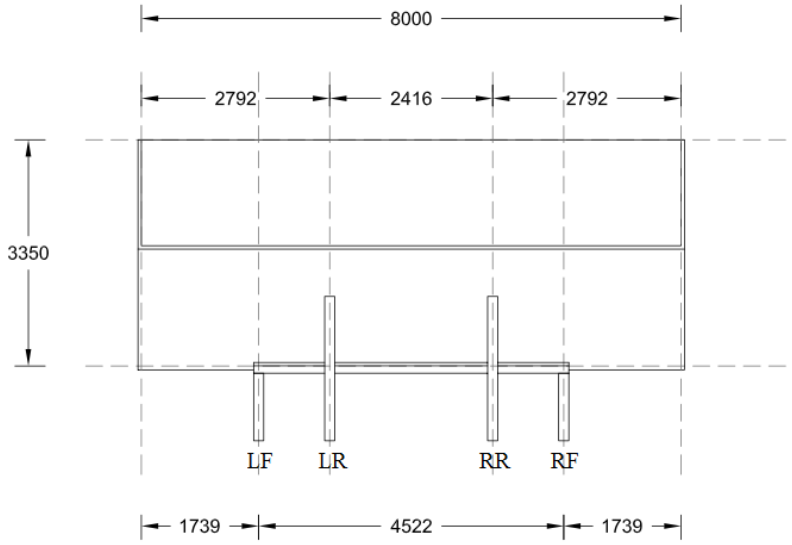

Figure 4.1 Caterpillar 797B standard body – Rear view

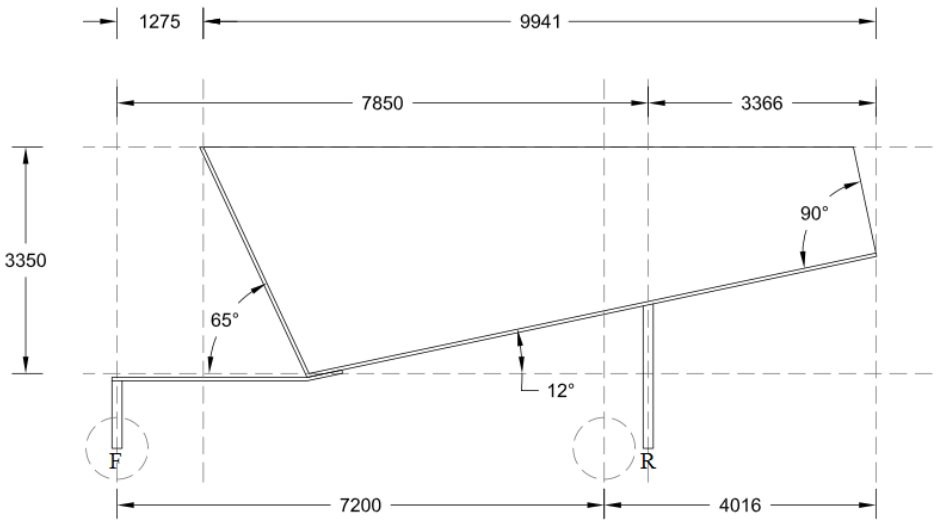

Figure 4.2 Caterpillar 797B standard body – Side view

After drawing the full scale 797 truck body, the dimensions were scaled to a 1:25 scale body as illustrated in figures 4.3 and 4.4. Linear dimensions were scaled directly, volumetric and weight scaling was a cube-root approach. As shown in the pictures the front struts, F, are located further ahead of the truck body and the rear struts, R, under the rear of truck body and also the front and bottom plates are angled.

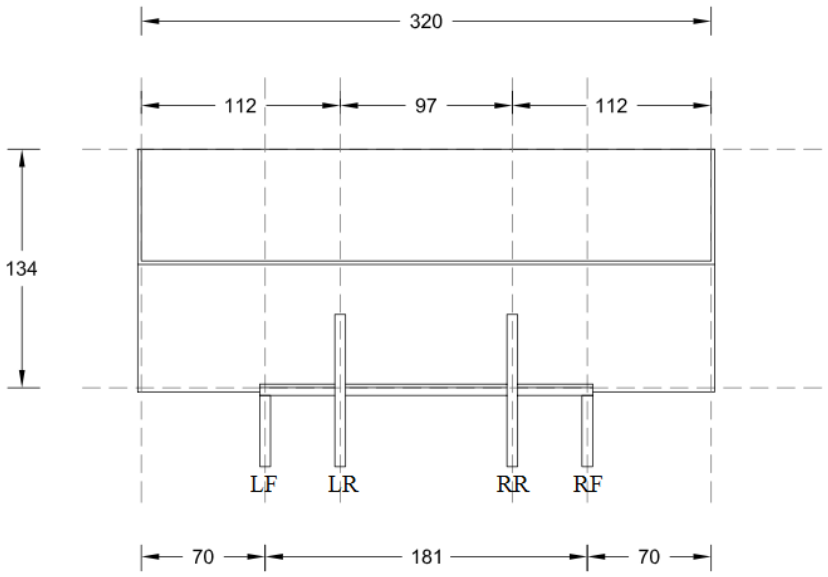

Figure 4.3 Caterpillar 797B 1:25 scale body – Rear view

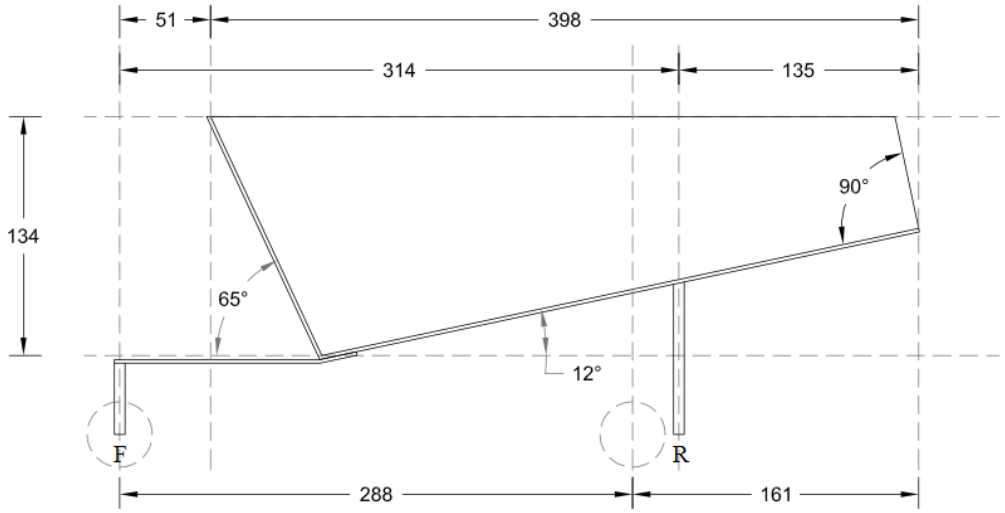

Figure 4.4 Caterpillar 797B 1:25 scale body – Side view

The 1:25 scale body side and bottom plates were cut out of a 3mm steel sheet and welded. Four bolts were also welded in the strut locations to attach the load cells representing in suspension struts. Since the front strut locations are ahead of the truck body, a single steel plate was welded to the body to attach the load cells.

In order to meet the purpose of the test, which was to study the shovel load cone interactions and also the payload shape and its relationship with the payload balance, the strut readings under load were simulated.

Four 50 lb S-shape Artech model 20210-50 load cells were acquired and installed in the strut locations to measure the forces applied on the struts at the 1:25 scale. The 3-D design of the 1:25 scale body is shown in figure 4.5.

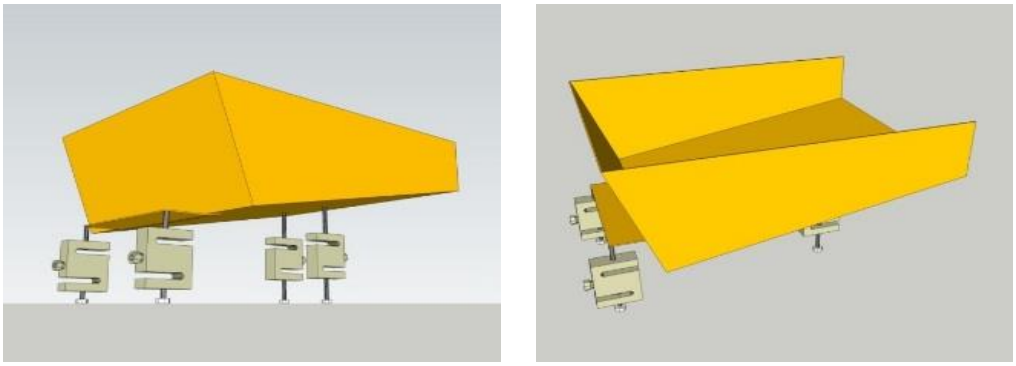

Figure 4.5 3-D design of the 1:25 scale truck body

The load cells were wired to a SoMat eDAQ data acquisition device, each cell powered by a separate 10v power source. The data was acquired using eDAQ software installed on a Panasonic Toughbook as shown in figure 4.6.

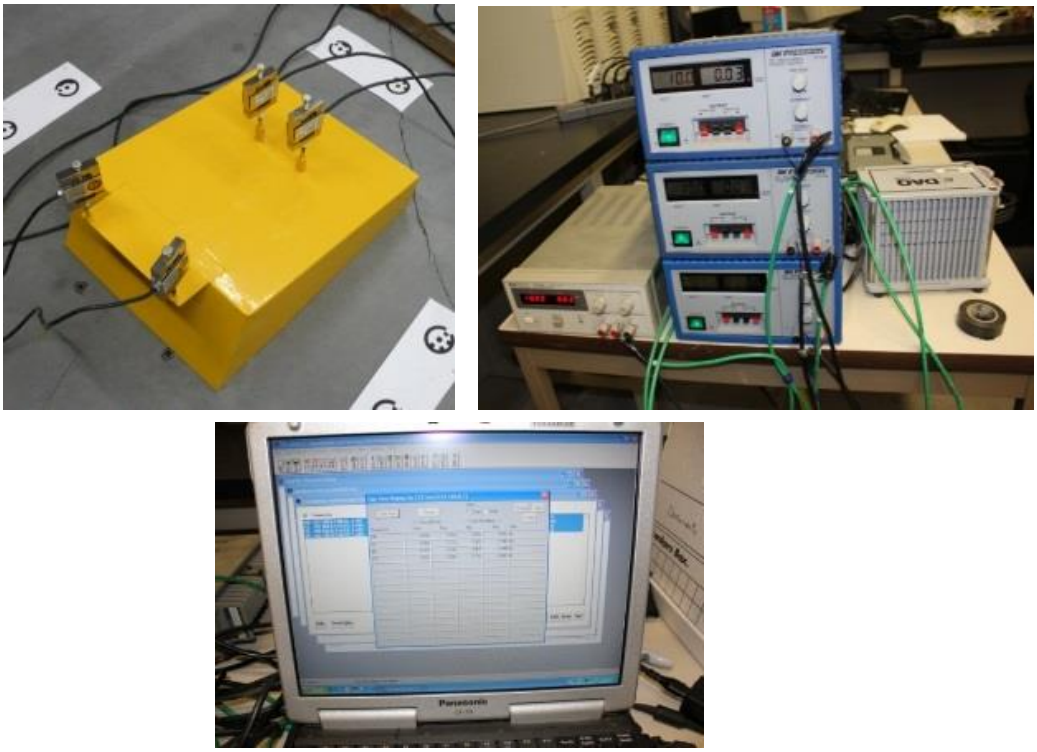

Figure 4.6 Load cell installation, power sources, eDaq software

4.2 Stiffness

Stiffness is defined to describe the force required to reach a certain deformation of a structure as shown in the expression 16.

"Stiffness" = "load" / "Deformation" [16]

Or stiffness of the material can be defined by the expression 17.

$$E = \frac{\sigma}{\varepsilon} \qquad [17]$$

Where the modulus of elasticity E (Young's modulus) represents the "material stiffness" and σ and ε are the stress and strain respectively. This is the Hooke's law of elasticity. A stiff material has a high Young's modulus and has a high resistance to elastic deformation under load. The unit for stiffness is the same as stress unit and it is N/m^2 or Pascal (Baumgart, 2000).

The stiffness of the steel plates used to build the scale model of the truck body is very high that the structure would experience very minimum deformation under the payload that is to be not higher than 25kg. Therefore, the stiffness of the model has little effect on the load cell readings which is insignificant.

4.3 Material types

Three types of material were used to progressively load the scale truck body. Oil sand and two type of unconsolidated soils that the Unified Soil Classification System (USCS) classifies as gravel and sand. The materials used in the test are shown in figure 4.10 in three piles and from left to right they are:

- Sand (≥ 50% of coarse fraction passing No.4 (4.75 mm) sieve, (USCS))
- Oil sand
- Gravel (> 50% of coarse fraction retained on No. 4 (4.75 mm) sieve, (USCS))

The gravel and limestone have similar particle size distributions. All material size distributions are shown in figures 4.7, 4.8 and 4.9.

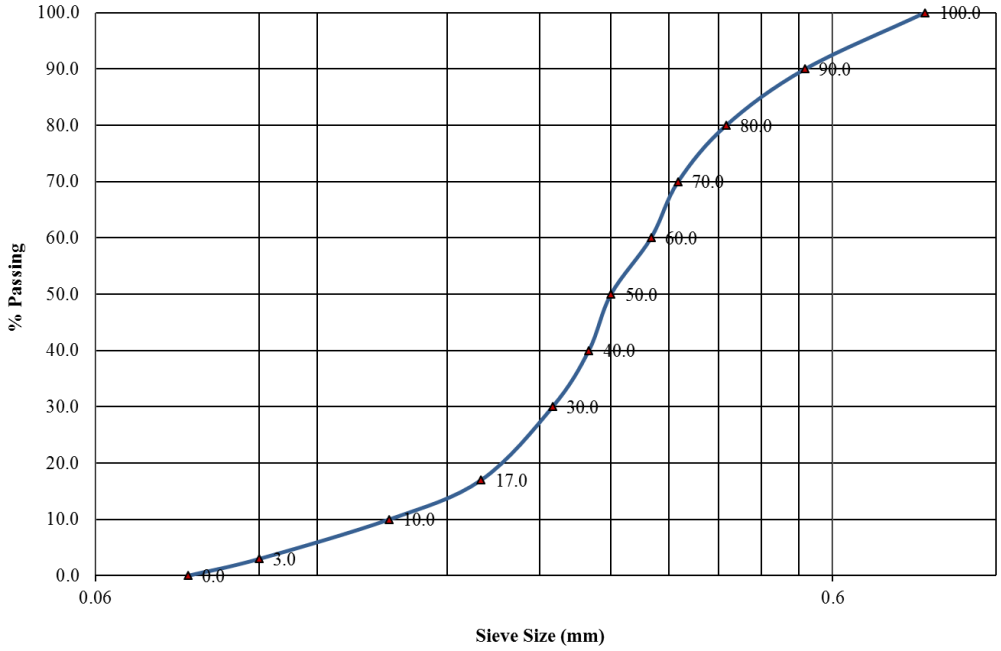

Figure 4.7 Susan Lake screened sand sieve analysis

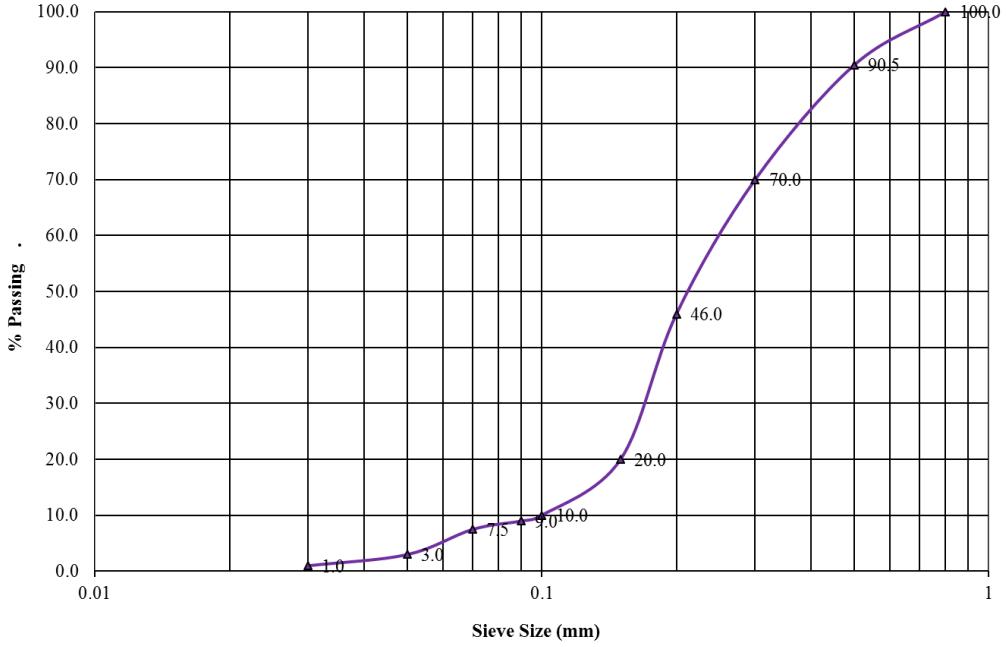

Figure 4.8 Oil sand sample sieve analysis

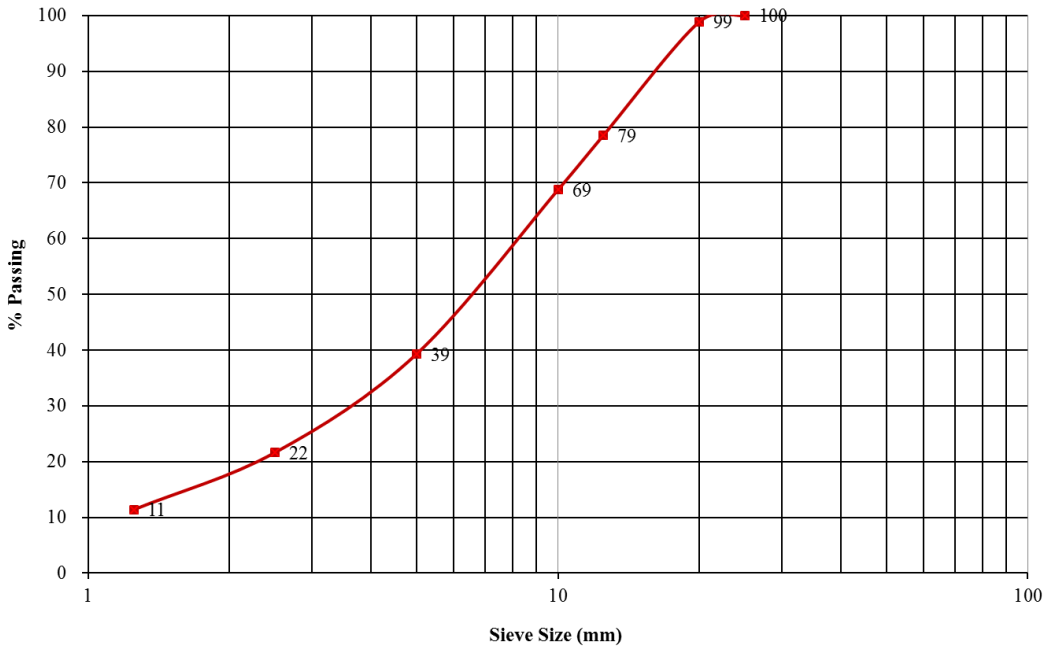

Figure 4.9 Limestone sample sieve analysis

To load the scale truck body, a scoop was used as shown in the figure 4.10 to simulate the field observed dump process. Water was also sprayed on the sand to suppress the dust and to increase the moisture for a more realistic representation of the material.

Figure 4.10 Loading tool (Left), Material types (Right)

4.4 PhotoModeller Scanner

Initially, photogrammetry software, Photomodeller Scanner, was acquired and used to create a point cloud of the payload using the PhotoModeller Dense Surface Modelling (DSM) technology in order to extract the measurements of the payload angle of repose, height, volume and shape.

A Panasonic digital camera was also used to take high resolution pictures to be used in modelling by Potomodeller. Before, the laboratory test was commenced, the camera had to be calibrated. A few target points were printed and placed on the ground and twelve pictures were taken from different angles. Figure 4.11 shows the final result of the calibration process.

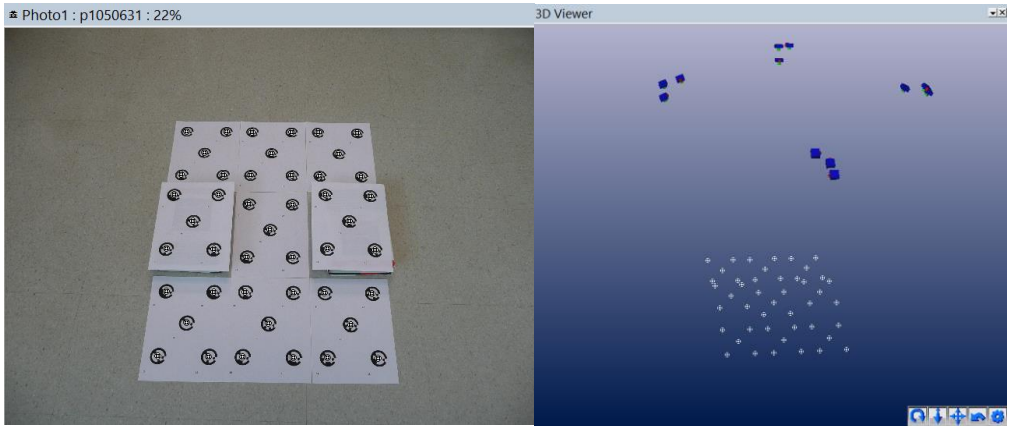

Figure 4.11 Digital Camera calibration in Photomodeller Scanner

In preparation for the laboratory test the same target points were placed around the scale truck body for the PhotoModeller to use them as the required reference points. After each scoop of material was placed in the scale truck body, five to six high resolution photos were taken from various angles to be imported into the Photomodeller Scanner to create a point cloud applying the DSM technique as shown in the figure 4.12.

However, after trying few set of pictures to simulate the payload shape the researcher realized that the models created in PhotoModeller are not accurate enough to be reliable sources for taking measurements. As a result, high

resolution pictures were taken and interpretation was performed in conjunction with the data acquired from the load cells.

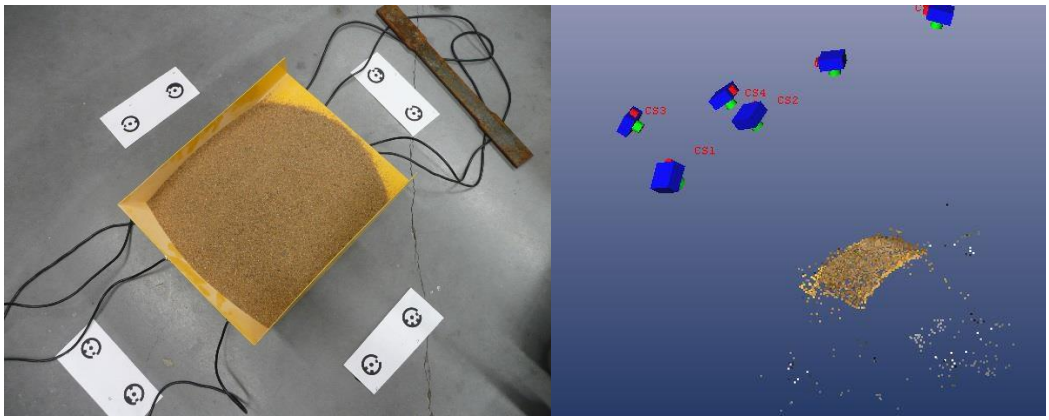

Figure 4.12 An example of the payload model created by PhotoModeller

High resolution pictures of the payload shape in the truck body were studied to better understand the shape of each shovel bucket load as well as the final payload in the scale truck body. For each material a constant angle of repose and cone shape per load pass and final truck payload were evaluated to simplify the problem for this thesis. The material piles placed on a flat floor are cone shaped with similar angles of repose for all three materials.

4.5 Density

It was assumed that the material placed in the truck body was homogeneous allowing the volume of the material to be calculated using a constant loose density determined for each material, and the weight of the material placed in the truck body from the load cell readings. As a result, the loose density of the materials were determined using a digital scale and a container of known volume, figure 4.13. Basically, an amount of material that was a good representative of the full load in the scale truck body was placed on the scale. The weight and volume of the soil were determined allowing a loose density to be calculated. Table 4.1 shows the loose density of the materials used in the test.

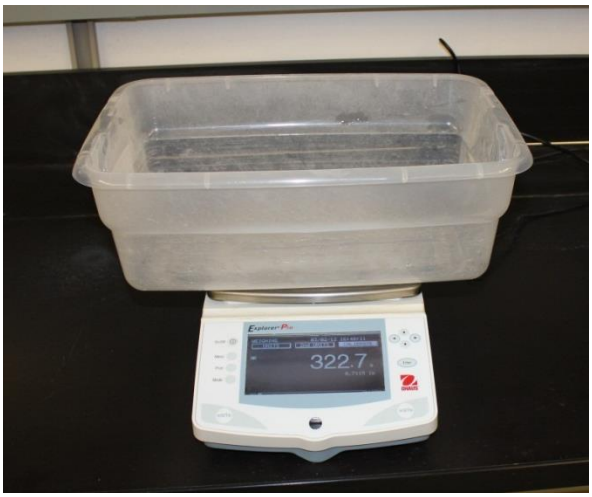

Figure 4.13 Digital scale and container

As shown in table 4.1, the density of sand is 1.9 t/m^3. The density of at face oil sand with approximately 10.5 percent bitumen content is 2.08 t/m^3.

Intact soil in its natural and original state is usually more compacted than when it is disturbed, and loose. As a result, the loose material will have a lower density than the at face material.

The density of the loose oil sand used in the laboratory test is much lower than the density of loose oil sand in the field generating scaling error. The reason is that a very small portion of oil sand is used to load a scale truck body; as a result, the weight of the particles in the pile is not high enough to cause re-compacting. In addition, since the oil sand used in the test was stored in an open container, it was somewhat dried out.

Table 4.1 Density of gravel, oil sand and sand

	Total weight (g)	Container (g)	Volume (l)	Density (kg/m^3)
Gravel	7568	323	4	1811
Oil sand	6040	323	5	1143
Sand	9808	323	5	1897

4.6 Calibration

Calibration was conducted in two parts; firstly to calibrate the load cells and the scale truck body prior to the test, and secondly to calibrate the load cell readings for the tare balance state of the scale model.

4.6.1 Calibration of load cells and the scale truck body

First, before running each loading sequence a hand held level was used to assure that the angle of the inclined floor planes are set at 12º and 65º and also the truck body is level across before each loading sequence was commenced as shown in figure 4.14.

Figure 4.14 Cansel hand held level

Secondly, all four load cell readings were calibrated to zero. As a result, the tare weight of the scale truck body and the load cells were eliminated. The resulting load cell readings then represented the payload in the truck body.

4.6.2 Calibration of the load cell readings

Calibrating the data and interpretation after the test was also critical. Since the load cell readings were set to zero before each test run and the tare weight of the scale truck was eliminated, the load cell readings need to be calibrated to reflect the total suspended weight on the struts (cells). According to the Caterpillar specification sheet for 797B truck, the GVW of Cat 797B truck is about 620 tonnes, of which, approximately 515 tonnes is the suspended weight on

the struts. If the payload is 365 tonnes then 150 tonnes is the weight of the frame, truck body and other components above the struts. However, in the laboratory the tare weight is eliminated before each loading sequence; therefore, the load cell readings need to be calibrated to reflect the total suspended load on the struts.

As shown in table 4.2, the load distribution on the front and rear axles are 43.5% and 56.5% respectively when the truck is empty. As a result, the payload weight needs to apply 36.6% to the front axle and 63.4% to the rear axle to create a final load distribution of 33.3% and 66.7% on the front and rear axles respectively. As a result, when the load cell readings were scaled up, 65 tonnes were added to the front axle and 85 tonnes to the rear axle to calibrate the readings to reflect the tare weight of the truck.

Table 4.2 load distribution chart

	Load Distribution		
	Empty	Loaded	Payload
Front	43.5%	33.3%	36.6%
Rear	56.5%	66.7%	63.4%

Although all the measurements were taken as accurate as possible to build the scale truck body, some scaling error needed to be addressed. For instance, the load cells position in the scale truck body were not exactly at 1:25 scale of the struts positions in the full scale 797B truck body. This was addressed by an offset in the data treatment to assure the tare balance was achieved in prior to test loading.

After the scale truck was fully loaded and balanced visually, the load cell forces were collected. The calibration constants were calculated so that the 36.6 to 63.4 percent nominal payload distribution was achieved on the front and rear axles respectively as suggested by the Caterpillar 797B specification sheet (Caterpillar, 2010).

Table 4.3 shows the five samples of the load cell reading of fully loaded scale truck used to generate the calibration factor for the front and rear load cell readings.

Table 4.3 load cell reading calibration

Calibration								
Date	Sample	Axles	Readings	Percentage	Difference	Axles	Average	C factor in %
Feb-02	1	Front	12.1	43.1	-6.5			
	1	Rear	15.9	56.9	6.5			
	2	Front	12.3	41.9	-5.3			
	2	Rear	17.0	58.1	5.3			
	3	Front	14.3	44.6	-8.0	Front	-5.8	94.2
	3	Rear	17.8	55.4	8.0	Rear	5.8	105.8
	4	Front	16.3	40.0	-3.3			
	4	Rear	24.5	60.0	3.3			
	5	Front	15.7	42.7	-6.1			
	5	Rear	21.0	57.3	6.1			

4.7 Analyzing the laboratory data

Table 4.4 illustrates a sample of the laboratory data collected from the load cells and analyzed. Load cell readings were recorded and calibrated, the truck KPIs were calculated and the data were scaled up to be comparable with the field data. And finally, scaled up truck KPIs were calculated and plotted.

Table 4.4 Laboratory data sample

		Raw Data (lbs)				Calibrated				KPIs			Load Distribution (Percentage)					Scale Up (tonne)				KPIs		
Date	Pass	LF	RF	LR	RR	LF	RF	LR	RR	Rack	Roll	Pitch	LF	RF	LR	RR	R Axle	LF	RF	LR	RR	Rack	Roll	Pitch
02-Feb-12	1	1.02	1.29	0.73	1.41	0.96	1.22	0.77	1.49	-0.47	-0.97	-0.09	21.6	27.4	17.4	33.6	49.0	39.32	41.13	47.99	53.10	3.30	-6.92	-20.63
02-Feb-12	2	1.21	3.21	1.04	3.58	1.14	3.02	1.10	3.79	-0.80	-4.57	-0.72	12.6	33.4	12.2	41.8	46.0	40.60	53.98	50.31	69.40	5.71	-32.47	-25.14
02-Feb-12	3	1.62	4.62	1.69	5.62	1.53	4.35	1.79	5.95	-1.33	-6.98	-1.86	11.2	32.0	13.1	43.7	43.2	43.34	63.41	55.20	84.73	9.46	-49.60	-33.18
02-Feb-12	4	2.48	5.19	3.26	7.03	2.34	4.89	3.45	7.44	-1.44	-6.54	-3.66	12.9	27.0	19.0	41.1	39.9	49.09	67.22	67.00	95.32	10.20	-46.46	-46.01
02-Feb-12	5	3.69	6.5	4.54	8.46	3.48	6.12	4.80	8.95	-1.50	-6.79	-4.16	14.9	26.2	20.6	38.3	41.1	57.19	75.99	76.61	106.07	10.66	-48.26	-49.51
02-Feb-12	6	5.87	6.2	7.47	8.46	5.53	5.84	7.90	8.95	-0.74	-1.36	-5.48	19.6	20.7	28.0	31.7	40.3	71.77	73.98	98.63	106.07	5.23	-9.65	-58.95
03-Feb-12	1	1.49	0.5	1.92	0.76	1.40	0.47	2.03	0.80	0.29	2.16	-0.96	29.8	10.0	43.1	17.1	39.8	60.2	42.47	35.85	56.93	48.21	-2.09	15.34	-26.82
03-Feb-12	2	2.16	2.03	3.02	2.41	2.03	1.91	3.20	2.55	0.52	0.77	-1.80	21.0	19.7	33.0	26.3	40.7	59.3	46.95	46.08	65.19	60.61	-3.71	5.45	-32.77
03-Feb-12	3	3.48	3	4.42	3.88	3.28	2.83	4.68	4.11	0.12	1.02	-2.68	22.0	19.0	31.4	27.6	41.0	59.0	55.78	52.57	75.71	71.66	-0.85	7.27	-39.01
03-Feb-12	4	4.35	4.17	5.75	5.58	4.10	3.93	6.08	5.90	0.01	0.35	-3.96	20.5	19.6	30.4	29.5	40.1	59.9	61.60	60.40	85.71	84.43	-0.07	2.48	-48.13
03-Feb-12	5	5.06	5.5	6.85	7.67	4.77	5.18	7.25	8.11	-0.45	-1.28	-5.41	18.8	20.5	28.6	32.1	39.3	60.7	66.35	69.30	93.97	100.13	3.22	-9.11	-58.46
03-Feb-12	6	6.03	6.22	8.14	8.84	5.68	5.86	8.61	9.35	-0.56	-0.92	-6.43	19.3	19.9	29.2	31.7	39.1	60.9	72.84	74.11	103.67	108.93	3.99	-6.53	-65.63
03-Feb-12	1	0.86	1.61	1.4	3.73	0.81	1.52	1.48	3.95	-1.76	-3.17	-3.10	10.4	19.6	19.1	50.9	30.0	70.0	38.25	43.27	53.02	70.53	12.49	-22.53	-42.02
03-Feb-12	2	2.3	4.44	2.68	6.31	2.17	4.18	2.84	6.68	-1.82	-5.86	-3.16	13.7	26.4	17.9	42.1	40.0	60.0	47.89	62.21	62.64	89.91	12.96	-41.59	-42.46
03-Feb-12	3	6.03	4.63	6.84	6.37	5.68	4.36	7.24	6.74	-0.82	1.82	-3.93	23.7	18.2	30.1	28.1	41.8	58.2	72.84	63.48	93.90	90.37	5.83	12.90	-47.94
03-Feb-12	4	7.54	6.79	8.98	8.82	7.10	6.40	9.50	9.33	-0.54	0.88	-5.33	22.0	19.8	29.4	28.9	41.8	58.2	82.95	77.93	109.98	108.78	3.82	6.22	-57.88
06-Feb-12	1	0.33	5.07	-0.16	3.59	0.31	4.78	-0.17	3.80	0.50	-8.43	1.46	3.6	54.8	-1.9	43.6	58.4	41.6	34.71	66.42	41.30	69.48	-3.53	-59.89	-9.65
06-Feb-12	2	2.56	4.36	7.34	3.06	2.41	4.11	7.77	3.24	6.22	2.83	-4.48	13.8	23.4	44.3	18.5	37.2	62.8	49.63	61.67	97.65	65.49	-44.20	20.12	-51.85
06-Feb-12	3	7.2	4.74	9.88	3.65	6.78	4.47	10.45	3.86	4.27	8.91	-3.07	26.5	17.5	40.9	15.1	44.0	56.0	80.67	64.21	116.74	69.93	-30.36	63.27	-41.78
06-Feb-12	4	6.13	6.4	8.44	11.8	5.77	6.03	8.93	12.48	-3.30	-3.81	-9.61	17.4	18.1	26.9	37.6	35.5	64.5	73.51	75.32	105.92	131.17	23.44	-27.05	-88.26
06-Feb-12	5	7.9	8.38	11.02	13.45	7.44	7.89	11.66	14.23	-2.12	-3.02	-10.55	18.1	19.1	28.3	34.5	37.2	62.8	85.35	88.57	125.31	143.57	15.05	-21.47	-94.95
06-Feb-12	1	1.44	1.85	2.17	2.88	1.36	1.74	2.30	3.05	-0.36	-1.14	-2.24	16.1	20.6	27.2	36.1	36.7	63.3	42.13	44.88	58.81	64.14	2.59	-8.08	-35.94
06-Feb-12	2	2.89	3.83	4.35	5.56	2.72	3.61	4.60	5.88	-0.39	-2.17	-4.15	16.2	21.5	27.4	35.0	37.6	62.4	51.84	58.12	75.19	84.28	2.80	-15.38	-49.51
06-Feb-12	3	5.2	4.94	7.65	7.13	4.90	4.65	8.09	7.54	0.31	0.80	-6.09	19.4	18.5	32.1	29.9	37.9	62.1	67.29	65.55	99.98	96.08	-2.17	5.65	-63.22
06-Feb-12	4	7.25	7.73	8.87	9.08	6.83	7.28	9.38	9.61	0.23	-0.67	-4.88	20.6	22.0	28.3	29.0	42.6	57.4	81.00	84.22	109.15	110.73	-1.63	-4.79	-54.66
06-Feb-12	5	7.68	7.98	10.43	10.59	7.23	7.52	11.03	11.20	0.11	-0.45	-7.49	19.6	20.3	29.8	30.3	39.9	60.1	83.88	85.89	120.87	122.08	-0.80	-3.21	-73.18

4.8 Loading the scale truck body

The test was conducted for all three material types. The scale truck body was progressively loaded with the scoop with the required number of passes. After each load pass pictures were taken from different angles and the load cell readings recorded.

During each round of testing, the shovel bucket loads were placed in different regions of the truck body to understand how the shovel cone shape loads intersect in order to shape the final truck payload.

4.8.1 Sand

As shown in figure 4.15, five load passes of sand were placed into the scale truck body. The sand small grain size made it ideal for the lab test since the other materials had larger grain size and they did not flow uniformly in a small scale load setting. The shape of each load pass clearly demonstrated the truncated cone shape discussed in next chapter.

As shown in table 4.4, the load cell readings were collected and after applying the calibration constant, the rack, roll and pitch values were calculated to study the relationship between the shovel bucket load locations in the scale truck body and the truck KPIs.

Even though the first load was placed in the corner of the scale truck body, the overall balance of the final payload was achieved placing the other loads in appropriate locations. It proves that a balance final payload can be achieved even after not properly placing few bucket loads in the truck body.

The first three loads were simulated using the Matlab program and interestingly Matlab also predicted load shapes very close to the actual ones shown in figure 4.15. It confirmed that the algorithm works well and has the capability of predicting the load shapes and how they interact with each other.

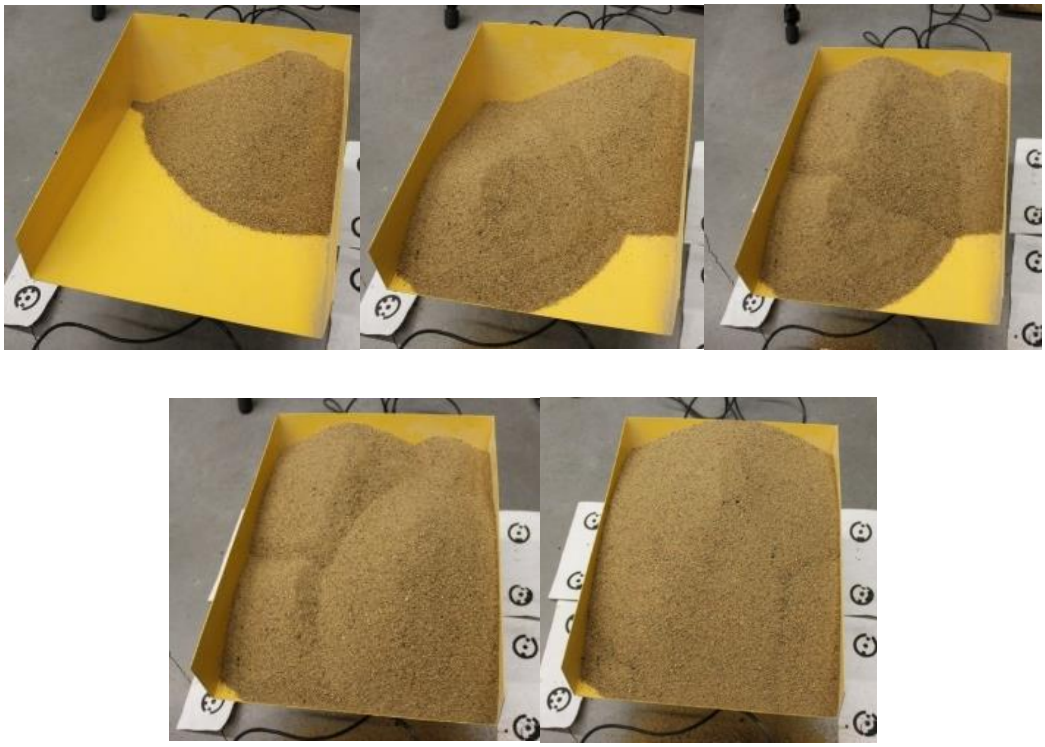

Figure 4.15 Five pass loaded scale truck body with sand

The calibrated load cell readings were used to generate the cumulative individual load cell forces and the front and rear axle load distributions which are plotted in figure 4.16.

As the first load was placed in the front right corner of the scale truck body illustrated in figure 4.15 and reflected in figure 4.16, the rear left cell was slightly lifted from the floor seen as a negative value in figure 4.16 with the first load pass because the scale truck body does not have other truck components attached to it; however, after the load cell readings were calibrated and scaled up to reflect the tare weight of the truck, there were not any negative values.

Figure 4.15 shows that the left rear corner of the scale truck body was not completely covered with sand. However, the right rear corner was covered, which confirms the load cell readings. As a result, higher roll and pitch events would be expected since the final payload was skewed to the right rear portion of the truck body.

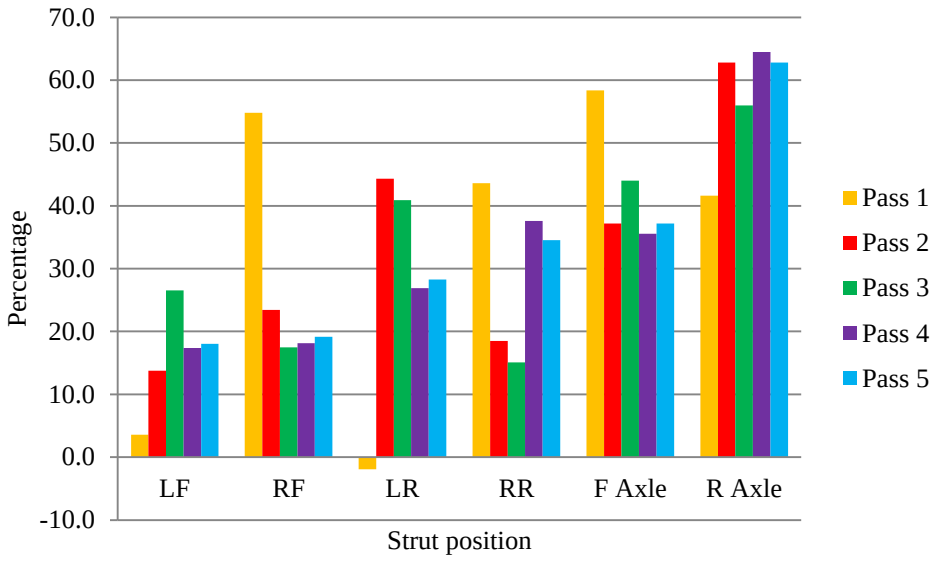

Figure 4.16 Strut load distribution for sand test

After the 5th shovel load pass, 63 percent of the load was distributed to the rear axle and 37 percent to the front axle. This ratio is very close to the calculated preferred 63.4 to 36.6 percent for the payload; however, the right rear cell showed a higher force than the left rear as shown in figure 4.16.

The load cell readings were scaled up to represent the real truck strut readings using equation 18. The cube-root law of scaling was applicable here. There may be a minor scaling error in the density of the material since the physical properties of the material in the field in a large scale are slightly different from those in the laboratory.

$$Field\ Payload = \left[\left(\sqrt[3]{Scale\ Payload}\right) \times 25\right]^3$$

or $$Field\ Payload = Scale\ Payload \times 25^3 \quad [18]$$

In addition, the load cell force unit (lbs) was converted to metric tonnes. The scaled up strut readings were plotted shown in figure 4.17. The total scaled-up payload is under 300 tonnes due to the density difference between the material

used in the laboratory and the field and also that the scale truck body was not fully loaded.

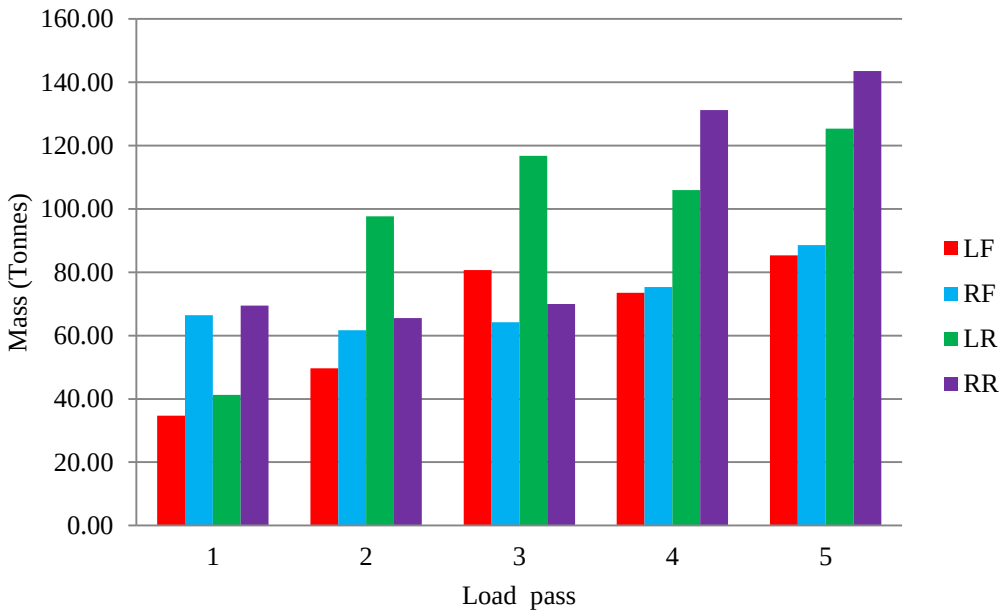

Figure 4.17 Scaled-up strut mass for sand test

The scaled up right rear value after the final load was slightly higher than the right rear that is clearly shown in the picture of the loads.

Comparing the individual strut loads after the scale truck body was fully loaded, it was noticeable that the left and right rear load cell readings were not equal as well as the right and left front load cell readings which would impose high rack and roll values. The rack and roll values will be worse when the truck is in motion.

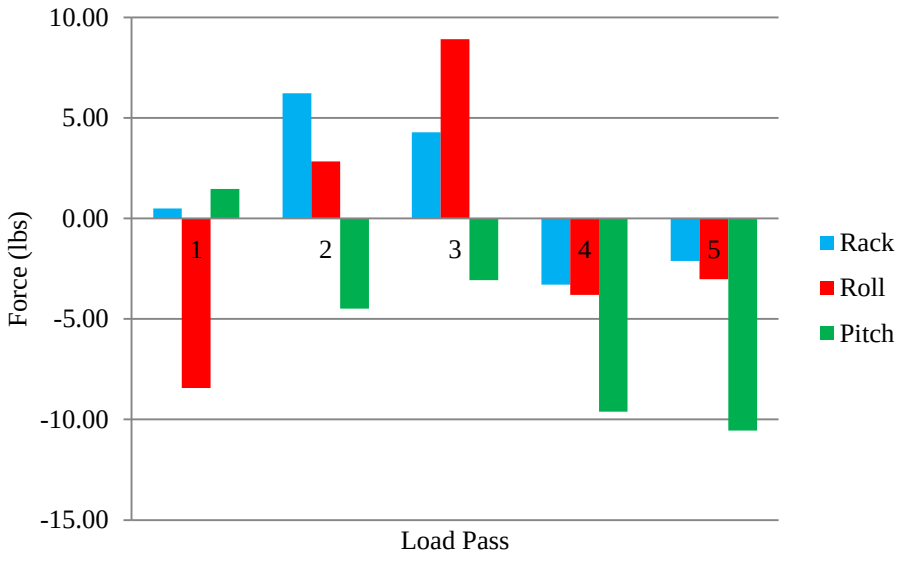

Figure 4.18 Rack, roll and pitch for sand test

The front and rear axle load distribution ratio in the scaled up values was very close to the manufacturer specification of 66.7 to 33.3 percent. As a result, the pitch values shown in figure 4.19 were within the acceptable range (-1/3 of the payload + tare weight). The roll values changed from negative to positive to negative due to the bucket load passes being placed in each corner of the truck body. The final payload was favoring the right rear corner of the truck body. As a result, the rack and roll values did not reach zero.

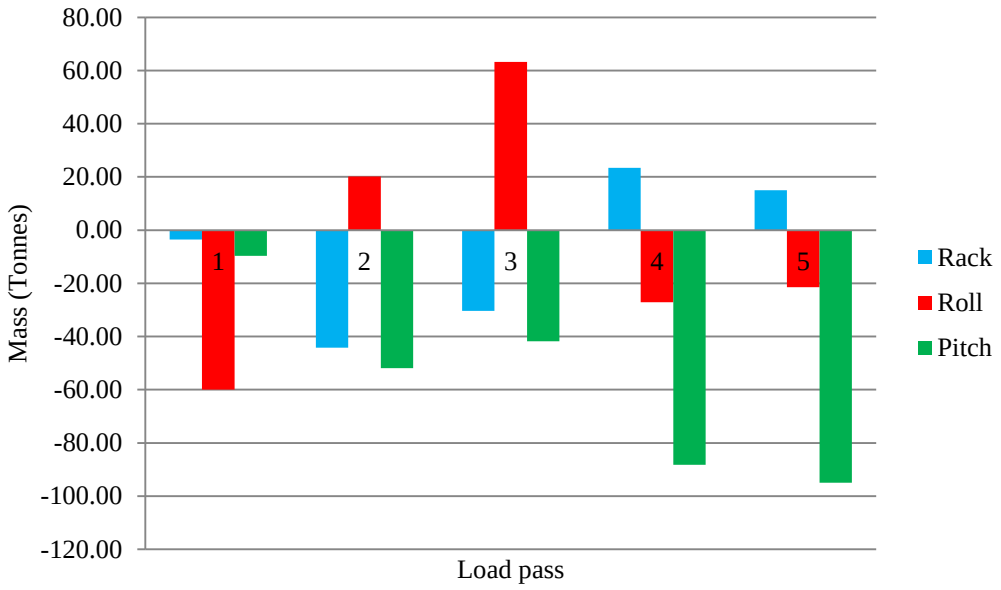

Figure 4.19 Scaled-up rack, roll and pitch for sand test

4.8.2 Gravel

Here, gravel was targeted as the loading material to load the scale truck. As shown in figure 4.20, the first and second shovel bucket loads were placed slightly to the right and back of the truck body. The third and fourth loads were placed to the left of the center line and front of the scale truck body to balance the final payload.

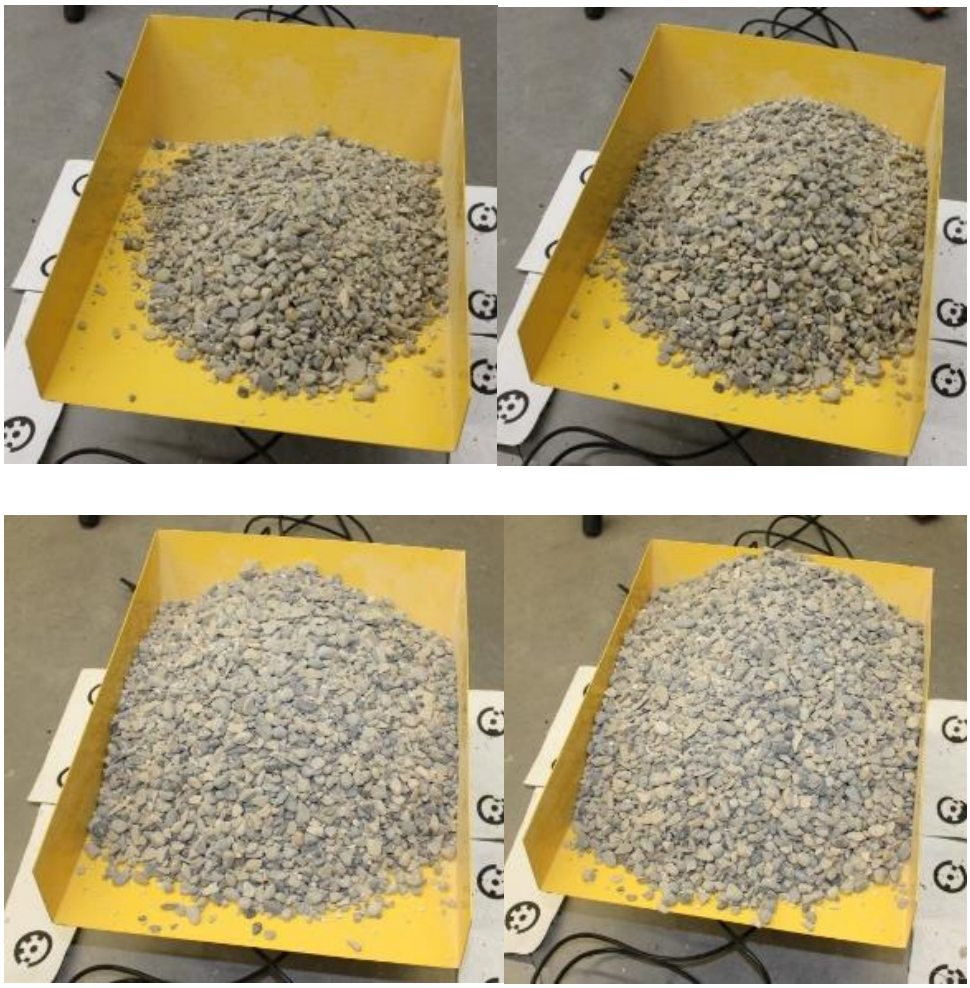

Figure 4.20 Loaded scale truck body with gravel

The load cell readings, figure 4.21, also show that the first and second bucket loads were placed in the right and rear corner of the scale truck body. The third and fourth loads were placed in the other corners to balance the final payload. However, the front and rear axle load distribution percentiles were different from the preferred payload distribution of 36.6% to 63.4% to achieve the manufacturer specification of 33 to 67 percent after applying the tare weight of the truck.

This showed that if the shovel bucket loads were not placed in the accurate location from the very first load passes, it became very difficult to correct and achieve a perfect final payload balance at the end. Not only that but also the load

cell readings clearly reflected the payload location on the truck body. It was nearly impossible to achieve a perfect payload balance through visual placement of shovel bucket loads in a truck body.

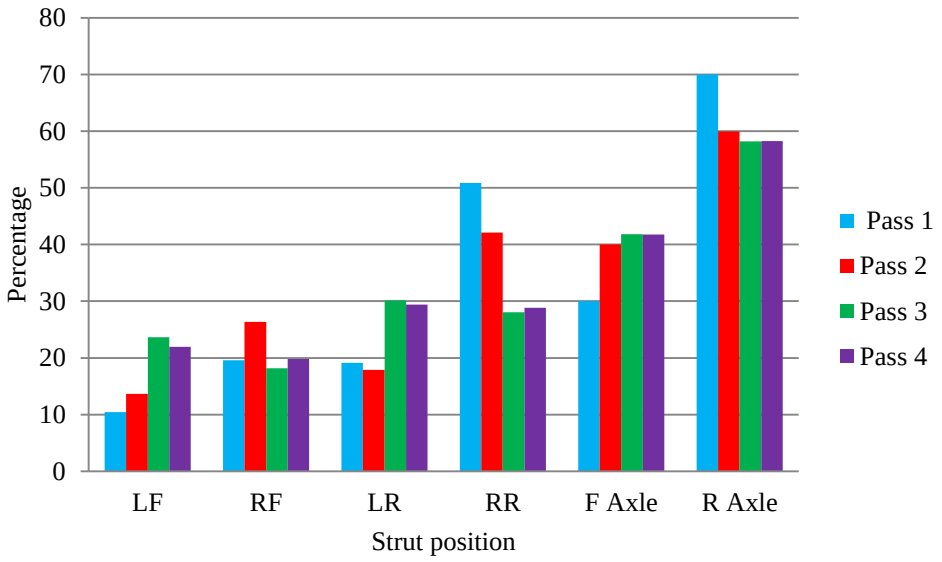

Figure 4.21 Strut load distribution for gravel test

The adverse effects of an unbalanced payload were clearly visible in the truck KPIs shown in figure 4.22. The high rack and roll values for the final payload magnified the significance of the unbalanced payload. These values would increase when the truck is in motion because of the non-uniformity of road surfaces in the mining industry. The pitch value was also smaller than expected which showed that more stresses were transferred to the front struts which would magnify when a loaded truck descends a slope.

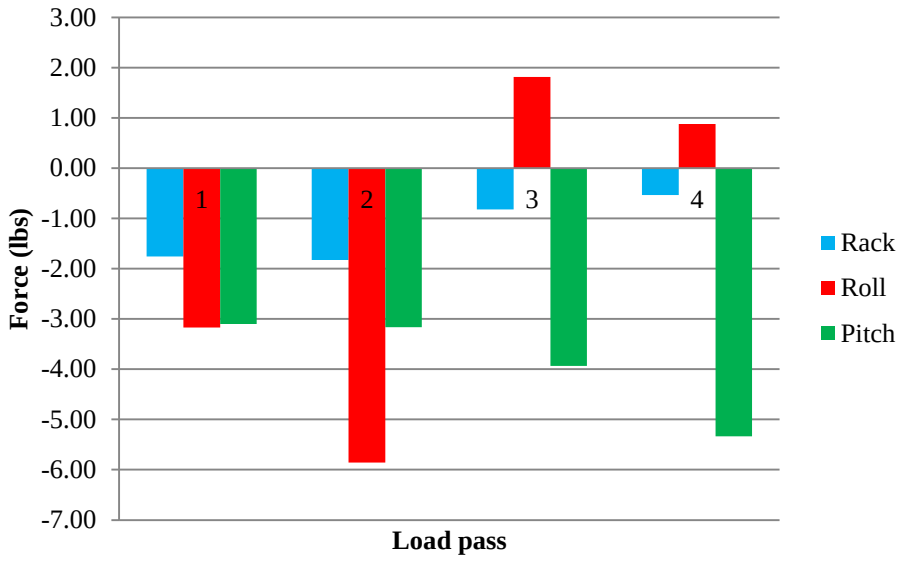

Figure 4.22 Rack, roll and pitch for gravel test

Figure 4.23 illustrates the scaled up strut masses after each bucket load pass. The final payload seemed to be evenly distributed across the truck body. However, the OEMs recommended front and rear axle load distribution was not achieved.

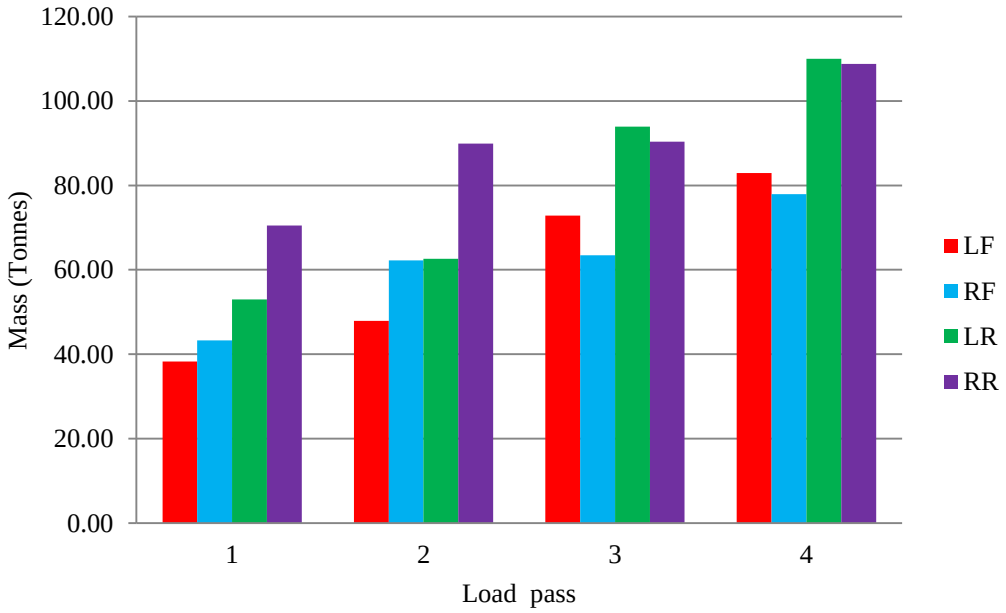

Figure 4.23 Scaled-up strut mass for gravel test

Figure 4.24 illustrates the scaled up rack, roll and pitch values after each bucket load. The rack values are changed from negative to positive values after scaling up the load cell readings and adding the tare weight of the truck.

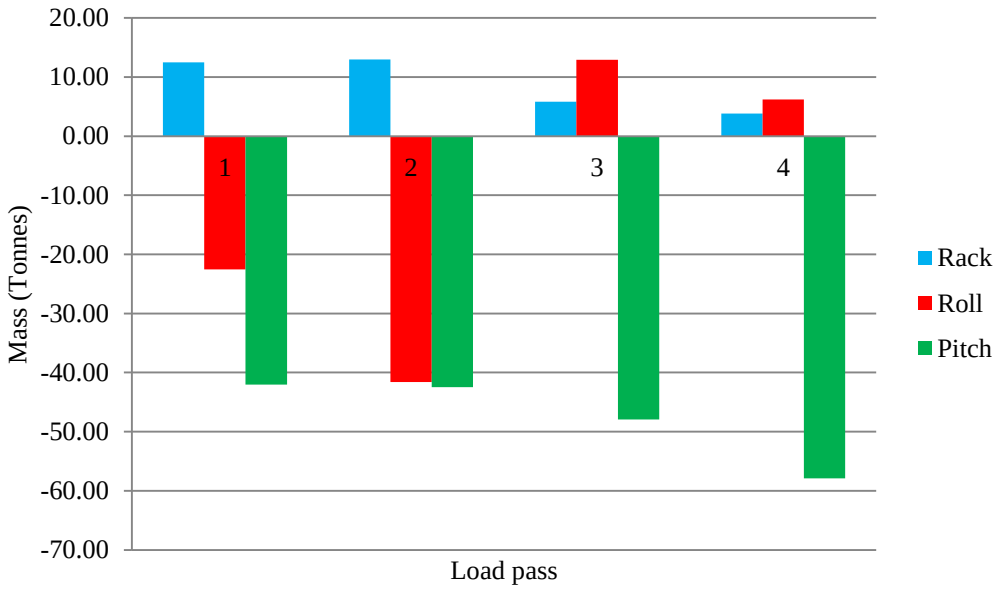

Figure 4.24 Scaled-up rack, roll and pitch for gravel

4.8.3 Oil sand

As field tests were conducted in an oil sand mine, oil sand was used to conduct the field target set of tests in the laboratory. Because of the small scale equipment and also that the oil sand used in the test were disturbed, bigger lumps were observed in the piles and the overall density of the oil sand dropped. As a result, the truck body was completely loaded after six shovel bucket passes.

Studying figure 4.25, it can be seen that the first load was slightly to the left; however, after that it became difficult to really say whether the other loads were placed in the appropriate locations or not without referring to the load cell readings.

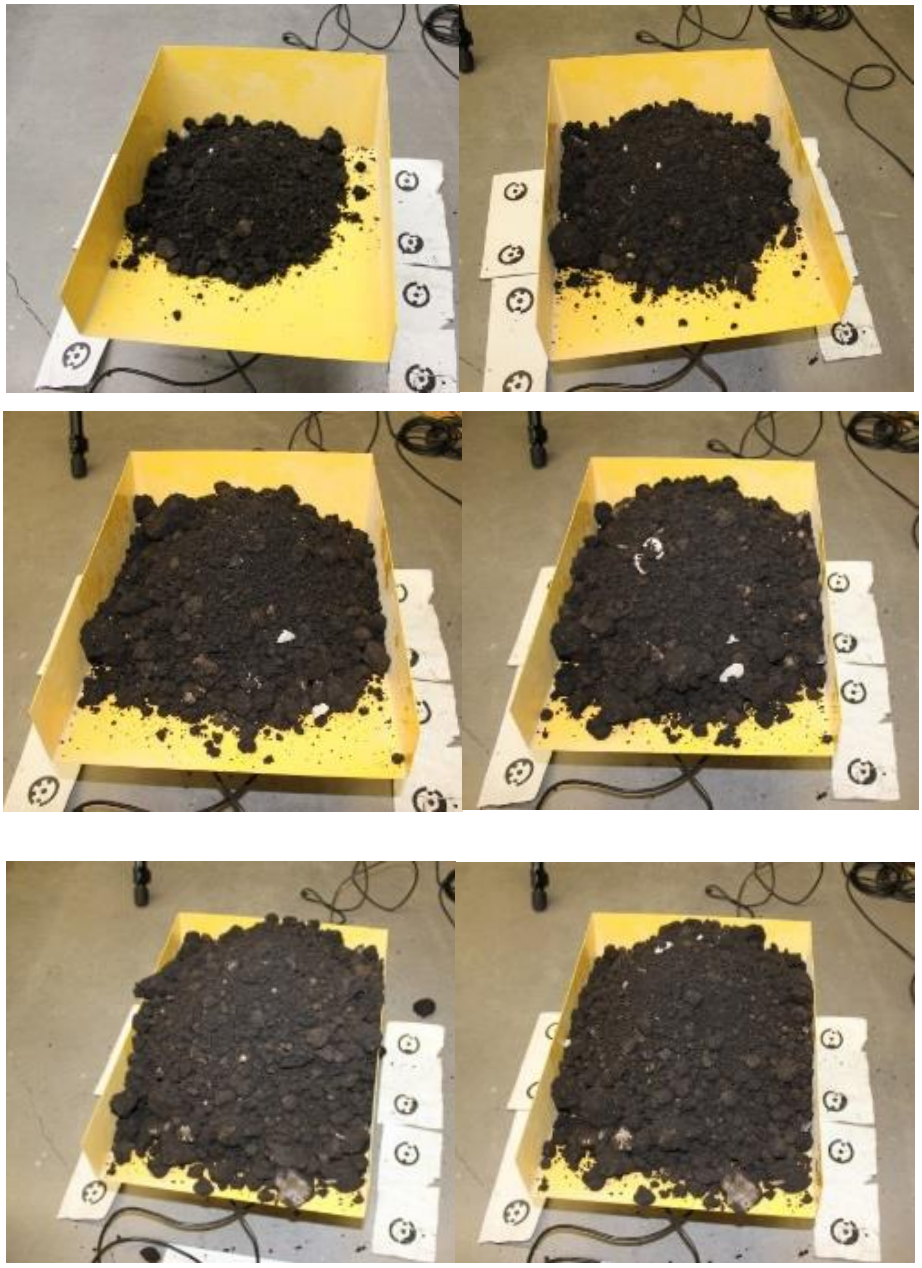

Figure 4.25 Loaded scale truck body with oil sand

Figure 4.26 shows the load cell readings during the test. The readings were studied to understand what has happened during the test. For example, if the front right and left strut readings correspond with the payload pictures, it can be determined that since the first load pass was placed slightly to the left of the center line, the other loads were slightly placed on the right side to offset the first load but it seems that it was overshot and the final payload was slightly on the

right side of the centerline that will pose high roll values. The final front and rear axles load distribution is 39 to 61 percent.

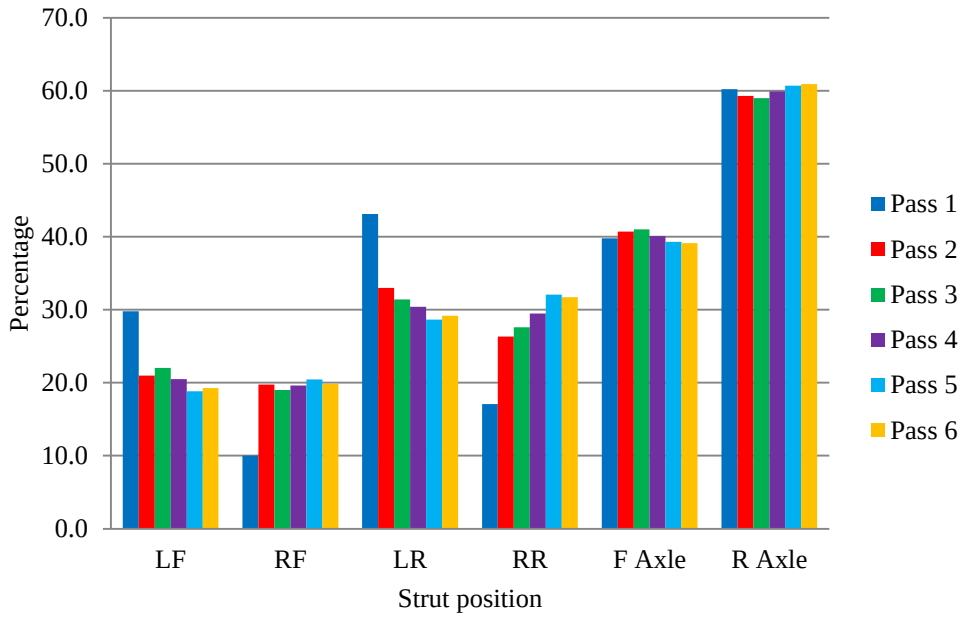

Figure 4.26 Strut load distribution for oil sand test

Investigating the final payload visually, it seems that the load is perfectly balanced; however, the truck KPIs shown in figure 4.27 do not agree with this observation. The rack and roll values are higher than zero and not only that but the pitch value is lower than the preferred value.

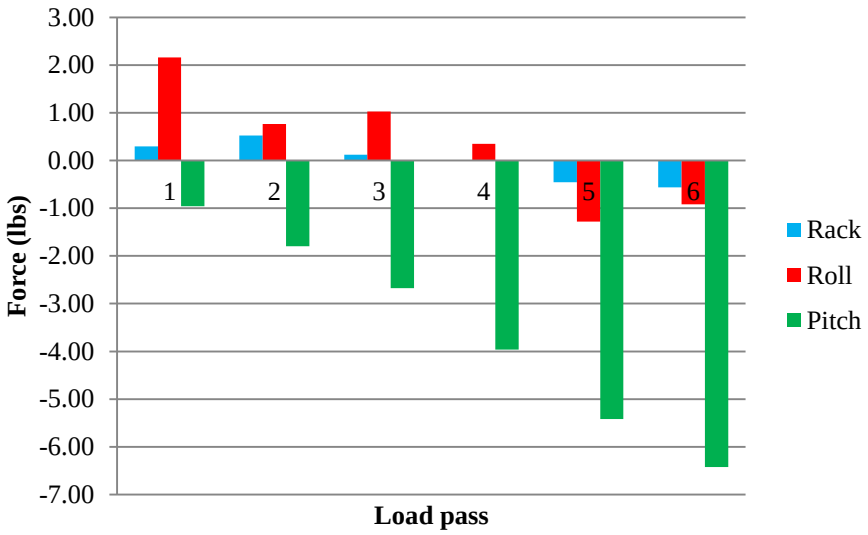

Figure 4.27 Rack, roll and pitch for oil sand test

The load cell readings were scaled up to represent the field scale readings shown in figure 4.28. After the sixth shovel load pass, more than 100 tonnes was applied on the rear struts and just under 80 tonnes on the front struts indicating that the preferred 67 to 33 percent load distribution on the rear and front axles was not achieved. As a result, high pitch values should be expected.

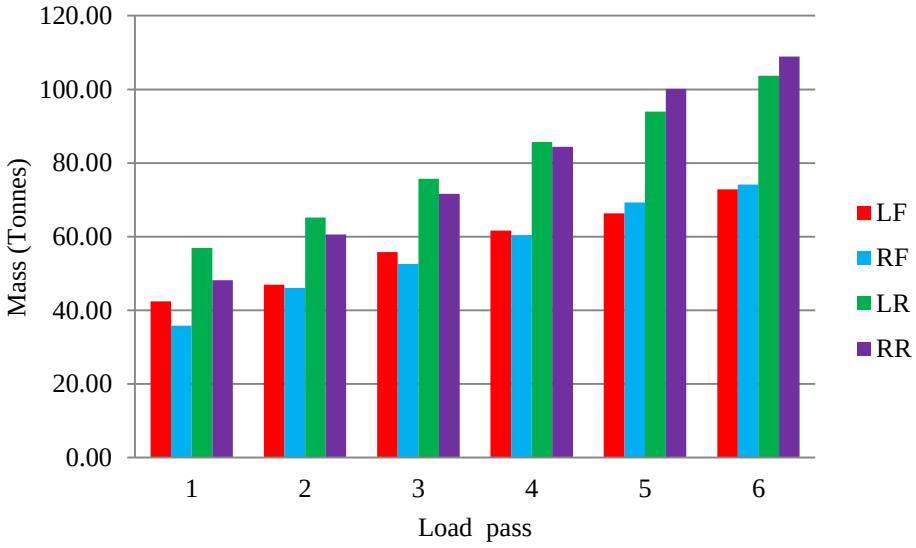

Figure 4.28 Scaled-up strut mass for oil sand test

Figure 4.29 shows the scaled up truck KPIs. The pitch values are significantly lower than one third of the tare weight showing that the load distribution on the front and rear axles are not close to the manufacture recommended 33 to 67 percent respectively.

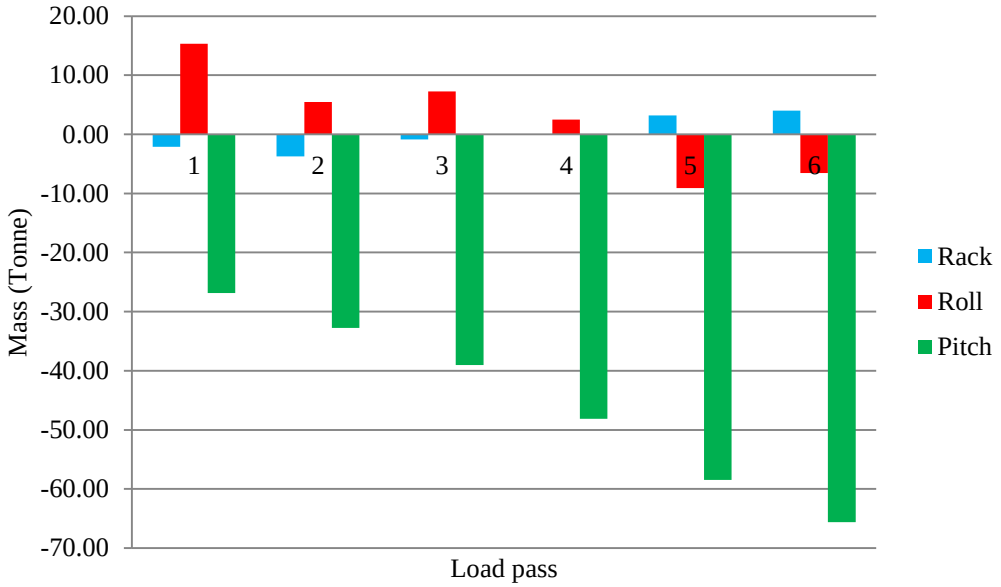

Figure 4.29 Scaled-up rack, roll and pitch for oil sand test

4.9 Conclusions

After conducting this laboratory test the following were concluded:

a. Conical shapes are generated with successive shovel bucket loads in the scale truck body and also in the final payload.
b. All three material types behave almost the same during the loading sequence with cones interacting and revealing individual angle of repose.
c. Load cell readings clearly reflect the shovel bucket load location within the truck body.
d. If the first bucket loads are not placed in the appropriate location, it became very difficult to correct and achieve a final payload balance in the last one or two bucket loads.

e. It was very difficult to visually locate the shovel bucket load in the truck body to achieve a final payload balance, even though much greater visibility is present in the laboratory setting than the field setting.
f. A slight shift in payload location within the truck body has a huge adverse effect on truck KPIs.

5. Mathematical and numerical models

In this chapter the mathematical theory of the conical shape of the placed material and their interactions with one another and also the numerical analysis to develop a truck payload balance algorithm will be discussed.

5.1 Mathematical theory

The haul truck payload profile varies with shovel load placement practices and the material angle of repose. It is ideally a cone that the three truck body side walls and floors cut through; however, the payload conical shape can vary due to heterogeneity of the loaded materials, the location of the truck with respect to the shovel location and also the pit floor profile on which the truck is sit.

Any types of soil that are free dumped from a static discharge point shape cones with constant side slopes that is the angle of repose of the material. Piles of loose material were placed adjacent to each other as shown in figure 3.1 in the laboratory. Each pile remained in a cone shape since the loose material has a relatively constant angle of repose. Each time the same mass of material was placed on the ground, it shaped an identical cone; however, when they came to contact with each other they behaved differently. The angle of repose still stayed the same and the mass of the material piles did not change; however, since they intersected with each other, the intersection volume of the two cones were added to the second cone volume to shape a larger volume.

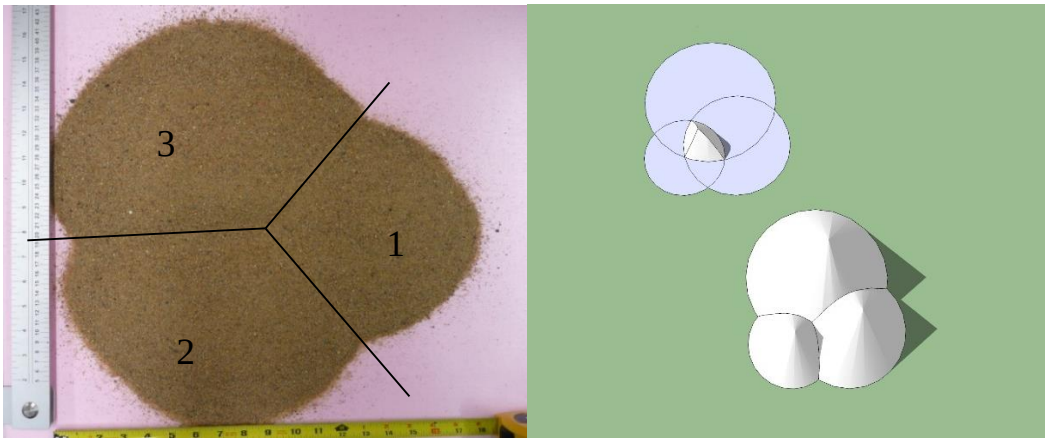

Figure 5.1 Three piles of sand interacting with one another on the left and three cones interaction analyses on the right

Since the material mass is known as well as the angle of repose, the height of the cone and consequently the base of the second cone can be determined if the common volume of the cones is determined.

In a two cone interaction with known masses, the volume of the second cone is given by the following expression.

Cone 2 volume (V_2) = Cone 1 volume (V_1) + Volume of the Cone 1 and 2 intersection (V_3) [19]

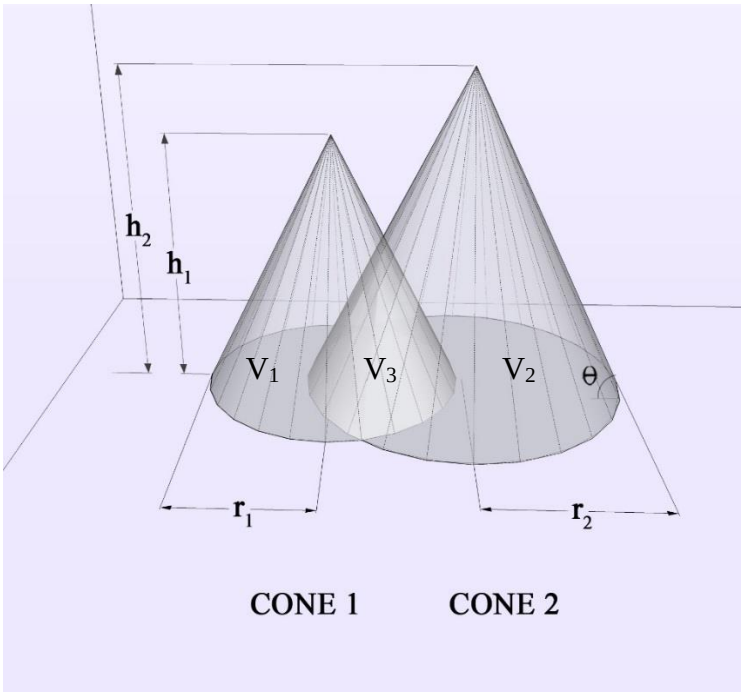

Figure 5.2 Two intersecting cones

Since the angle of repose and density of the loose material are generally known, the height of the first cone "h_1" can be determined as well as the radius "r_1" of the first cone. As a result, the volume of the cone can be determined by equations 19 and 20.

The volume of the second cone can also be calculated using the same method if the cone does not come in contact with the first cone. However, if the second cone intersects with the first cone, the common volume of the cones has to be added to the volume of the first cone to calculate the volume of the second.

$$\frac{1}{3}\pi {r_2}^2 h_2 = \frac{1}{3}\pi {r_1}^2 h_1 + V_3 \qquad [20]$$

Where $h_1 = r_1 \tan\theta \; and \; h_2 = r_2 \tan\theta$.

In reality, the cones interact not only with one another but also with the truck body. This makes the calculation more complex.

The chosen concepts were used to develop a numerical method using Matlab to calculate the cone intersection volumes that leads to reconstructing the cumulative shape of the shovel load passes within the truck body. If each shovel load pass creates a truncated cone shape in the truck body, since the angle of repose of the material is relatively constant and the shovel bucket capacity is known, the shape of the load pass can be reconstructed.

The location of the cone within the truck body can also be identified using the strut forces. Also, the location of the strut with respect to the truck body is constant therefore the center of the gravity of the cone created by the first shovel load pass can be located and the cumulative weight of the shovel load passes can be determined. Then the Matlab algorithm, predicts the second load pass location within the truck body to shift the center of the gravity of the payload to the predefined ideal location to achieve the manufacturer nominal load distribution on axles and struts after the truck is fully loaded. As a result, an algorithm has been developed to simulate the shovel load passes within the truck body to enhance the truck final payload balance.

5.2 Numerical analysis

The geometrical shape and interaction of shovel load passes within a truck body were discussed previously. In addition, a mathematical algorithm to simulate cone shaped interactions within the truck body to generate a final payload was discussed. However, since a parametric approach is highly complex, a numerical algorithm was developed.

5.2.1 Objectives

The objectives of the numerical analysis were to:

a. Calculate the volume of truncated cones in a truck body.
b. Calculate the volume of cone intersections.
c. Simulate the shovel load pass shapes within the truck body using the strut forces by load pass.
d. Predict the shovel load pass location to achieve an even load distribution on all 6 tires.
e. Simulate the truck payload after each shovel load pass to determine the next bucket load location.

5.2.2 Procedure

The flow chart illustrated in figure 5.3 demonstrates the working steps of the algorithm. The input data to the algorithm are the strut pressure readings, the struts location with respect to the truck body, the optimum centroid of the payload after each load pass that would progressively form a balanced final payload and the truck body shape.

After the first shovel bucket pass, the strut pressure readings are used to determine the centroid of the payload and also the accumulative payload tonnage. Then, the payload shape is reconstructed. All the possible locations for the next full bucket pass within the truck body are evaluated. The best location is identified to assist the shovel operator in placing the next load into the truck body to continue on a path to achieve a final balanced payload.

Iterating, the strut readings are collected after the second bucket pass, which is used to simulate the actual payload. A third cone interaction analysis is performed to suggest the best location for the third shovel pass, and so on.

Finally, the strut pressures are recorded after the third shovel load pass to reconstruct the payload and show the payload shape.

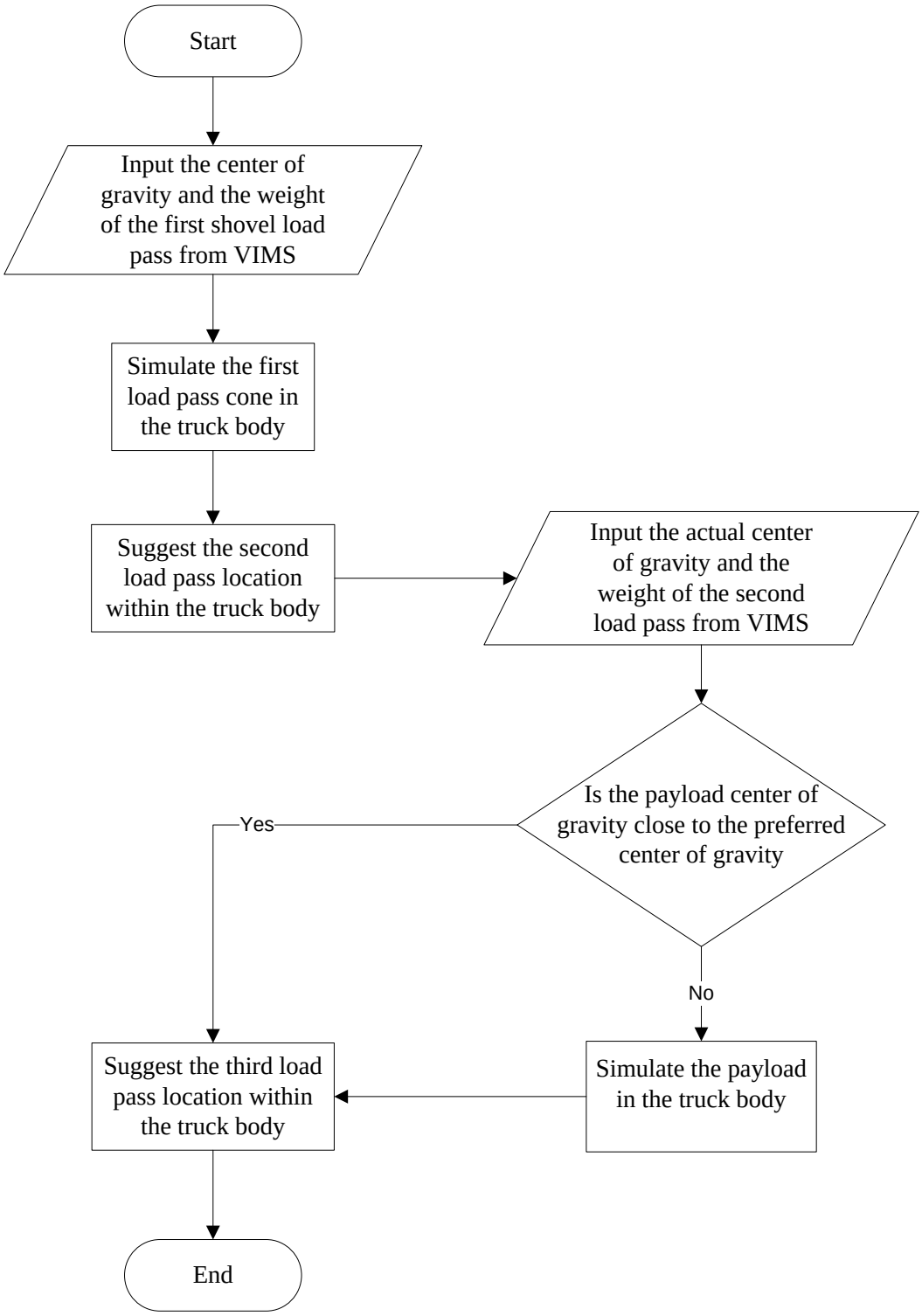

Figure 5.3 Numerical analysis flow chart

5.2.3 Algorithm

To develop an example numerical algorithm, an angle of repose for the material was assumed to be constant at 27 degrees with each shovel pass volume is assumed at 50 m^3. These input parameter can be changed requiring a small modification in the algorithm. The center of gravity of the payload was also input to the algorithm via interface with a spread sheet calculated from the strut pressure readings after each load pass.

A mesh network was defined using X, Y and Z matrices. Each cubical mesh defined as 0.2m×0.2m×0.2m allowed generating of 25,000 elements in a physical 200m^3 body volume. The Z values were set to the front wall and bottom of the truck body where these are defined by two inclined planes that make 70 and 12 degrees with x axis respectively. Equations 21 and 22 define the truck body front wall and floor and figure 5.4 illustrates the truck floor planes configuration.

$$Z0(i,j)= - \tan(70*pi/180) * X(i,j)+3.35 \qquad [21]$$

$$Z0(i,j)= \tan(12*pi/180)*(X(i,j)-3.35/\tan(70*pi/180)) \qquad [22]$$

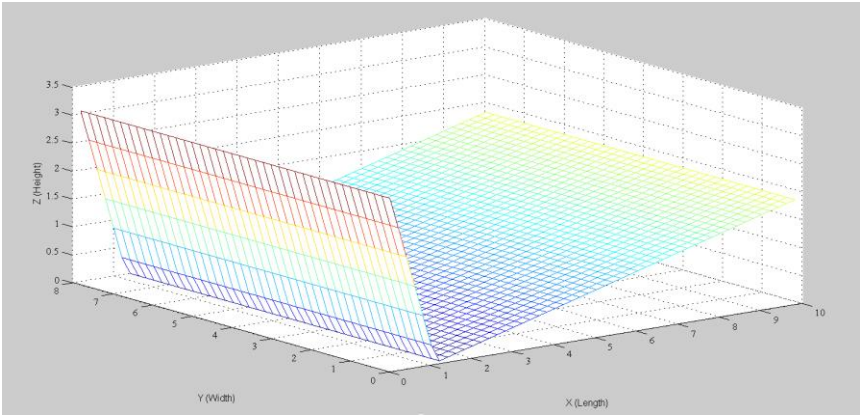

Figure 5.4 Trcuk floor planes and the 3D spacial configuration of the mesh network

Expression 23 is an implicit Cartesian equation of a right cone with a base radius r and a height h oriented along the z axes as show in figure 5.5 (Weisstein, 2013).

$$\frac{(x-x_0)^2+(y-y_0)^2}{c^2} = (z-z_0)^2 \quad [23]$$

Where $c = \frac{r}{h}$

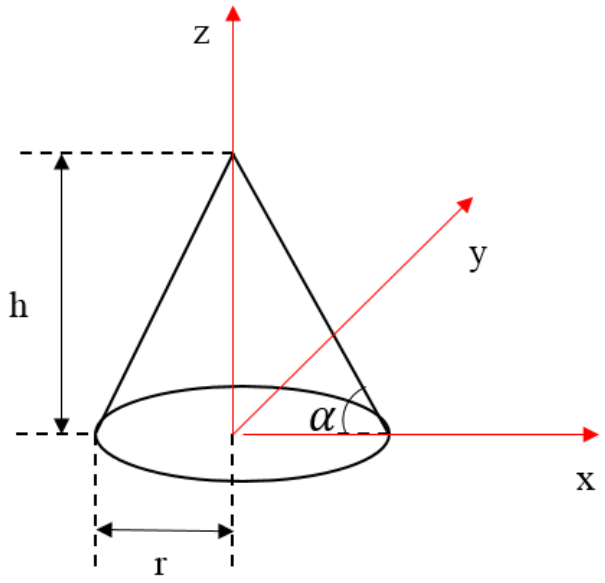

Figure 5.5 a right cone of height h and radious r

If $\tan\alpha = \frac{h}{r}$ then

$$z = z_0 - \frac{\sqrt[2]{(x-x_0)^2+(y-y_0)^2}}{\tan\alpha} \quad [24]$$

Where α is the angle of repose of the material that shapes the conical pile. Equation 24 as shown below in expression 25 is used to generate the cone in the numerical method.

Z= h-sqrt((X-X1).^2+(Y-Y1).^2)/tan(alfa) [25]

Five functions are also defined called “cgopt”, “hvalue”, “volumeq”, “centerg” and “shovel” provided through appendices 8.3.1.1 to 8.3.1.5.

The “cgopt” is the function of the difference between the calculated centre of gravity that would provide “balance” and the actual centre of gravity indicated by the truck strut sensors. “fminsearch’ is an optimization function used in Matlab to minimize the value of the “cgopt”. Basically, this function will look for the closest calculated centre of gravity to the actual one (Mathews & Fink, 2004).

The “hvalue” function is defined to change the cone height for the set 50 cubic meter volume. The algorithm searches for a cone that satisfies the two conditions of the volume and centre of gravity by changing the cone height to satisfy the 50 cubic meter volume and by moving the cone within the truck body search area to find the best position to allow closest centre of gravity to the balance location.

The “volumeq” function is used to calculate the total volume of the cones in the truck body for each iteration.

The “centerg” function calculates the centre of gravity of each constructed cone that is used by the optimization function to establish a center of gravity that provides a balanced load.

The “shovel” function is to plot the activity of providing a suggested placement location for the next shovel load pass. Above mentioned functions may be found in appendix 7.3.

5.2.4 Test scenario

The algorithm was run using the following balanced centre of gravity to test the functionality of the algorithm. The details of the calculations are presented in the appendix 8.3. Here, the visual output of the algorithm has been followed, such X1=3, Y1=5, X2=4.5 and Y2=3.5.

The conditions to run this scenario have been loosely set to allow the algorithm to run quicker; however, to achieve a higher accuracy the conditions could be tightened which would take longer to run the algorithm.

The balanced centre of gravity for the payload after the second and third loads were set as: Best X2=4.5, Best Y2=4, Best X3=4.5 and Best Y3=4.

Initially, the algorithm reconstructed the payload shape contained within the truck body after the first shovel payload pass was completed as shown in figure 5.6. The actual load in the scale truck body in the laboratory is also illustrated to further prove that the algorithm is able to closely model the load passes within the truck body.

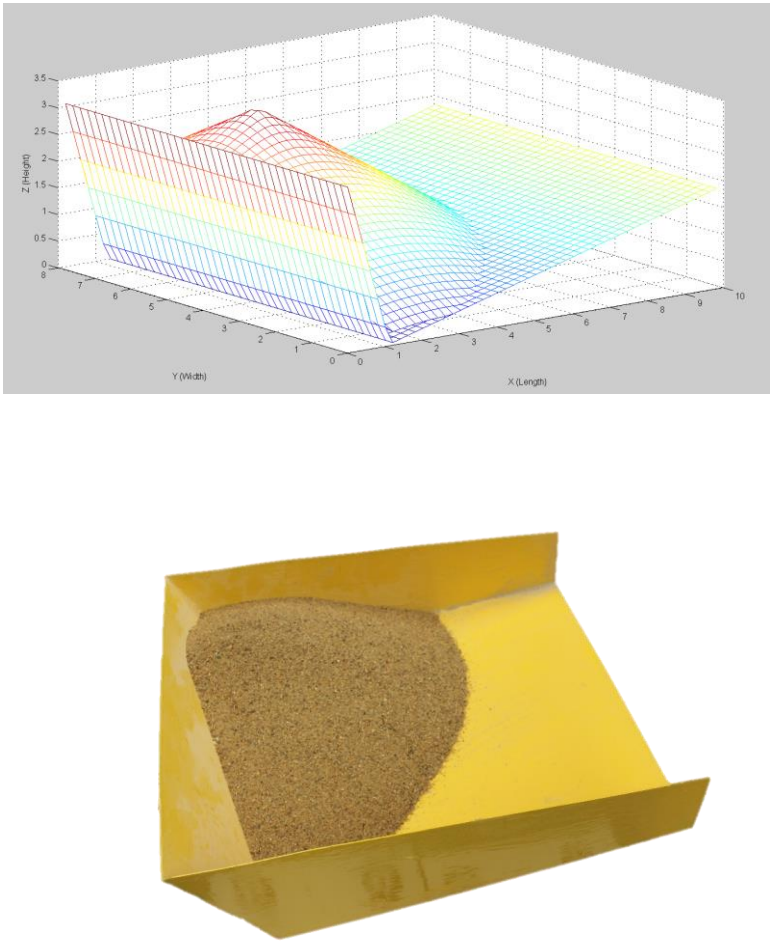

Figure 5.6 First load pass shape within the truck body

Then a preferred location to place the second payload pass was suggested that would narrow the centre of gravity of the payload after the second shovel load pass to the preferred location indicated above as shown in figure 5.7.

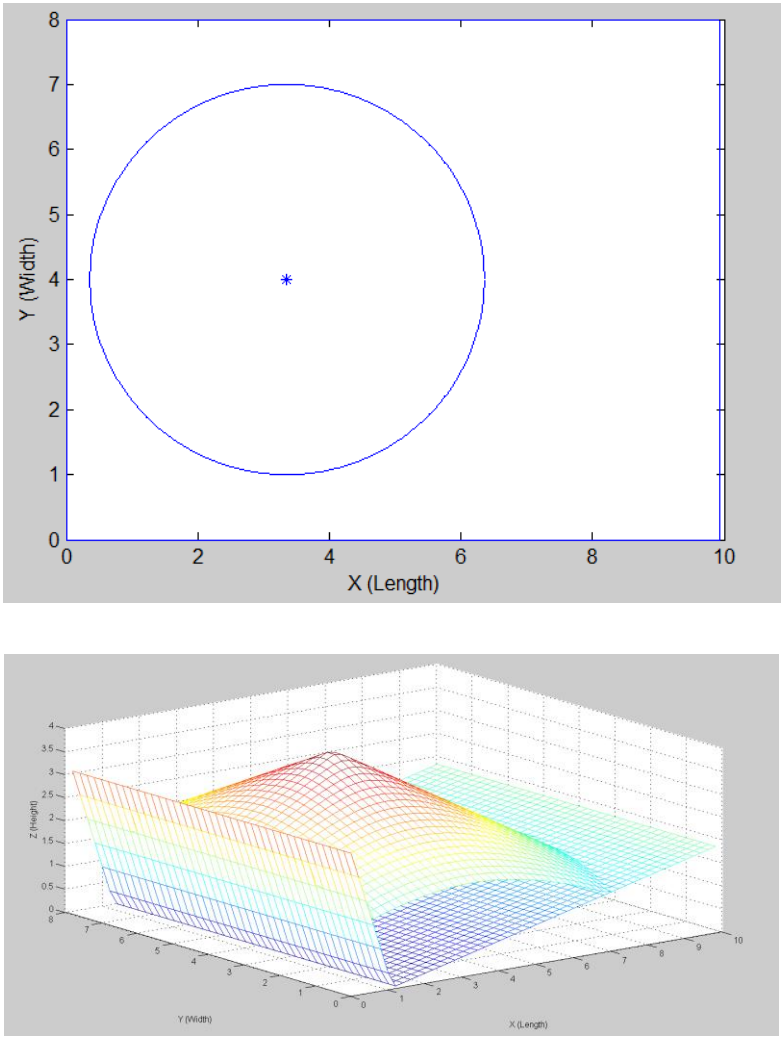

Figure 5.7 Suggested location for the second load pass within the truck body

After the second shovel load pass was performed, the centre of gravity of the payload was determined and entered into the algorithm. That allows the algorithm to reconstruct the actual payload (figure 5.8) in order to determine the third load pass location which would balance the final payload.

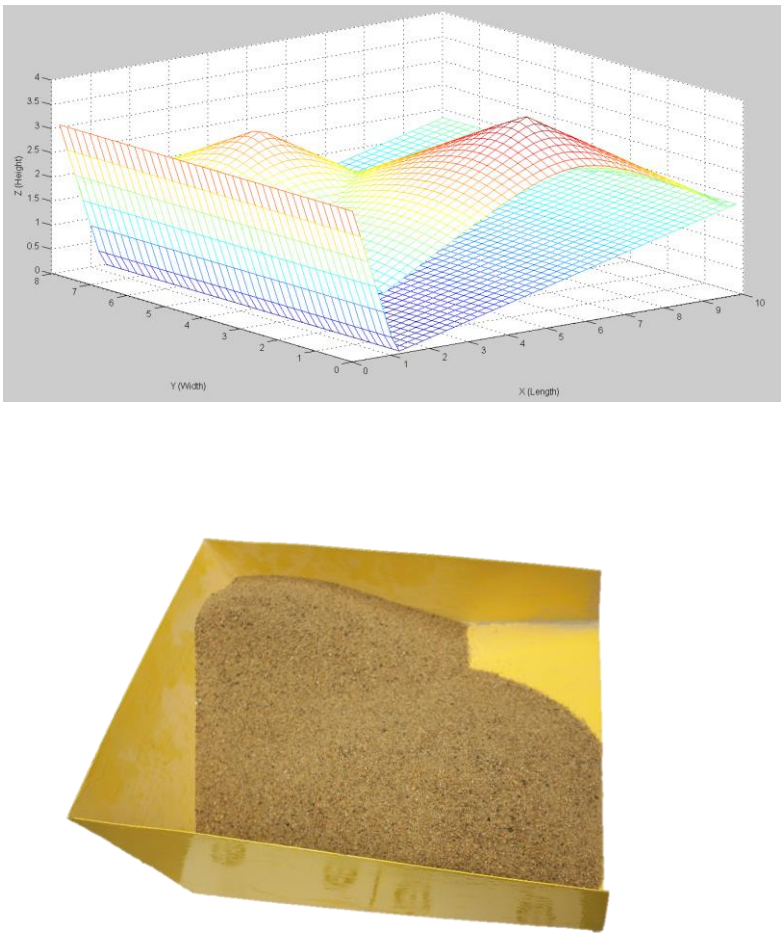

Figure 5.8 Payload after the second shovel load pass is performed

The algorithm suggested the third shovel pass preferred location and also the shape of the payload after the third shovel bucket pass was performed as shown in figure 5.9.

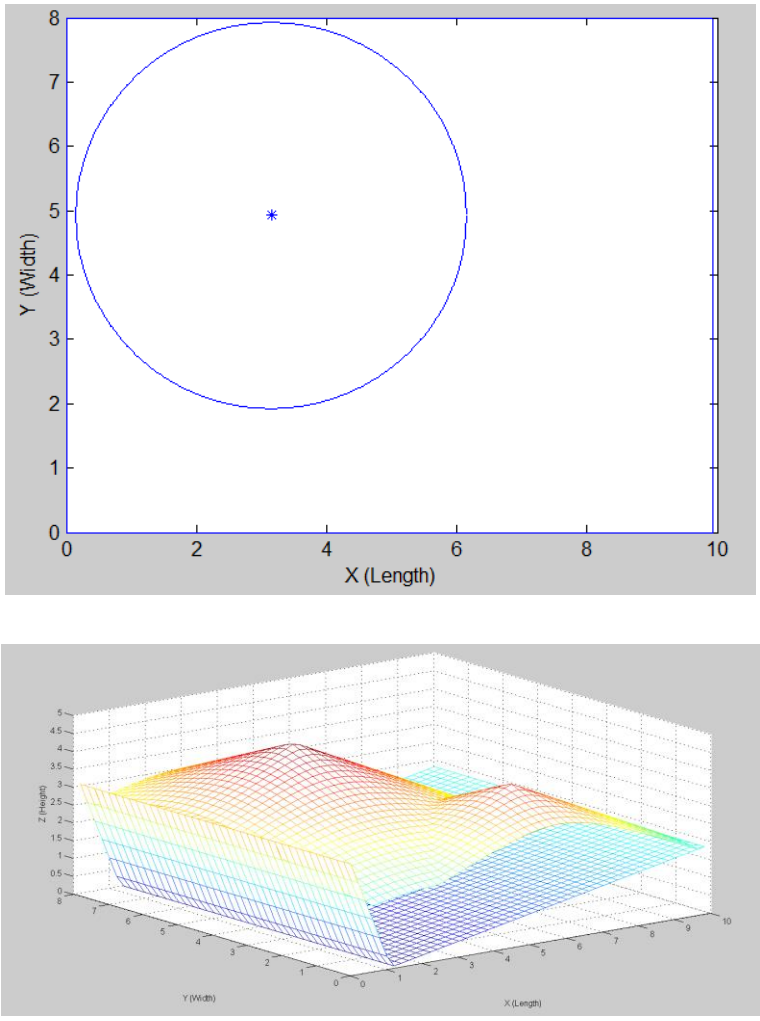

Figure 5.9 The truck payload shape after the third pass following the software instructions

5.3 Shovel operator payload balance assist system

A shovel operator assist system consists of a data acquisition system to collect the truck strut pressure readings, a wireless system to communicate the data from the trucks to the loading shovel, an algorithm to identify the center of gravity of the payload and to simulate and suggest a proper location for the successive shovel load passes to create a balanced payload before the truck moves away from the shovel.

Figure 5.10 illustrates a schematic of the shovel truck communication system and figure 5.11 shows the hardware for this communication system that is readily available on the market (Joseph & Chamanara, 2012). Future work is required to develop a shovel operator loading assist system that will be discussed in section 6.3.

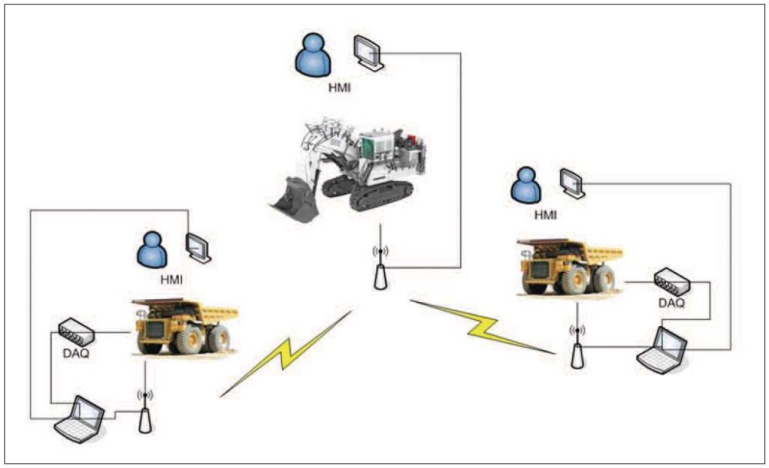

Figure 5.10 Schematic of an excavator and hauler communication system (Joseph & Chamanara, 2012).

Figure 5.11 Data acquisition, wireless transmitter and touch screeen processor (Joseph & Chamanara, 2012)

6. Discussions and Conclusions

6.1 Conclusions

Today's ultra-class mine haul trucks gross vehicle weights exceed 600 metric tonnes that subject the truck structure to excessive forces. Haul trucks are designed to bear these excessive forces evenly on all six tires. However, an unbalanced payload combined with an uneven mine haul road profile could adversely affect an even load distribution on the tires, and consequently on the truck structure. This would subject the truck structures to high stresses when the truck is in motion.

Various mine KPIs have been developed to monitor the performance of the mining haul trucks; such as, rack, roll, pitch, TKPH and WBC. In addition, various studies have proven that high rack, roll and pitch events subject the truck structure to excessive stresses that reduce the life of the components of the truck and consequently the life span of the truck. In addition, this increases the operational cost of the truck fleet. And also, it subjects the truck drivers to high level of the whole body vibration which jeopardizes the safety of the operators.

In this research study, it was also determined that the unbalanced payload will deteriorate the operating condition, causing the truck structure to undergo more sever adverse forces. Currently, shovel operators rely on their sight to balance the truck payload performing the shovel load passes. Operators have difficulty judging the lateral distances from their position across the truck body that will lead to side load events.

Very basic visual aids such as hanging reflective cones are used to aid the shovel operators to shape balanced loads within the truck body; however, a reliable and accurate shovel operator aid system does not exist. This would assist industry to reduce cost and to increase the haul truck fleet reliability.

With the goal of developing a shovel operator loading aid system, the shovel loading sequence was studied. It was determined that the free dumped

loose material would shape cone piles. It was also determined that each shovel load pass shape a truncated cone interacting with the truck body walls and floor as well as the preceding pass cone shape within the truck body. Since the angle of repose of the material and loose density are effectively constant, the height of the cone can be determined if the mass of the material is known. However, since each cone interacts with other cones, the common volume of several cones become important; therefore, a mathematical method is needed to calculate the intersection volume of the cones. The common volume of the cones needs to be added to the second cone to be able to model the second cone shape within a truck body.

Since the analytical mathematical approach was complex, a numerical method was developed using Matlab to model successive shovel load passes within a truck body. In this model, various optimization functions were used to suggest the preferred next shovel load pass locations within the truck body.

The input of the program was determined from the truck onboard system. Caterpillar trucks are equipped with an onboard condition monitoring system, VIMS, which records strut pressure readings at 1 Hz. The strut locations are fixed with respect to the truck body and the effective bearing areas of the struts are known; therefore, the pressure units can be easily converted to force units. From the strut forces, the truck payload and the center of gravity of the payload can be determined.

This information was fed into the numerical algorithm with the output of the algorithm used to develop a shovel operator loading visual aid. Basically, the preferred location of the shovel payload pass can be illustrated on a computer screen to the shovel operator in real time, subject to a short-range acquired wireless system in place between the trucks and shovel when in close proximately to one another.

It is suggested that such a shovel operator loading aid system would improve the sequential placement of payload and balance of trucks, that intern

would improve the truck KPIs significantly and consequently improve the truck fleet productivity, efficiency and safety.

6.2 Contributions of the research

Even though, the need to develop an algorithm to properly load haul trucks has been identified in previous research works, no mathematical approach has been previously suggested to develop an algorithm to simulate the bucket passes conical interaction in the truck body.

Introduction of the concept of intersecting cones to model cyclic placement of loose material into any types of container is the main contribution to the body of knowledge. The numerical analysis introduced based on this concept could be applied to determine any conical shaped substances interaction in the space to determine their common volume and the center of gravity of their cumulative mass.

In addition, correlating the payload to rack impacts that increase the fatigue damage cycles is also a contribution to the engineering knowledge. Applying the approach of this thesis, the structural life of any mobile equipment could be determined based on the number of adverse rack events and their magnitudes experienced by the machine.

Utilizing the truck on board system to develop a truck payload balance algorithm is unique with significant contribution to the industry as outlined in section 6.1.

Finally, a scientific paper published in the Canadian Institute of Mining (CIM) journal and a pre-reviewed paper presented at the 23rd World Mining Congress in Montreal are the outcomes of this research (Chamanara & Joseph, 2013; Joseph & Chamanara, 2012).

6.3 Errors

In this research only one truck body type is considered with two flat inclined planes at the bottom and vertical side planes. However, there are many different types of truck body mainly costume made according to the material types as well as the climate. For instance, there are body types with rubber floor and three floor inclined planes rather than two and so on. Despite that only one type of truck body is considered in this research the approach and algorithm can be applied to all kind of truck bodies.

There are laboratory measurement and calibration errors associated with the scale truck body, which are not significant and do not negatively impact the research outcome.

There may have been some minor errors with the strut pressure readings in the field due to the strut not being properly charged and maintained and also when the data is analysed to convert the strut pressure units to force units and so on.

Some assumptions have been made through the thesis such as the angle of repose and density of the materials that might vary at different sites; which, can be fed back to the algorithm to obtain more accurate results.

Initial strut pressure readings might be slightly off due to the truck being on an uneven ground while be loaded.

6.4 Future work

In order to develop a shovel operator loading assist system a short range wireless system needs to be developed to enable the trucks' on board system to communicate with the loading shovel when the trucks back into the digging face to be loaded.

A truck position estimation system needs to be employed to determine the truck orientation to the loading shovel. There are already few systems introduced

using various sensors including laser rangefinders as well as stereo cameras (Brothwick, 2009; A. Stentz, J. E. Bares, S. Singh, & P. Rowe, 1999).

In addition, a shovel bucket position estimation needs to be developed to determine the shovel bucket position with respect to the truck body.

The truck payload balance algorithm introduced in this research could be used in conjunction with above mentioned systems to develop a visual shovel operator loading assist system to show the position of the bucket with respect to the truck body and the ideal location of the shovel bucket pass in the truck body on a screen to aid the shovel operator in the loading process.

Finally, the truck payload balance algorithm needs to be field tested and improved. In process of improving the algorithm, various scenarios needs to be evaluated. For instance, when the digging pit floor is not even and the truck is sitting on an unbalance ground. The strut pressure readings need to be calibrated after each shovel bucket load pass to reflect the actual payload location within the truck body.

The ultimate goal is to develop a reliable system including a simple wireless communication system between truck on board systems and shovels; utilizing the algorithm to aid the shovel operator to balance the truck payload before the truck leaves the digging face.

7. References

Abd. Rahman, R., Nasir Tamin, M., & Kurdi, O. (2008). Stress analysis of heavy duty truck chasis as a preliminary data for its fatigue life prediction using FEM. *Jurnal Mekanikal*(26), 10.

Amarra, F., & El-Sayed, M. (2010). Albian Sands: Mine Truck 797B Frame Failure RCA. Calgary.

Baker, M. R. (2000). USA Patent No. US6157889 A. U. S. Pattent.

Balogun, F. A., Brunetti, A., & Cesareo, R. (2000). Volume of intersection of two cones. *Radiation Physics and Chemistry, 59*(1), 23-30.

Baumgart, F. (2000). Stiffness — an unknown world of mechanical science? *Injury, 31, Supplement 2*(0), 14-84. doi: http://dx.doi.org/10.1016/S0020-1383(00)80040-6

Berezan, J. J., Joseph, T. G., & Valle, V. d. (2004). Monitoring whole body vibration effects on ultra-class haulers *CIM Bulletin, 97*(1082), 4.

Beyer, W. A., Fawcett, L. R., Mauldin, R. D., & Swartz, B. K. (1987). The volume common to two congruent circular cones whose axes intersect symmetrically. *Journal of Symbolic Computation, 4*(3), 381-390. doi: http://dx.doi.org/10.1016/S0747-7171(87)80014-7

Boardman, B. (1990). Fatigue Resistance of Steels. In A. International (Ed.), *ASM Handbook, Properties and Selection: Irons, Steels, and High-Performance Alloys* (Vol. 1, pp. 673-688): ASM International.

Borthwick, J. R., Lawrence, P. D., & Hall, R. H. (2009). *Mining haul truck localization using stereo vision.* Paper presented at the 14th IASTED International Conference on Robotics and Applications, RA 2009, November 2, 2009 - November 4, 2009, Cambridge, MA, United states.

Brothwick, J. R. (2009). *Mining Haul Truck Pose Estimation and Load Profiling Using Stereo Vision.* (Master of Applied Science), The University of British Columbia.

Cannon, H. N. (1999). *Extended Earthmoving with an Autonomous Excavator.* (Master of Science), Carnegie Mellon University, Pittsburgh, PA. (CMU-RI-TR-99-10)

Caterpillar. (2013). Cat 7495 HF Electric Rope Shovel.

Caterpillar (Ed.). (2010). *797 Truck*: Caterpillar

Chakraborty, S. (2011). Scaling Laws *Mechanics Over Micro and Nano Scales*: Springer.

Chamanara, A., & Joseph, T. G. (2013, August 11-15, 2013). *Adverse effect of unbalanced payloads on mining haul truck KPIs.* Paper presented at the The 23rd World Mining Congress, Montreal, Canada.

Deslandes, J. V., & Marshall, G. A. (1986). *Factors affecting structural fatigue damage of mine haul trucks* Newman, Aust.

Duff, E. (2000). *Automated volume estimation of haul-truck loads.* Paper presented at the Australasian Conference on Robotics and Automation (ACRA), Melbourne, Australia

ERCB. (2013). *Directive 082*. Alberta: The Energy Resources Conservation Board.

Finning, C. (2010). Site Failure Report - Albian Sands (RHF Spindle). Fort McMurray.

Gu, Z., Mi, C., Wang, Y., & Jiang, J. (2012). A-type frame fatigue life estimation of a mining dump truck based on modal stress recovery method. *Engineering Failure Analysis, 26*(0), 89-99. doi: http://dx.doi.org/10.1016/j.engfailanal.2012.07.004

Hagenbuch, L. G. (2000). *Adapting the Off-Highway Truck Body Volumetric Process to Real World Conditions*. Paper presented at the International Off-Highway & Powerplant Congress & Exposition, Milwaukee, Wisconsin.

Hagenbuch, L. G. (2002). *Off-Highway Truck Body True Capacity . . . Why Can't I Get Rated Payload On My Off-Highway Trucks Without Hungry Boards And Tail Extensions?* Paper presented at the SME Annual Meeting February 25 - 27, , Phoenix, Arizona

Hagenbuch, L. G. (2011). US 7,917,266 B2. U. S. Patent.

Hitachi. (2013). Hitachi EX8000 Hydraulic Excavator.

Joseph, T. G. (2003). *Large mobile mining equipment operating on soft ground*. Paper presented at the The 18th International Mining Congress and Exhibition of Turkey, Antalya.

Joseph, T. G., & Chamanara, A. (2012). Hauler body payload balance. *CIM Journal, 3*(1), 9.

Komatsu. (2013). What is KOMTRAX? Retrieved June 24, 2013, from http://www.komatsuamerica.com/what-is-komtrax

Mathews, J. H., & Fink, K. D. (2004). Nelder-Mead Method - Numerical Optimization *Numerical Methods Using Matlab* (pp. 7). Upper Saddle River, New Jersey, USA: Prentice-Hall Inc.

Mi, C., Gu, Z., Yang, Q., & Nie, D. (2012). Frame fatigue life assessment of a mining dump truck based on finite element method and multibody dynamic analysis. *Engineering Failure Analysis, 23*(0), 18-26. doi: http://dx.doi.org/10.1016/j.engfailanal.2012.01.014

Mills, D. J. (2002). Assessing the effects of a mine profile on the performance of off-highway trucks. *Caterpillar of Australia - Project Management Consultant,* 10.

Prem, H. (1998). *Off-highway mine haul truck dynamics simulation*. Paper presented at the SAE International Off-Highway and Powerplant Congress and Exposition, Milwaukee, Wisconsin, USA.

SAE. (2012). Tonne Kilometer Per Hour Application - J1098_201203: SAE International.

Schexnayder, C., Weber, S. L., & Brooks, B. T. (1999). Effect of Truck Payload Weight on Production. *Journal of Construction Engineering and Management, 125*(1), 1-7.

Stentz, A., Bares, J., Singh, S., & Rowe, P. (1998). *A Robotic Excavator for Autonomous Truck Loading.* Paper presented at the 1998 IEEE/RSJ International Conference on Intelligent Robots and Systems, Victoria, BC.

Stentz, A., Bares, J., Singh, S., & Rowe, P. (1999). A Robotic Excavator for Autonomous Truck Loading. *Autonomous Robots, 7*(2), 175-186. doi: 10.1023/A:1008914201877

Stentz, A., Bares, J. E., Singh, S., & Rowe, P. (1999). A Robotic Excavator for Autonomous Truck Loading. *Auton. Robots, 7*(2), 175-186. doi: 10.1023/a:1008914201877

Weisstein, E. W. (2013). "Cone.". *MathWorld--A Wolfram Web Resource.*, 2013, from http://mathworld.wolfram.com/Cone.html

Whalen, D. O., Khaled. (2003). *Effect of Oil Sand Mining Operations on Haul Truck Dump Body Design*. Paper presented at the Operational Challenges in the Canadian Oilsands, Montreal.

Wikipedia. (2013, 2 August 2013). Sqaure-cube law. Retrieved 16 August 2013, 2013, from http://en.wikipedia.org/wiki/Square-cube_law

8. Appendices

8.1 Laboratory test

8.1.1 Test 1

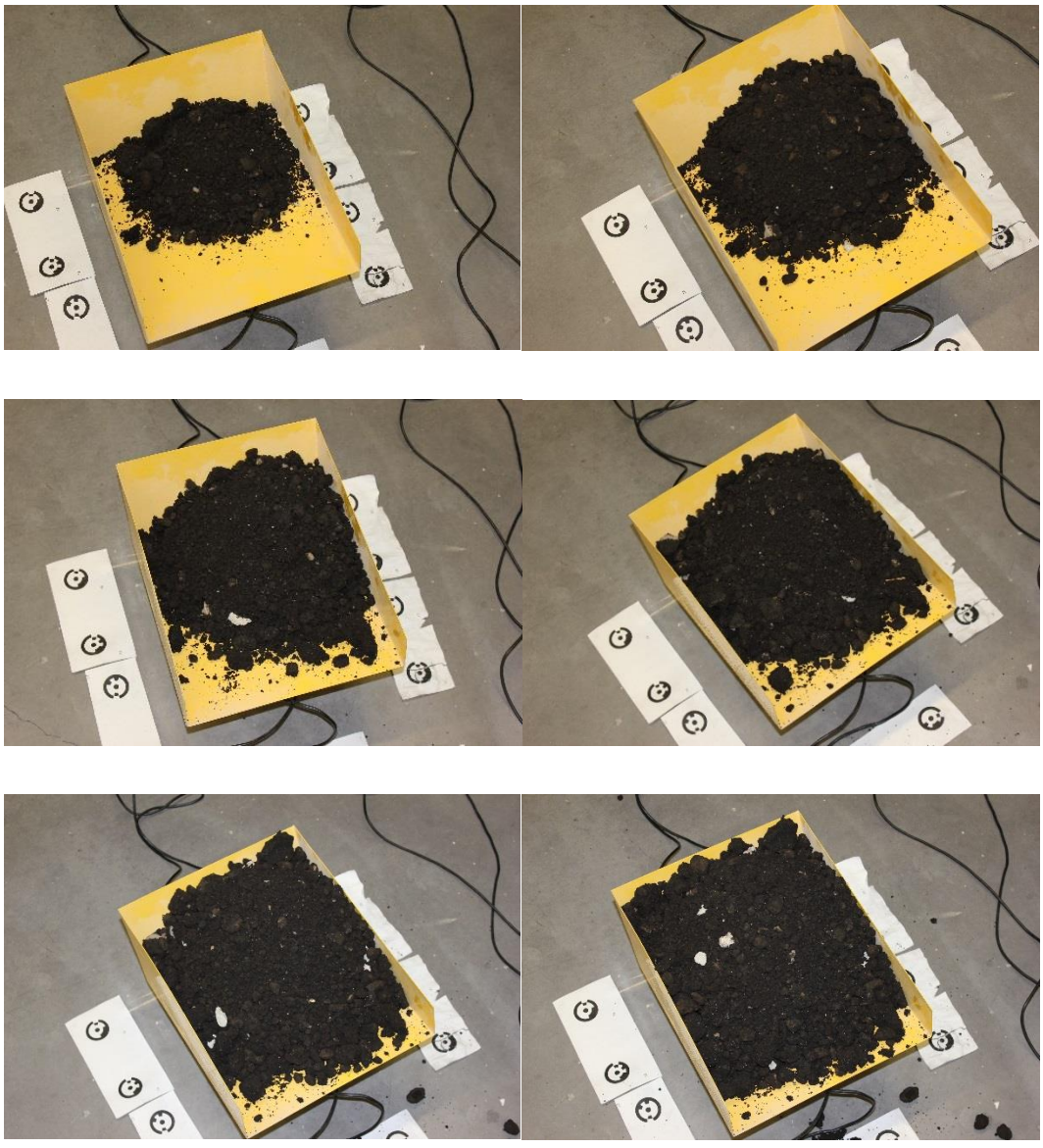

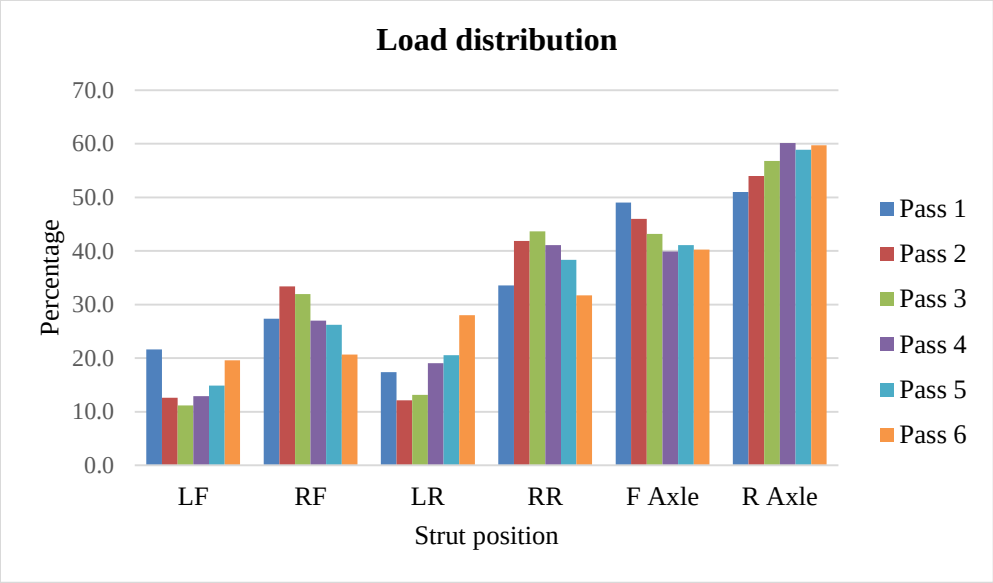
Load distribution
70.0
60.0
50.0
40.0
30.0
20.0
10.0
0.0
Percentage
LF
RF
LR
RR
F Axle
R Axle
Strut position
Pass 1
Pass 2
Pass 3
Pass 4
Pass 5
Pass 6

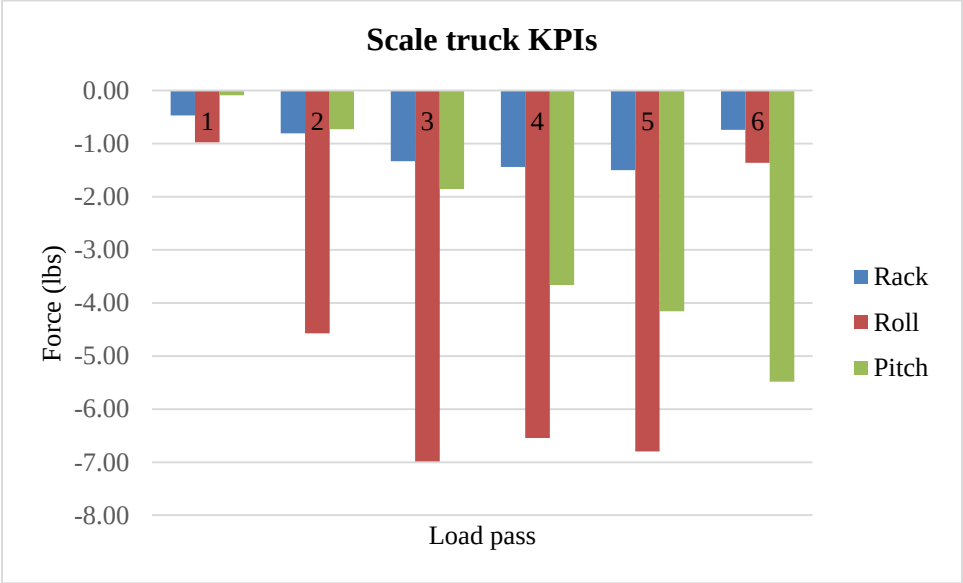
Scale truck KPIs
0.00
-1.00
-2.00
-3.00
-4.00
-5.00
-6.00
-7.00
-8.00
Force (lbs)
1
2
3
4
5
6
Load pass
Rack
Roll
Pitch

8.1.2 Test 2

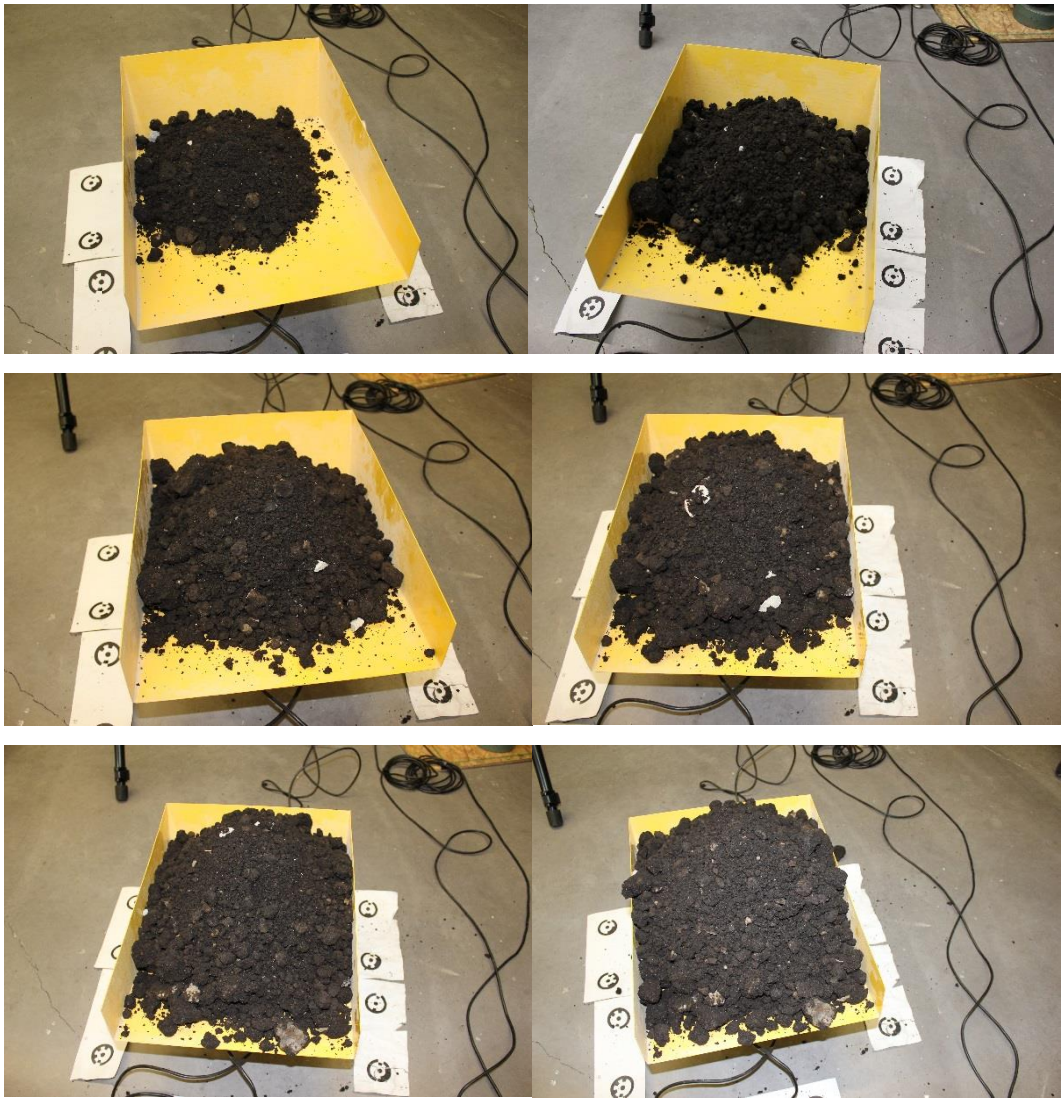

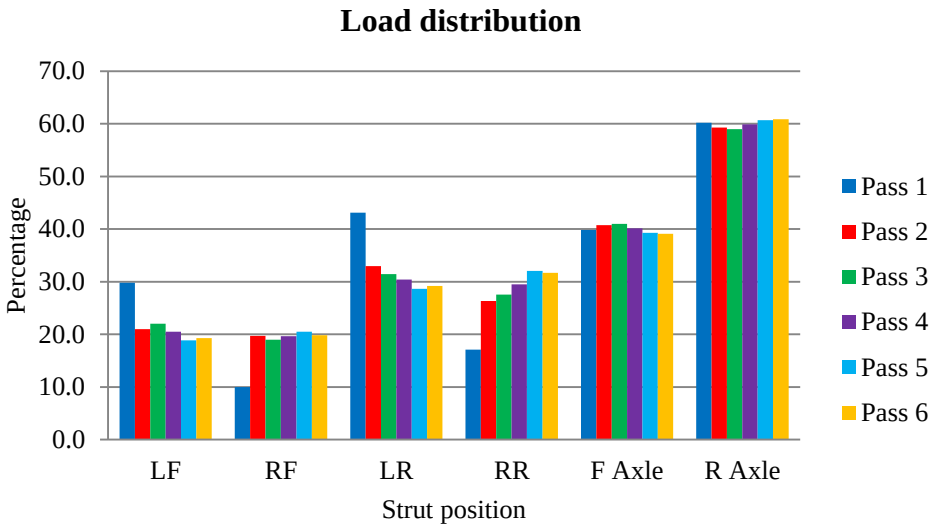
Load distribution
70.0
60.0
50.0
40.0
30.0
20.0
10.0
0.0
Percentage
LF
RF
LR
RR
F Axle
R Axle
Strut position
Pass 1
Pass 2
Pass 3
Pass 4
Pass 5
Pass 6

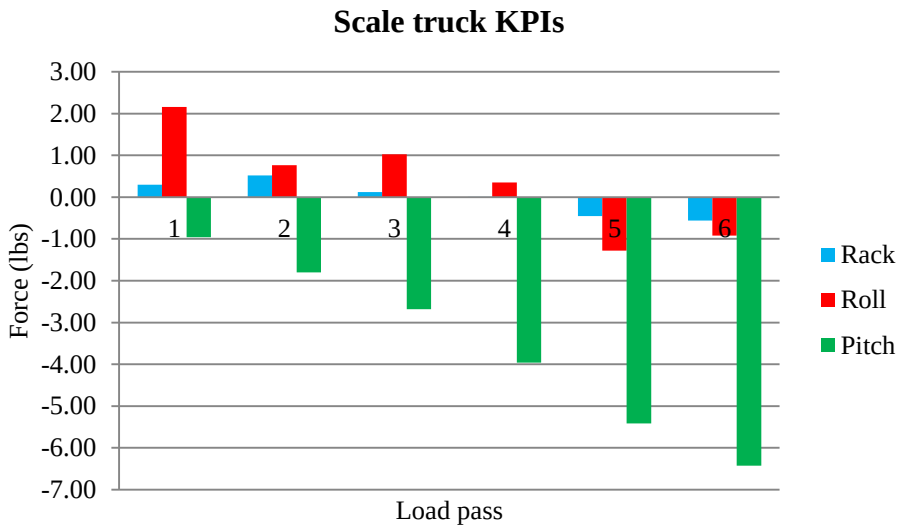
Scale truck KPIs
3.00
2.00
1.00
0.00
-1.00
-2.00
-3.00
-4.00
-5.00
-6.00
-7.00
Force (lbs)
1
2
3
4
5
6
Load pass
Rack
Roll
Pitch

8.1.3 Test 3

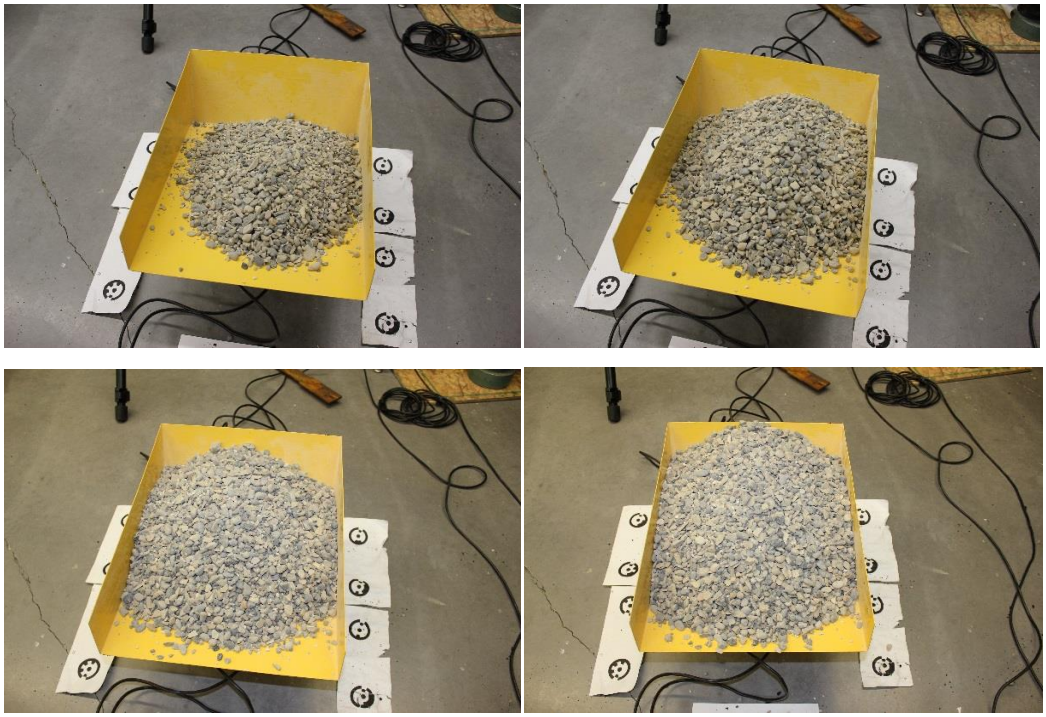

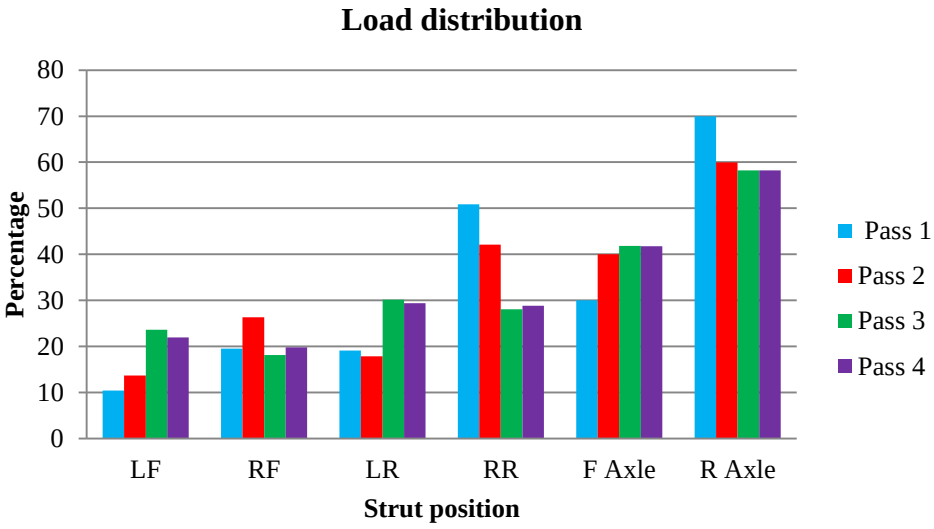
Load distribution
80
70
60
50
40
30
20
10
0
Percentage
LF
RF
LR
RR
F Axle
R Axle
Strut position
Pass 1
Pass 2
Pass 3
Pass 4

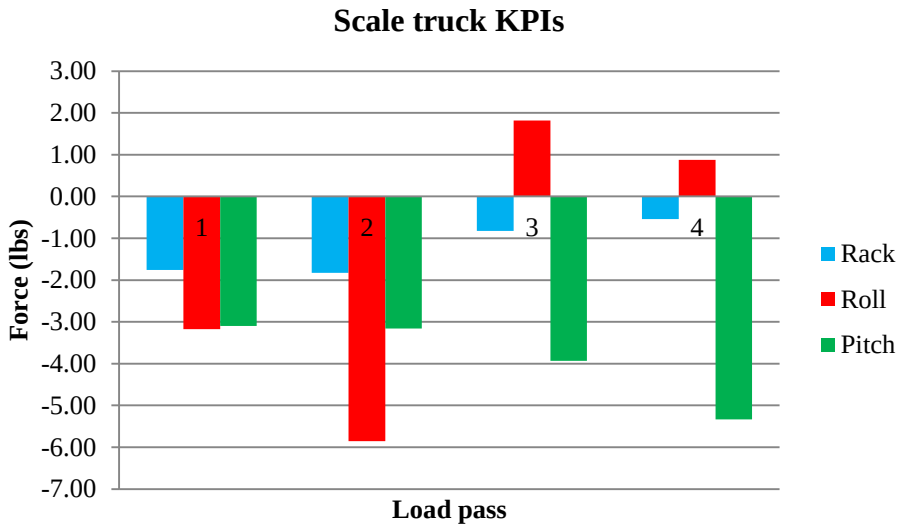
Scale truck KPIs
3.00
2.00
1.00
0.00
-1.00
-2.00
-3.00
-4.00
-5.00
-6.00
-7.00
Force (lbs)
1
2
3
4
Load pass
Rack
Roll
Pitch

8.1.4 Test 4

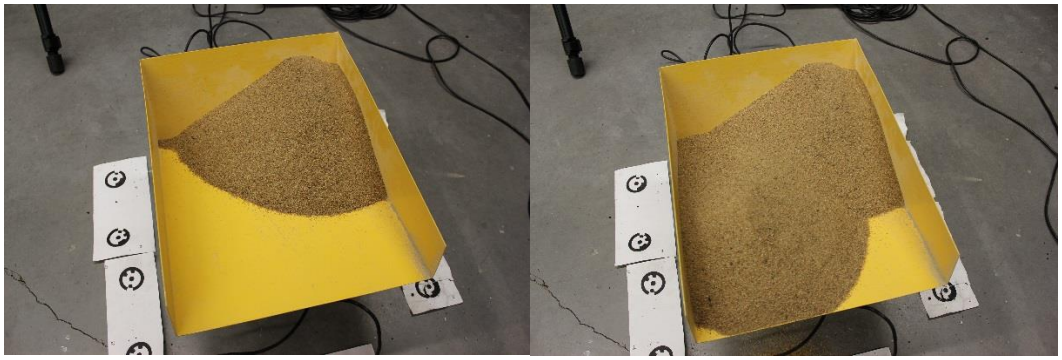

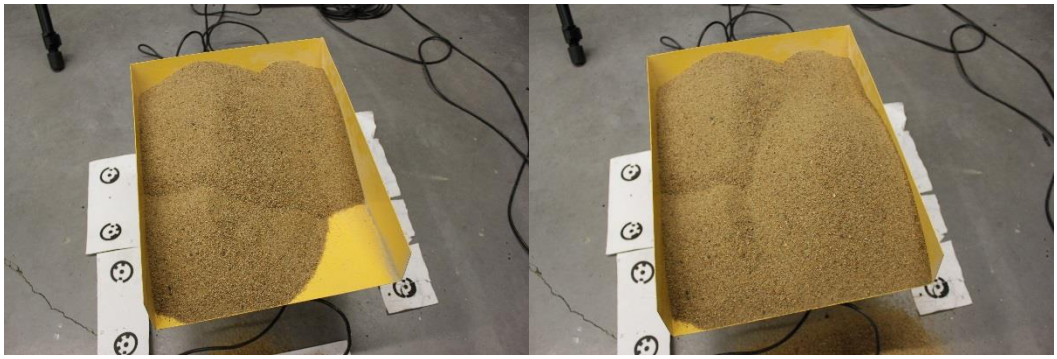

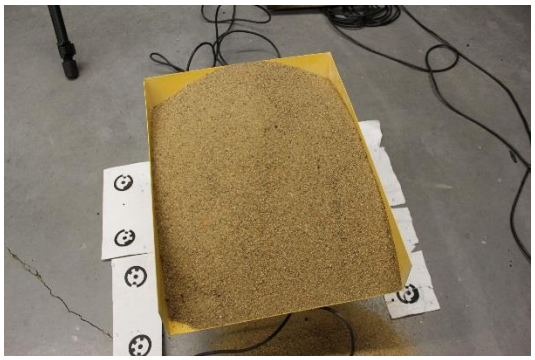

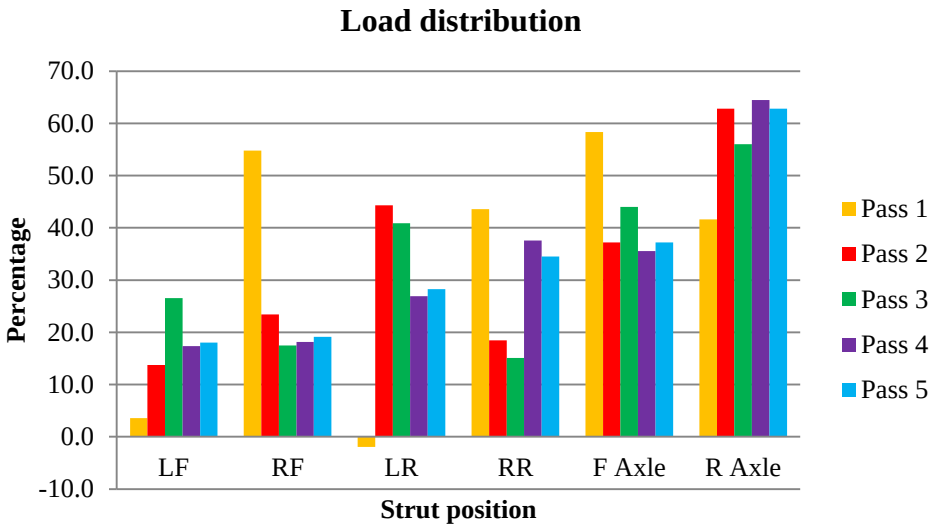
Load distribution
70.0
60.0
50.0
40.0
30.0
20.0
10.0
0.0
-10.0
Percentage
LF
RF
LR
RR
F Axle
R Axle
Strut position
Pass 1
Pass 2
Pass 3
Pass 4
Pass 5

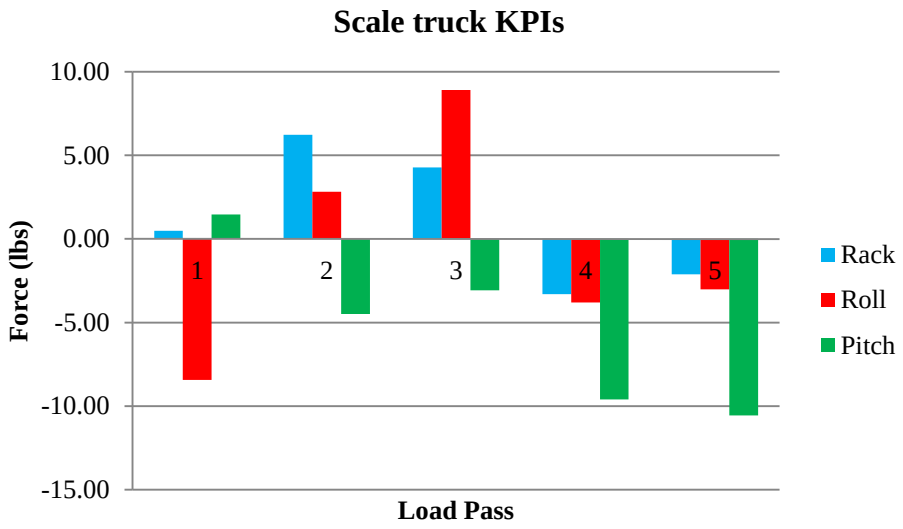
Scale truck KPIs
10.00
5.00
0.00
-5.00
-10.00
-15.00
Force (lbs)
1
2
3
4
5
Load Pass
Rack
Roll
Pitch

8.1.5 Test 5

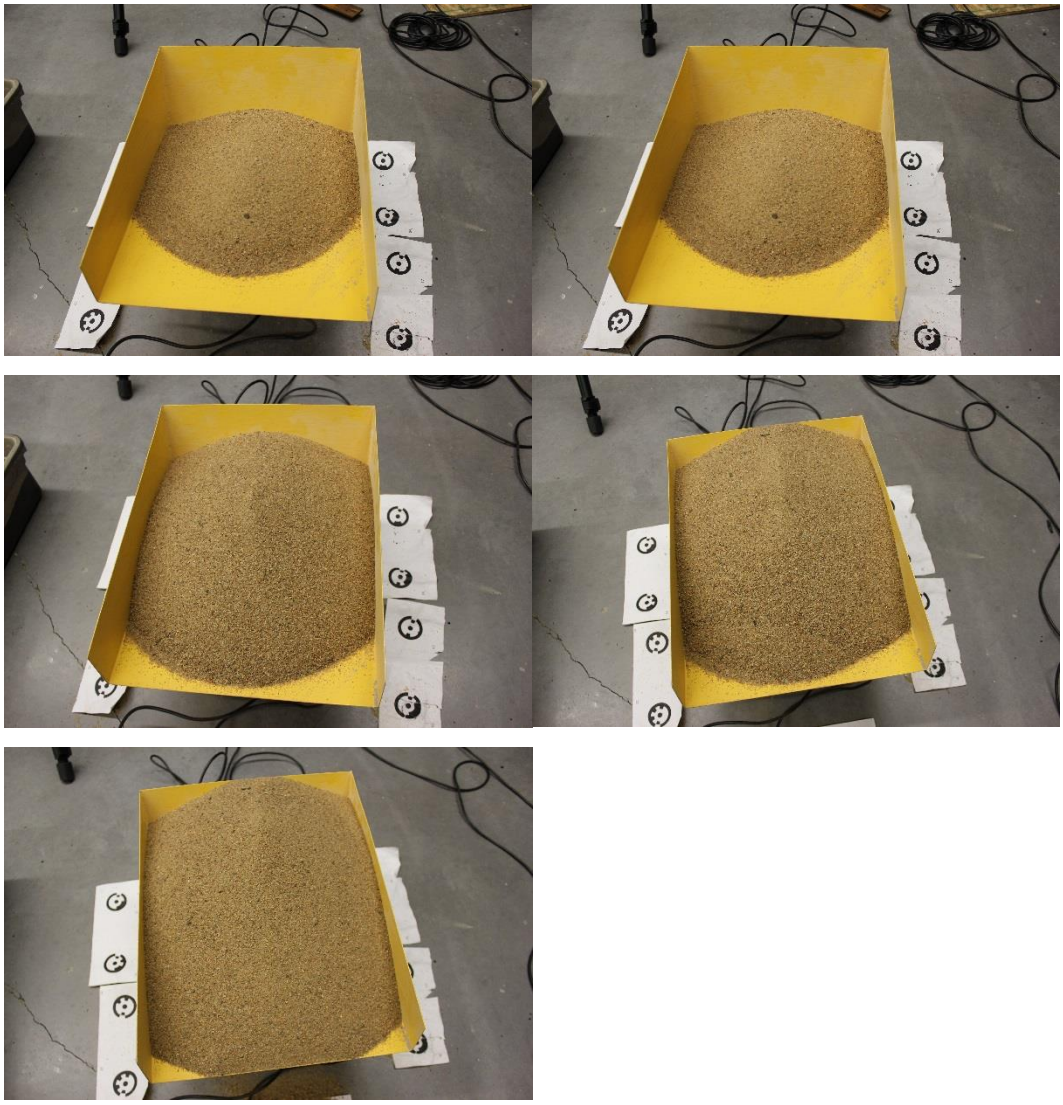

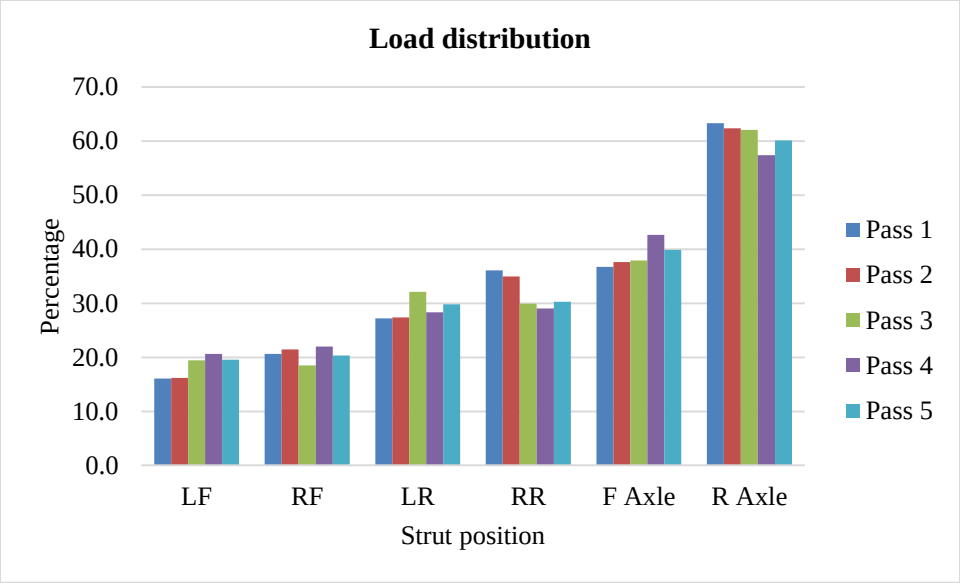
Load distribution
70.0
60.0
50.0
40.0
30.0
20.0
10.0
0.0
Percentage
LF
RF
LR
RR
F Axle
R Axle
Strut position
Pass 1
Pass 2
Pass 3
Pass 4
Pass 5

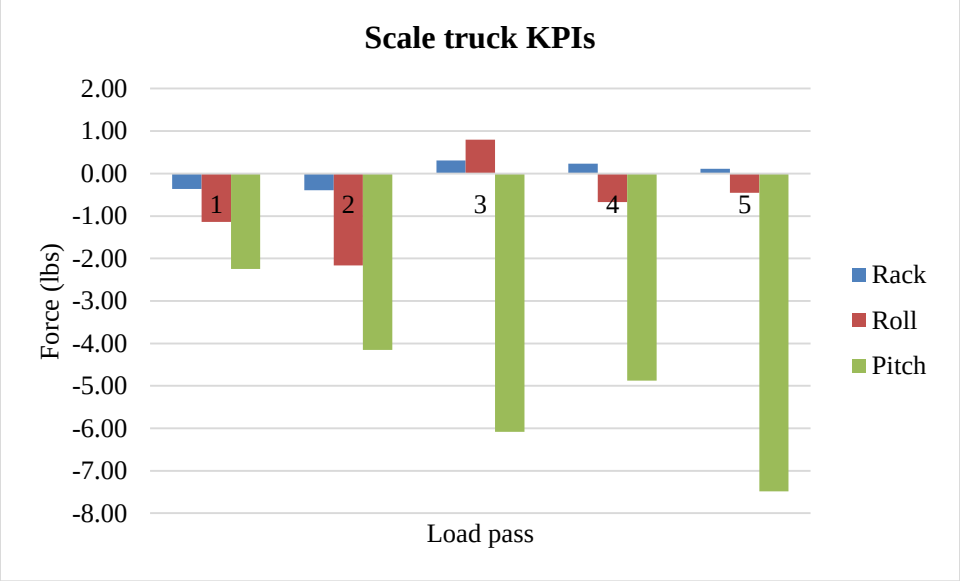
Scale truck KPIs
2.00
1.00
0.00
-1.00
-2.00
-3.00
-4.00
-5.00
-6.00
-7.00
-8.00
Force (lbs)
1
2
3
4
5
Load pass
Rack
Roll
Pitch

8.1.1 Test 6

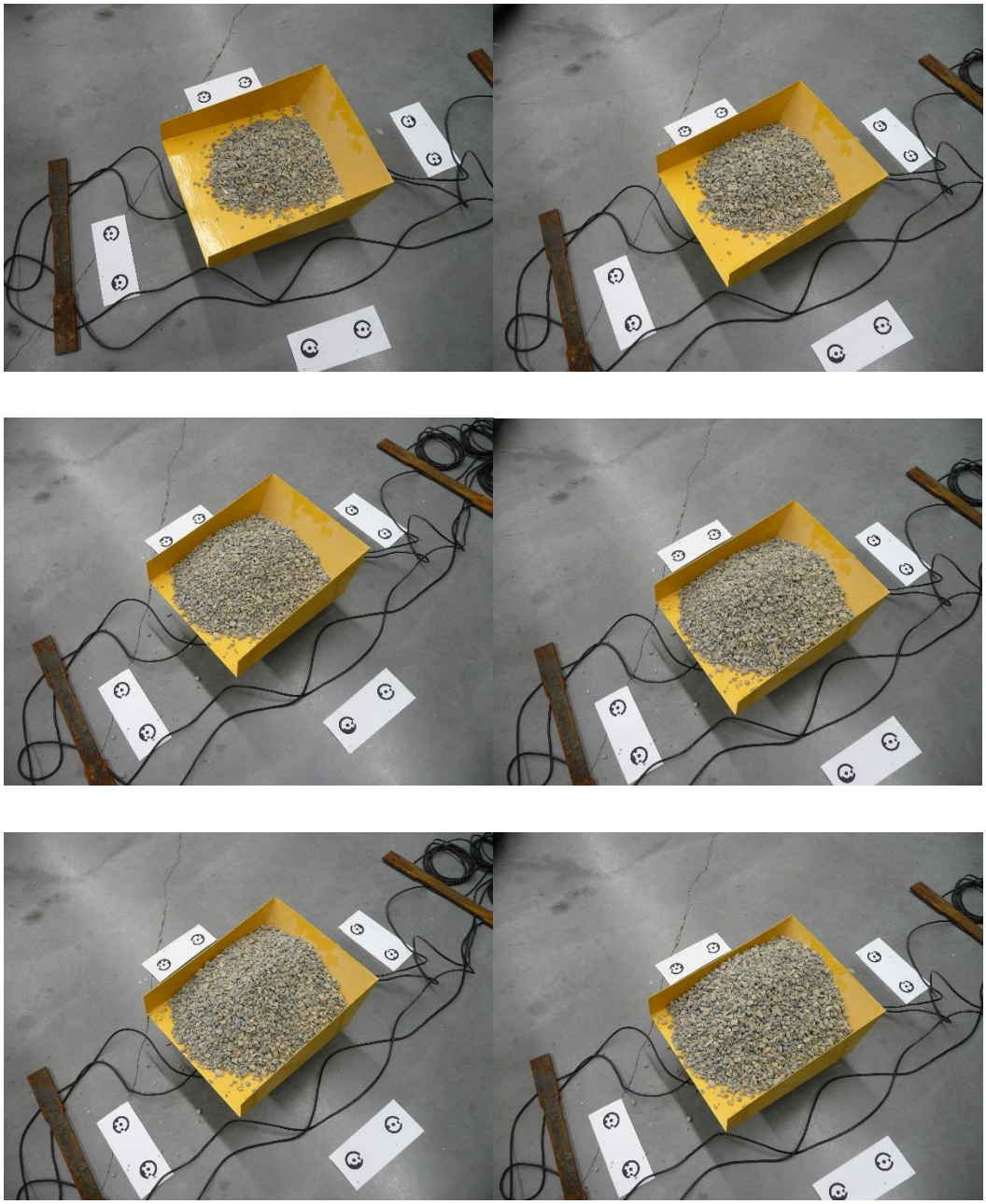

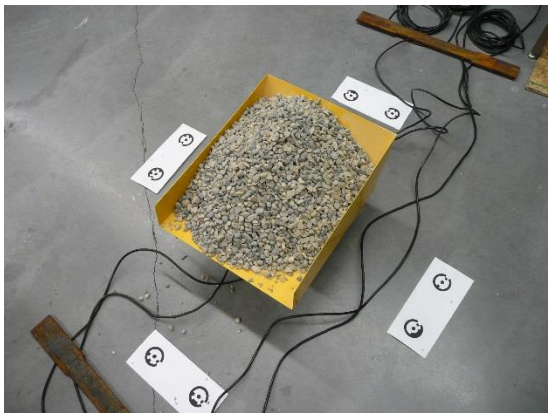

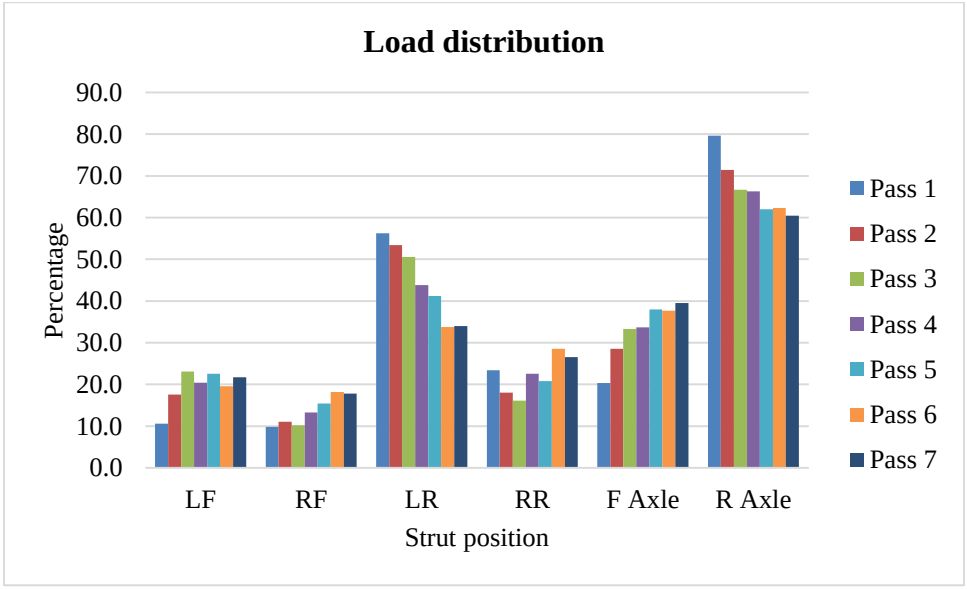
Load distribution
90.0
80.0
70.0
60.0
50.0
40.0
30.0
20.0
10.0
0.0
Percentage
LF
RF
LR
RR
F Axle
R Axle
Strut position
Pass 1
Pass 2
Pass 3
Pass 4
Pass 5
Pass 6
Pass 7

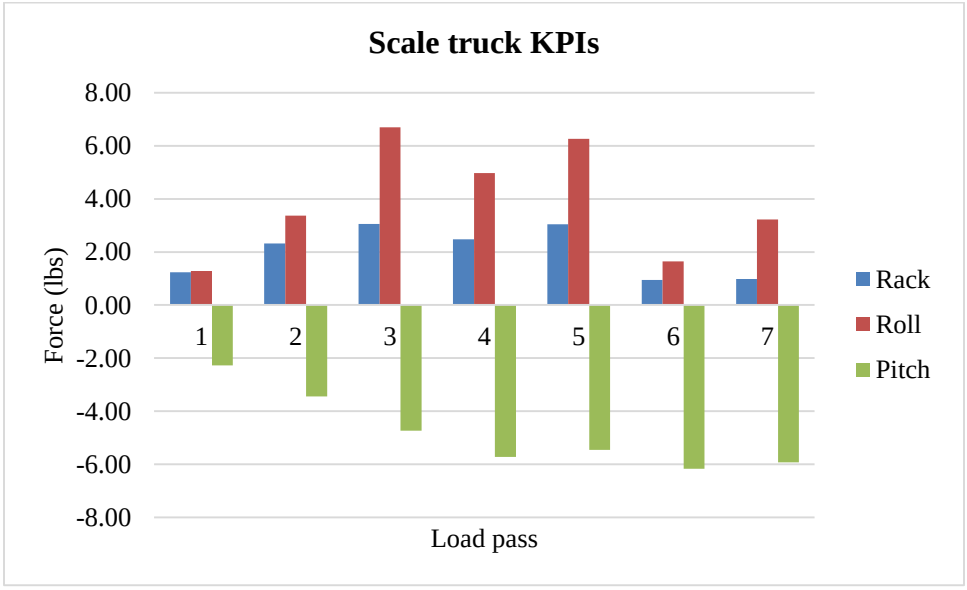
Scale truck KPIs
8.00
6.00
4.00
2.00
0.00
-2.00
-4.00
-6.00
-8.00
Force (lbs)
1
2
3
4
5
6
7
Load pass
Rack
Roll
Pitch

8.1.1 Test 7

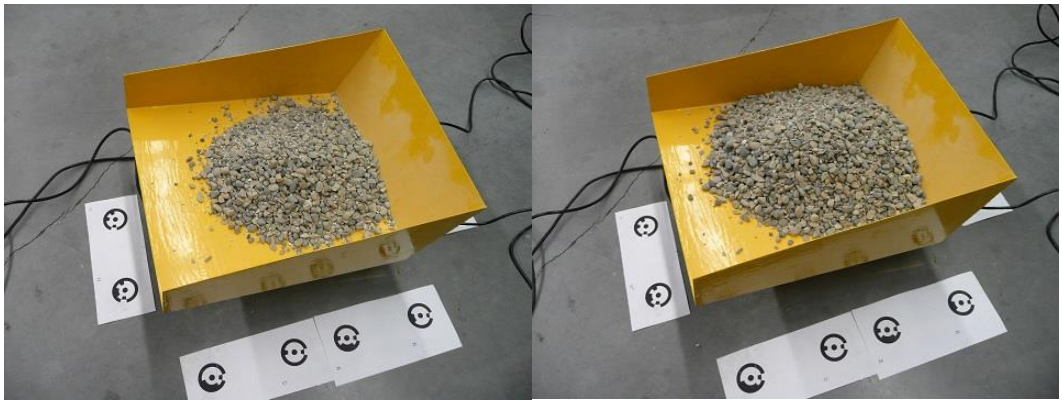

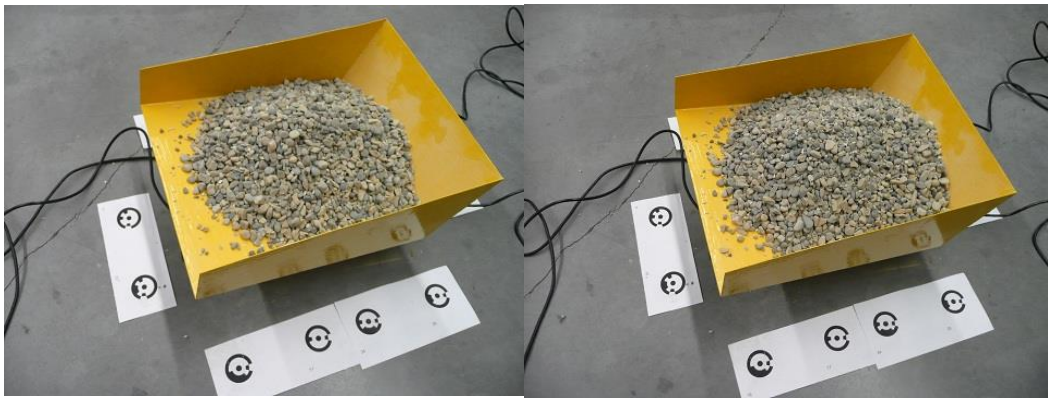

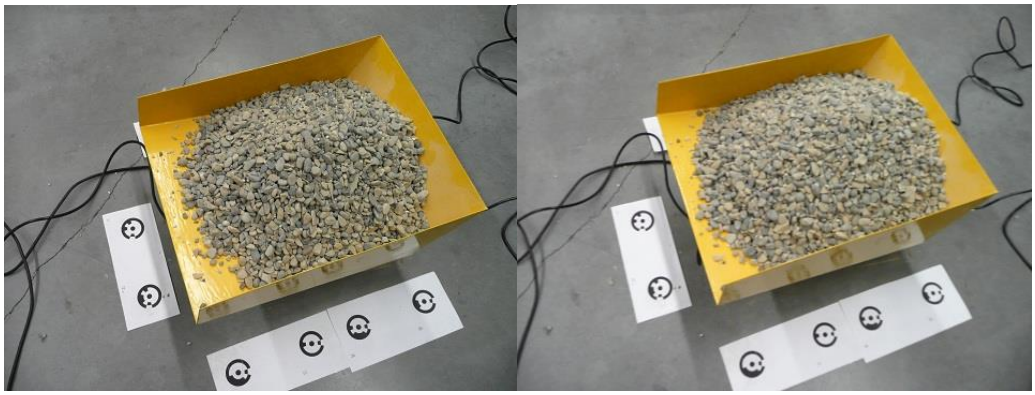

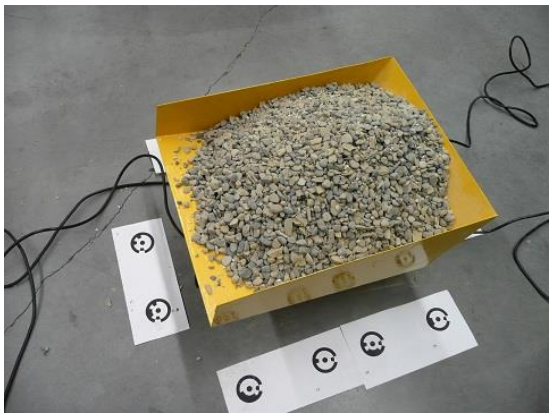

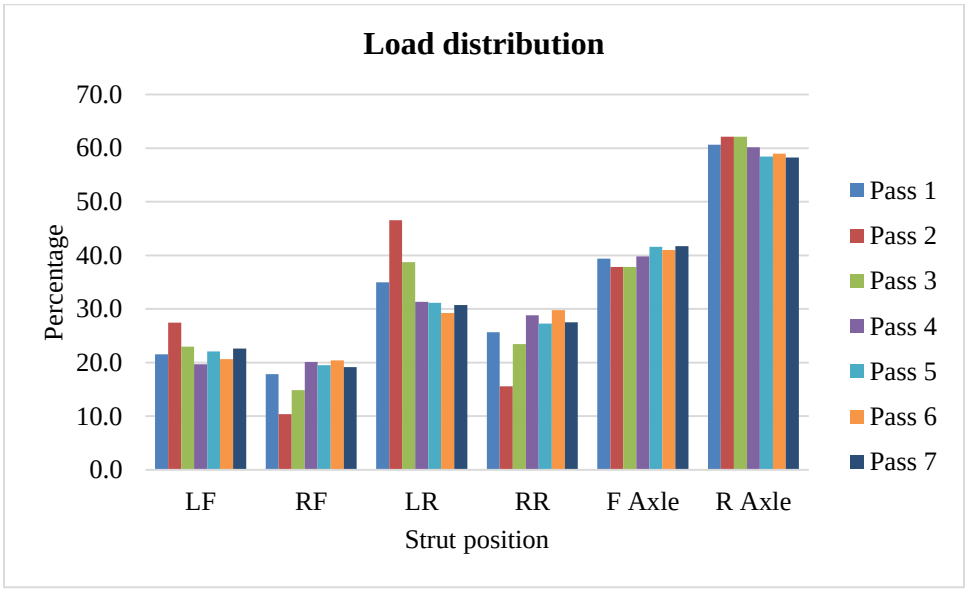
Load distribution
70.0
60.0
50.0
40.0
30.0
20.0
10.0
0.0
Percentage
LF
RF
LR
RR
F Axle
R Axle
Strut position
Pass 1
Pass 2
Pass 3
Pass 4
Pass 5
Pass 6
Pass 7

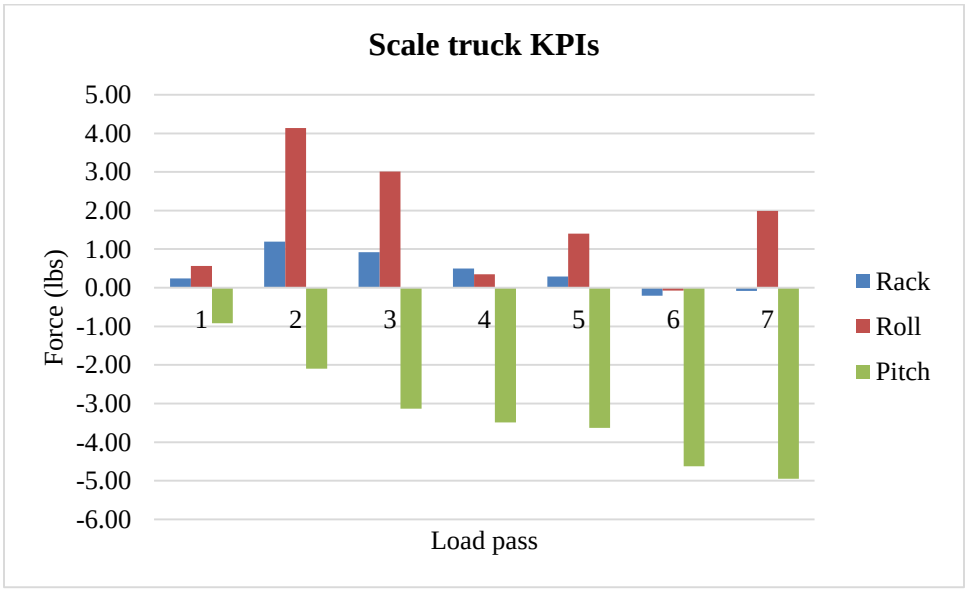
Scale truck KPIs
5.00
4.00
3.00
2.00
1.00
0.00
-1.00
-2.00
-3.00
-4.00
-5.00
-6.00
Force (lbs)
1
2
3
4
5
6
7
Load pass
Rack
Roll
Pitch

8.2 Field Study

8.2.1 136 truck

8.2.1.1 Cycle 1

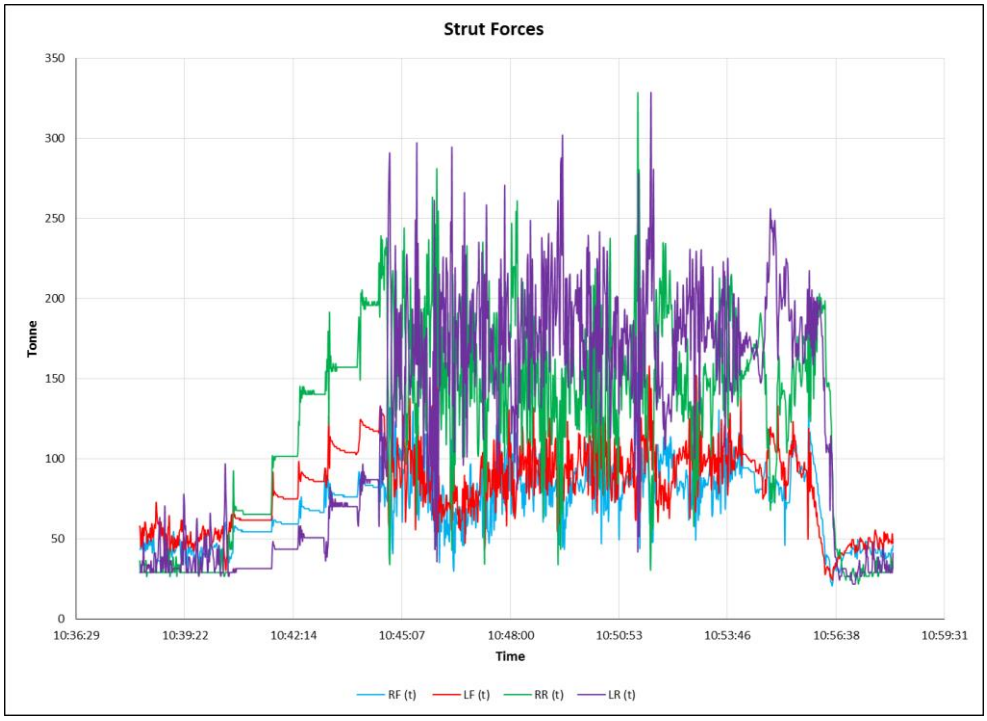
Strut Forces
350
300
250
200
150
100
50
0
Tonne
10:36:29
10:39:22
10:42:14
10:45:07
10:48:00
10:50:53
10:53:46
10:56:38
10:59:31
Time
RF (t)
LF (t)
RR (t)
LR (t)

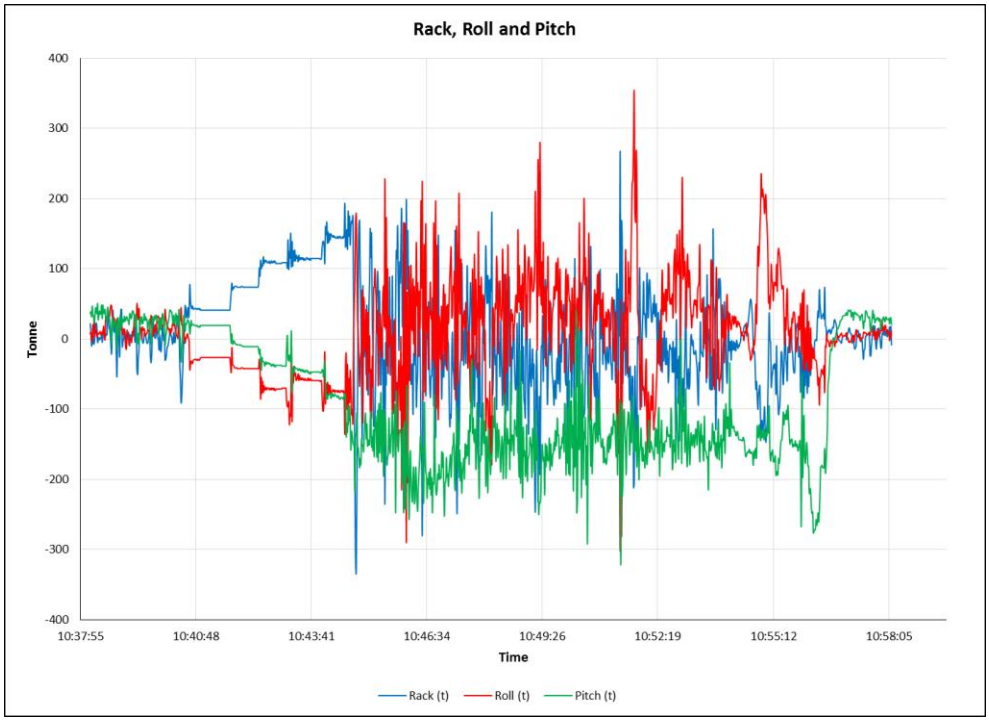
Rack, Roll and Pitch
400
300
200
100
0
-100
-200
-300
-400
Tonne
10:37:55
10:40:48
10:43:41
10:46:34
10:49:26
10:52:19
10:55:12
10:58:05
Time
Rack (t)
Roll (t)
Pitch (t)

8.2.1.2 Cycle 2

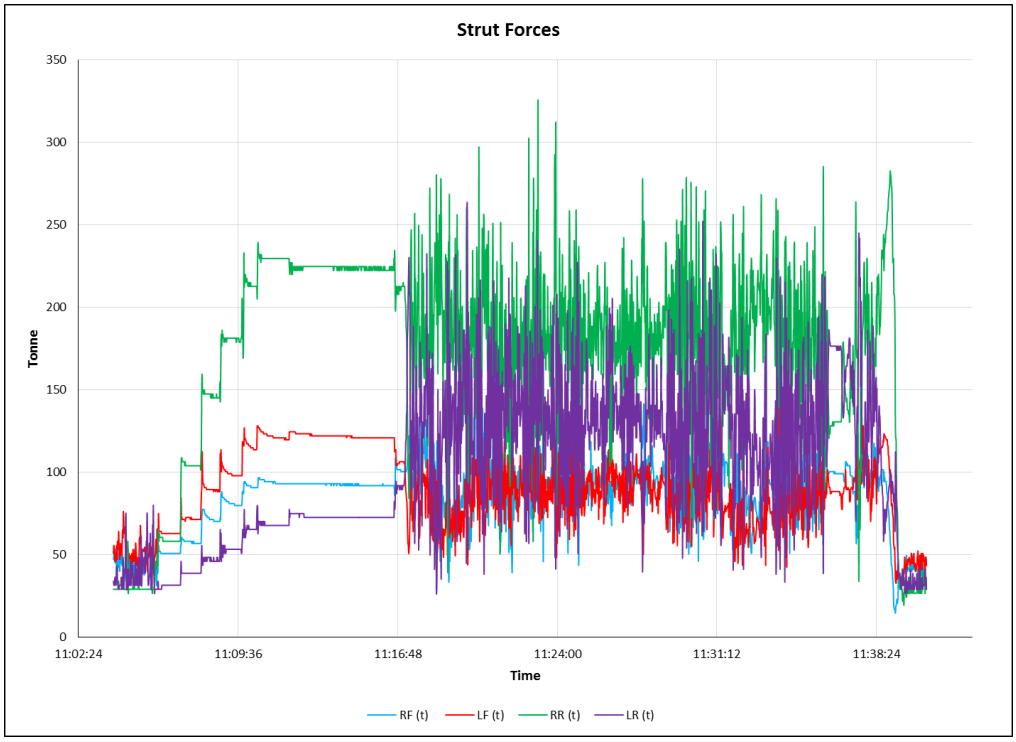
Strut Forces
350
300
250
200
150
100
50
0
Tonne
11:02:24
11:09:36
11:16:48
11:24:00
11:31:12
11:38:24
Time
RF (t)
LF (t)
RR (t)
LR (t)

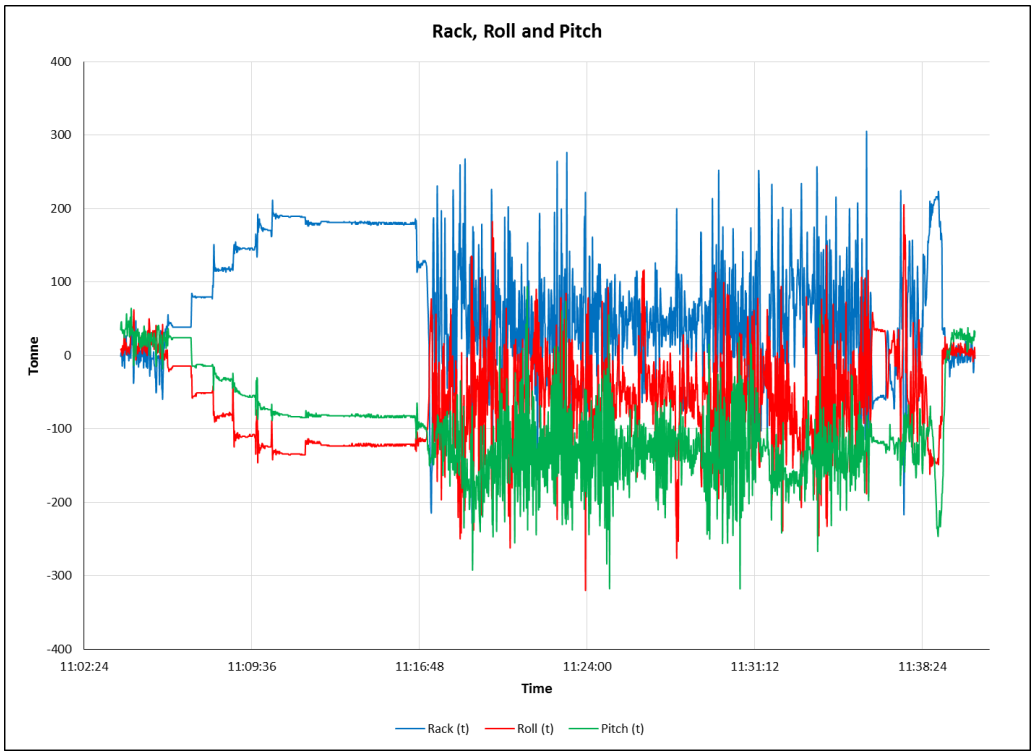
Rack, Roll and Pitch
400
300
200
100
0
-100
-200
-300
-400
Tonne
11:02:24
11:09:36
11:16:48
11:24:00
11:31:12
11:38:24
Time
Rack (t)
Roll (t)
Pitch (t)

8.2.1.3 Cycle 3

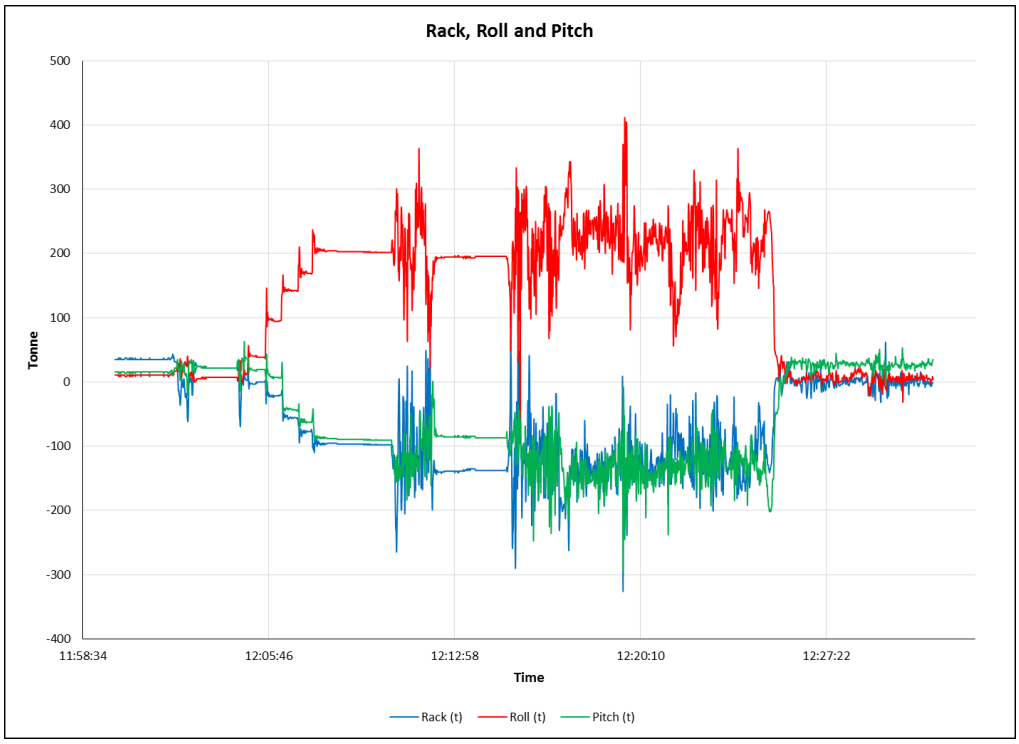
Rack, Roll and Pitch
500
400
300
200
100
0
-100
-200
-300
-400
Tonne
11:58:34
12:05:46
12:12:58
12:20:10
12:27:22
Time
Rack (t)
Roll (t)
Pitch (t)

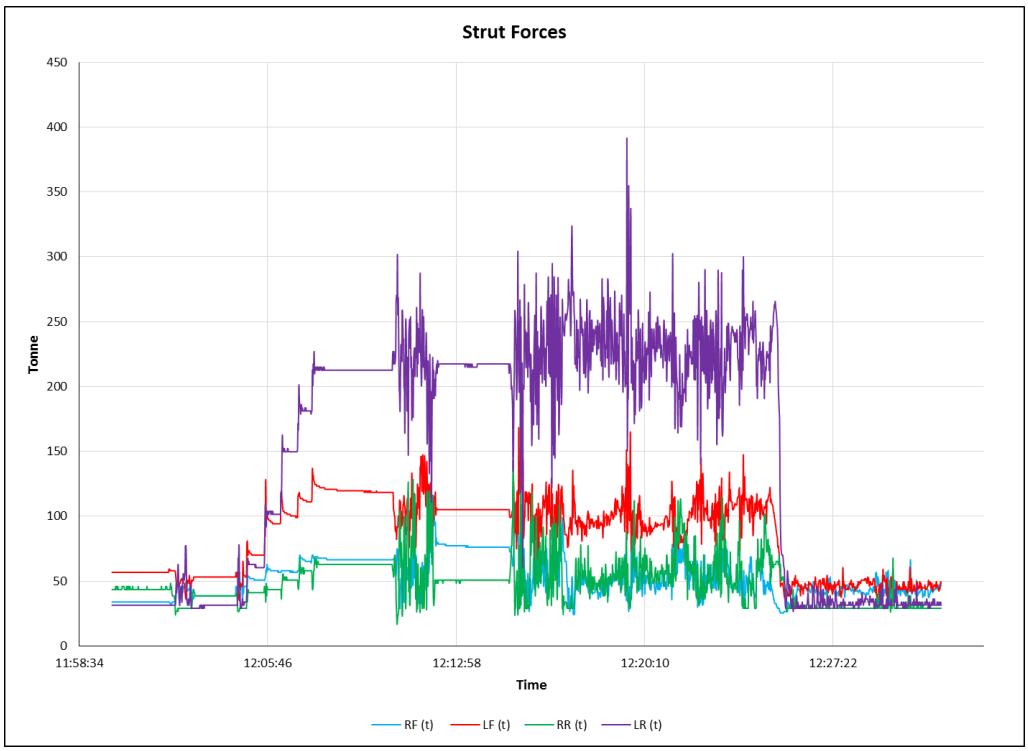
Strut Forces
450
400
350
300
250
200
150
100
50
0
Tonne
11:58:34
12:05:46
12:12:58
12:20:10
12:27:22
Time
RF (t)
LF (t)
RR (t)
LR (t)

8.2.2 137 Truck

8.2.2.1 Cycle 1

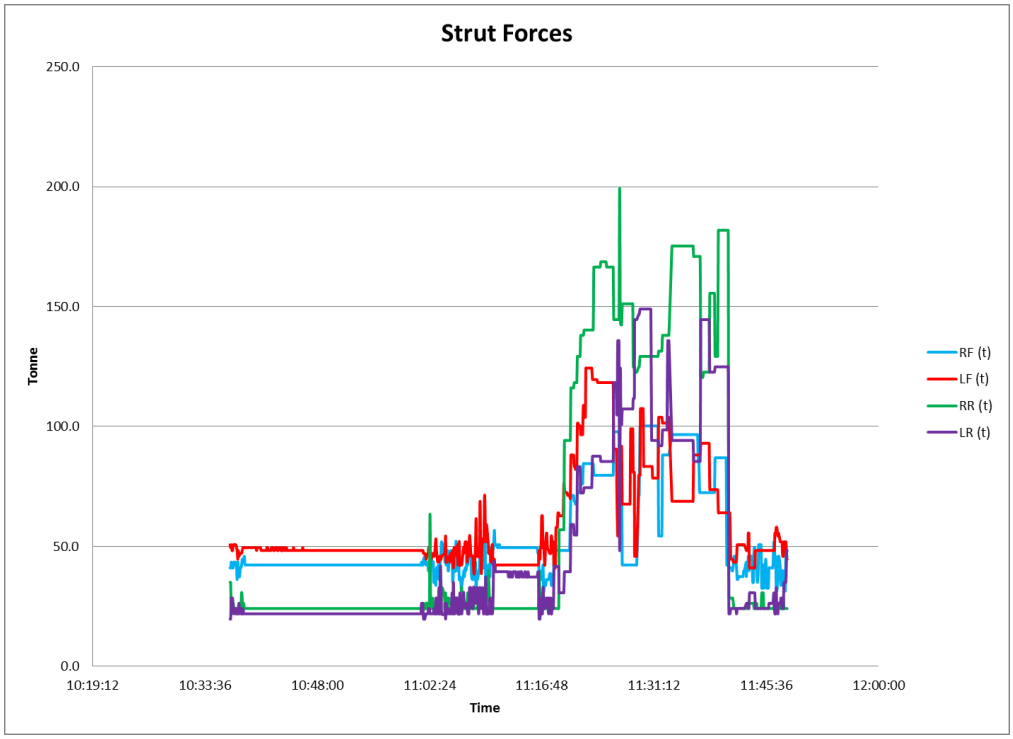
Strut Forces
250.0
200.0
150.0
100.0
50.0
0.0
Tonne
10:19:12
10:33:36
10:48:00
11:02:24
11:16:48
11:31:12
11:45:36
12:00:00
Time
RF (t)
LF (t)
RR (t)
LR (t)

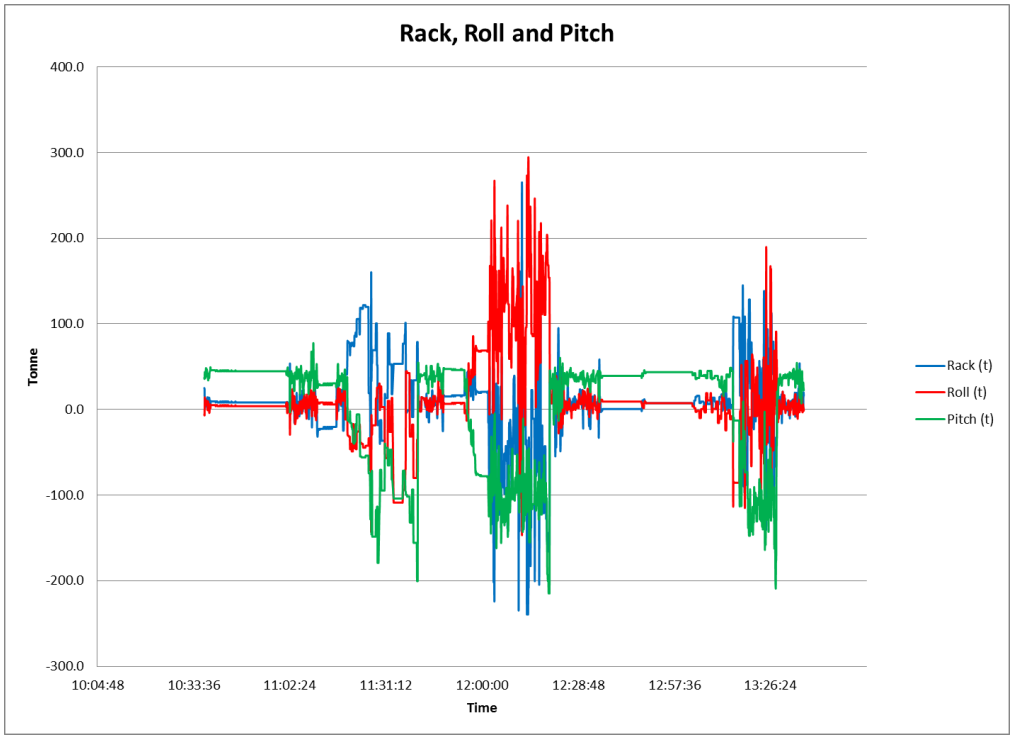
Rack, Roll and Pitch
400.0
300.0
200.0
100.0
0.0
-100.0
-200.0
-300.0
Tonne
10:04:48
10:33:36
11:02:24
11:31:12
12:00:00
12:28:48
12:57:36
13:26:24
Time
Rack (t)
Roll (t)
Pitch (t)

8.2.2.2 Cycle 2

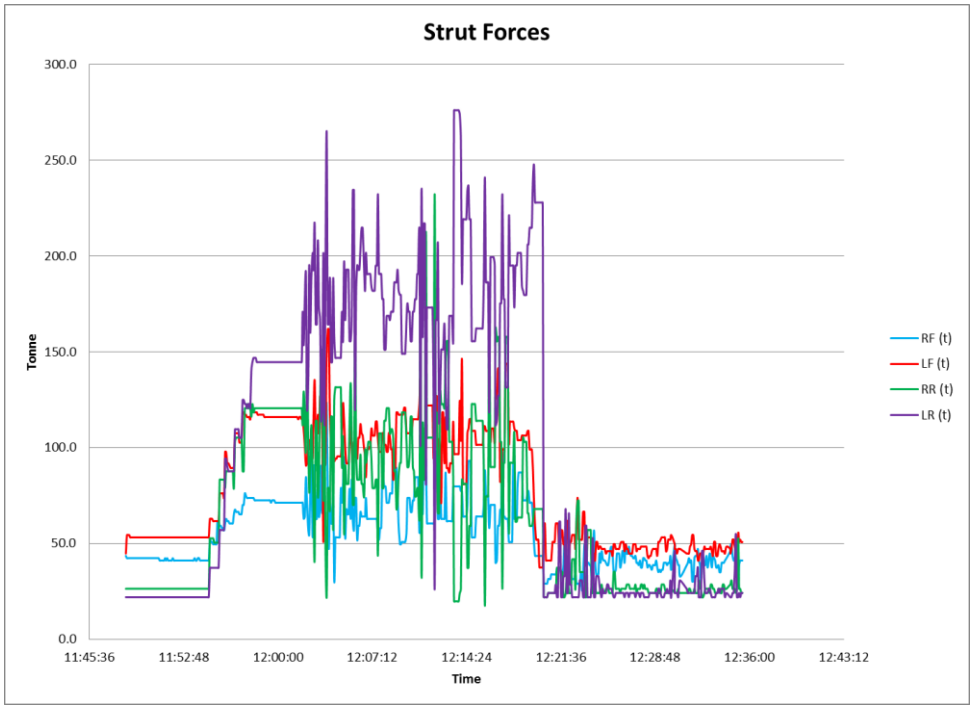
Strut Forces
300.0
250.0
200.0
150.0
100.0
50.0
0.0
Tonne
11:45:36
11:52:48
12:00:00
12:07:12
12:14:24
12:21:36
12:28:48
12:36:00
12:43:12
Time
RF (t)
LF (t)
RR (t)
LR (t)

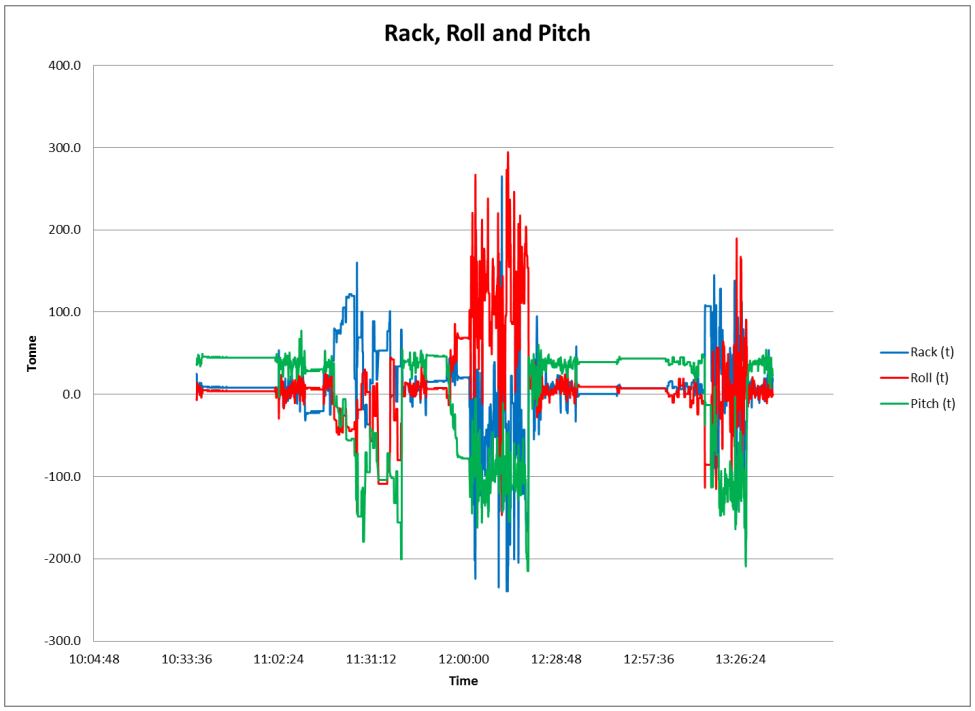
Rack, Roll and Pitch
400.0
300.0
200.0
100.0
0.0
-100.0
-200.0
-300.0
Tonne
10:04:48
10:33:36
11:02:24
11:31:12
12:00:00
12:28:48
12:57:36
13:26:24
Time
Rack (t)
Roll (t)
Pitch (t)

8.3 Numerical Algorithm

8.3.1 Matlab program

```
clc;clear all; close all;
global L W d alfa X Y CG1 Z0 V0 X1 Y1 surff
L=9.94;W=8;d=0.2;alfa = (90-27)*pi/180;V0=50;
for i=1: round(L/d)
   for j=1:round(W/d)
      X(i,j)=-d/2+i*d;
      Y(i,j)=-d/2+j*d;
      if X(i,j)< 3.35/tan(70*pi/180)
         Z0(i,j)= - tan(70*pi/180) * X(i,j)+3.35;
      else
         Z0(i,j)= tan(12*pi/180)*(X(i,j)-3.35/tan(70*pi/180));
      end
   end
end
surff=Z0;
%% Input
% CG1 is the CG from sensors
% CG1=[3;3];
CG1X=input('Enter CG1X :')
CG1Y=input('Enter CG1Y :')
CG1=[CG1X;CG1Y];
CGold=CG1;
```

```
%% Optimisation
[XY1] = fminsearch(@cgopt,CG1,optimset('TolX',1e-4,'TolFun',1e-
4,'MaxIter',100,'Display','iter'))
X1=XY1(1);Y1=XY1(2);
%% Post processing
h=hvalue(Z0,X1,Y1);
H1=h
XX1=X1;
YY1=Y1;
 Z= h-sqrt((X-X1).^2+(Y-Y1).^2)/tan(alfa);
profile= max(Z,Z0);
mesh(X,Y,profile)
hold on
mesh(X,Y,surff)
hold on
plot (CG1(1),CG1(2),'*')
 zz=profile-surff;
Best_CGXX=d^2*sum(sum(X.*zz))/(V0)
Best_CGYY=d^2*sum(sum(Y.*zz))/(V0)
%% Second Cone
% CG1 is the desired CG for 2 cones
CG1=[4.5;4];
 Z0=profile;
 X2=2*CG1(1)-X1;
```

```
Y2=2*CG1(2)-Y1;
 [XY2] = fminsearch(@cgopt,[X2,Y2],optimset('TolX',1e-
4,'MaxIter',120,'Display','iter'))
X2=XY2(1);Y2=XY2(2);
 figure
shovel(X2,Y2)
 %% Post processing
h=hvalue(Z0,X2,Y2);
 H2=h
XX2=X2;
YY2=Y2;
kk=0;m=1;
while m>0
   for y=0:.2:8
   z= h-sqrt((9.94-X2)^2+(y-Y2)^2)/tan(alfa);
   if z>1.85
      kk=kk+1;
   end
   end
      if kk>0
      X2=X2-0.2;
      h=hvalue(Z0,X2,Y2);
      m=1;
   else
```

```
        m=0;
    end
    kk=0;
end
X2
Y2
Z= h-sqrt((X-X2).^2+(Y-Y2).^2)/tan(alfa);
profile= max(Z,Z0);
figure
mesh(X,Y,profile)
hold on
mesh(X,Y,surff)
hold on
plot (CG1(1),CG1(2),'*')
 zz=profile-surff;
Best_CGXX2=d^2*sum(sum(X.*zz))/(2*V0)
Best_CGYY2=d^2*sum(sum(Y.*zz))/(2*V0)
 %% Second prime Cone
% Here, CG1 is the actual CG after 2nd cone read from sensors
% CG1=[3.2;4.5];
 CG1X=input('Enter CG2X :')
CG1Y=input('Enter CG2Y :')
CG1=[CG1X;CG1Y];
```

```
CGold=CG1;
[XY2prime] = fminsearch(@cgopt,[X2,Y2],optimset('TolX',1e-
4,'MaxIter',100,'Display','iter'))
X2prime=XY2prime(1);Y2prime=XY2prime(2);
 %% Post processing
h=hvalue(Z0,X2prime,Y2prime);
 H2prime=h
XX2prime=X2prime;
YY2prime=Y2prime;
 kk=0;m=1;
while m>0
   for y=0:.2:8
        z= h-sqrt((9.94-X2prime)^2+(y-Y2prime)^2)/tan(alfa);
      if z>1.85
      kk=kk+1;
   end
   end
     if kk>0
      X2prime=X2prime-0.2;
      h=hvalue(Z0,X2prime,Y2prime);
      m=1;
   else
      m=0;
   end
```

```
    kk=0;
end
 Z= h-sqrt((X-X2prime).^2+(Y-Y2prime).^2)/tan(alfa);
profile= max(Z,Z0);
figure
mesh(X,Y,profile)
hold on
mesh(X,Y,surff)
hold on
plot (CG1(1),CG1(2),'*')
 zz=profile-surff;
Best_CGXX=d^2*sum(sum(X.*zz))/(2*V0)
Best_CGYY=d^2*sum(sum(Y.*zz))/(2*V0)
%% Third Cone
% CG1 is the desired Center of Graity for all 3 cones
CG1=[4.5;4];
Z0=profile;
 X3=3*CG1(1)-2*CGold(1);
Y3=3*CG1(2)-2*CGold(2);
 [XY3] = fminsearch(@cgopt,[X3,Y3],optimset('TolFun',1e-
4,'MaxIter',100,'Display','iter'))
X3=XY3(1);Y3=XY3(2);
 %% Post processing
h=hvalue(Z0,X3,Y3);
```

```
H3=h
XX3=X3;
YY3=Y3;
 kk=0;m=1;
while m>0
   for y=0:.2:8
        z= h-sqrt((9.94-X3)^2+(y-Y3)^2)/tan(alfa);
      if z>1.85
      kk=kk+1;
   end
   end
      if kk>0
      X3=X3-0.2;
      h=hvalue(Z0,X3,Y3);
      m=1;
   else
      m=0;
   end
   kk=0;
end
X3
Y3
 figure
shovel(X3,Y3)
```

```
Z= h-sqrt((X-X3).^2+(Y-Y3).^2)/tan(alfa);
profile= max(Z,Z0);
figure
mesh(X,Y,profile)
hold on
mesh(X,Y,surff)
hold on
plot (CG1(1),CG1(2),'*')

zz=profile-surff;
Best_CGXX=d^2*sum(sum(X.*zz))/(3*V0)
Best_CGYY=d^2*sum(sum(Y.*zz))/(3*V0)
```

8.3.1.1 Cgopt function

```
function y=cgopt(x)
global CG1 Z0
 % figure
% mesh(Z0)
 [a,b]=CenterG(Z0,x(1),x(2));
y=(CG1(1)-a)^2+(CG1(2)-b)^2;
% aabb=[a;b]
```

8.3.1.2 Hvalue function

```
function h=hvalue(Z0,X1,Y1)
global alfa V0
h0=(150/pi/tan(alfa)^2)^(1/3);
h1=h0/2;
h2=1000000*h0;
error=9;
while error>0.001
      V=volumeq(Z0,X1,Y1,(h1+h2)/2);
      if V>V0
      h2=(h1+h2)/2;
   else
      h1=(h1+h2)/2;
   end
      error=abs(V-V0);
end
 h=(h1+h2)/2;
```

8.3.1.3 Volumeq function

```
function V=volumeq(Z0,X1,Y1,h)
 global L W d alfa X Y
 for i=1: round(L/d)
   for j=1:round(W/d)
      X(i,j)=-d/2+i*d;
```

```
        Y(i,j)=-d/2+j*d;
        Z(i,j)= h-sqrt((X(i,j)-X1)^2+(Y(i,j)-Y1)^2)/tan(alfa);

        if (Z(i,j)-Z0(i,j)) < 0
            Z(i,j)=0;
        else
            Z(i,j)=Z(i,j)-Z0(i,j);
        end
    end
end
 V = d^2*sum(sum(Z));
```

8.3.1.4 Centerg function

```
function [CGX,CGY]=CenterG(Z0,X1,Y1)
global L W d alfa X Y V0 XX1 YY1 surff
 h=hvalue(Z0,X1,Y1);
% XX1=X1; YY1=Y1;
% h = fminsearch(@hvalueq,10,optimset('TolX',1e-5,'MaxIter',1000));
 for i=1: round(L/d)
    for j=1:round(W/d)
        Zz(i,j)= h-sqrt((X(i,j)-X1)^2+(Y(i,j)-Y1)^2)/tan(alfa);
          if Zz(i,j)>Z0(i,j)
            Z(i,j)=Zz(i,j);
        else
```

```
            Z(i,j)=Z0(i,j);
        end
        if (Z(i,j)-surff(i,j)) < 0
            Z(i,j)=0;

        else
            Z(i,j)=Z(i,j)-surff(i,j);
        end
    end
end
 % d^2*sum(sum(Z))
 CGX=sum(sum(X.*Z))/(sum(sum(Z)));
CGY=sum(sum(Y.*Z))/(sum(sum(Z)));
```

8.3.1.5 shovel.m

```
function shovel(X1,Y1)

x=0:0.01:9.94;
y=0:0.01:8;

plot(x,0.*x)
hold on
plot(0.*y,y)
hold on
```

```
plot(x,0.*x+8)
hold on
plot(0.*y+9.94,y)
hold on
 % X1=9
% Y1=1
 R=3;
 if X1-R<0
    x1=0;
else x1= X1-R
end
if X1+R>9.94
    x2=9.94;
else x2= X1+R;
end
x=x1:0.01:x2;
y1=Y1+(R^2-(x-X1).^2).^0.5;
for i=1: length(x)
    if y1(i) >8 y1(i)=8;
    end
end
y2=Y1-(R^2-(x-X1).^2).^0.5;
for i=1: length(x)
    if y2(i)<0 y2(i)=0;
```

```
    end
end


plot(x,y1)
hold on
plot(x,y2)
hold on
plot (X1,Y1,'*')
```

8.3.2 Matlab Test

Enter CG1X :3

CG1X = 3

Enter CG1Y :5

CG1Y = 5

Iteration	Func-count	min f(x)	Procedure
0	1	0.110954	
1	3	0.0317322	initial simplex
2	4	0.0317322	reflect
3	6	0.00144919	reflect
4	7	0.00144919	reflect
5	9	0.00137462	contract outside
6	11	0.00064008	contract inside
7	13	0.000130279	contract inside
8	15	0.000130279	contract inside
9	17	7.33561e-005	contract outside
10	19	3.56761e-005	contract inside
11	21	6.93256e-006	contract inside
12	23	6.93256e-006	contract inside
13	25	6.93256e-006	contract inside
14	27	4.75685e-006	contract outside
15	29	6.63914e-007	contract inside
16	31	6.63914e-007	contract inside
17	33	3.36303e-007	reflect
18	35	2.98738e-007	contract inside
19	37	1.99844e-007	contract inside
20	39	3.88598e-008	contract inside
21	41	3.88598e-008	contract inside
22	42	3.88598e-008	reflect

23	44	1.5029e-008	contract inside
24	46	7.05962e-009	contract inside
25	48	2.80098e-010	contract inside
26	50	2.80098e-010	contract outside
27	52	2.80098e-010	contract inside
28	54	2.80098e-010	contract outside
29	56	2.80098e-010	contract inside
30	60	5.25378e-011	shrink

Optimization terminated:
the current x satisfies the termination criteria using OPTIONS.TolX of 1.000000e-004
and F(X) satisfies the convergence criteria using OPTIONS.TolFun of 1.000000e-004

XY1 =
2.9354
5.5597
H1 =
3.1236
Best_CGXX = 3.0001
Best_CGYY = 5.0002

Iteration	Func-count	min f(x)	Procedure
0	1	0.217927	
1	3	0.19752	initial simplex
2	5	0.167395	expand
3	7	0.12278	expand
4	8	0.12278	reflect
5	10	0.120211	reflect
6	12	0.0647567	expand

7	13	0.0647567	reflect
8	15	0.00384793	expand
9	17	0.00384793	contract outside
10	19	0.00384793	contract outside
11	20	0.00384793	reflect
12	21	0.00384793	reflect
13	22	0.00384793	reflect
14	24	0.00188939	contract inside
15	26	0.000908502	contract outside
16	28	0.000821496	contract inside
17	30	0.000104743	contract inside
18	32	0.000104743	contract inside
19	34	8.81809e-005	contract outside
20	36	2.17506e-005	contract inside
21	38	2.17506e-005	contract inside
22	40	1.29482e-005	contract outside
23	42	7.00542e-007	contract inside
24	44	7.00542e-007	contract inside
25	45	7.00542e-007	reflect
26	47	7.00542e-007	contract inside
27	49	7.00542e-007	contract outside
28	51	1.69729e-007	contract inside
29	53	1.69729e-007	contract outside
30	55	1.68877e-007	contract outside
31	57	4.22012e-008	contract inside
32	59	4.22012e-008	contract inside
33	61	1.79856e-008	reflect
34	63	1.33596e-008	contract inside
35	65	1.33596e-008	contract outside
36	67	3.74595e-009	contract inside
37	69	3.74595e-009	contract inside

38	71	3.74595e-009	contract inside
39	75	3.74595e-009	shrink
40	77	1.67309e-009	reflect
41	79	3.46626e-010	reflect
42	81	3.46626e-010	contract inside

Optimization terminated:
the current x satisfies the termination criteria using OPTIONS.TolX of 1.000000e-004
and F(X) satisfies the convergence criteria using OPTIONS.TolFun of 1.000000e-004

XY2 = 3.3577 4.0000
x1 = 0.3577
H2 = 3.9621
X2 = 3.3577
Y2 = 4.0000
Best_CGXX2 = 3.5006
Best_CGYY2 = 4.0007
Enter CG2X :4.5
CG1X = 4.5000
Enter CG2Y :3.5
CG1Y = 3.5000

Iteration	Func-count	min f(x)	Procedure
0	1	1.24999	
1	3	1.12104	initial simplex
2	5	0.975729	expand
3	7	0.729906	expand
4	9	0.527407	expand
5	11	0.182571	expand

6	13	0.0656189	expand
7	15	0.051675	reflect
8	17	0.051675	contract outside
9	19	0.051675	contract inside
10	21	0.0439631	reflect
11	23	0.0352978	expand
12	25	0.0191521	reflect
13	27	0.0063456	reflect
14	29	0.0063456	contract outside
15	30	0.0063456	reflect
16	32	0.000186695	contract inside
17	34	0.000186695	contract inside
18	36	0.000186695	contract inside
19	37	0.000186695	reflect
20	39	0.000186695	contract inside
21	41	0.000186695	contract outside
22	43	4.79224e-005	contract inside
23	44	4.79224e-005	reflect
24	46	4.79224e-005	contract inside
25	48	3.93393e-005	contract inside
26	50	9.73179e-006	contract inside
27	52	1.98014e-006	contract inside
28	54	1.98014e-006	contract outside
29	56	8.54881e-007	contract inside
30	58	7.37875e-007	contract outside
31	60	2.29367e-007	contract inside
32	62	1.9667e-007	contract inside
33	64	1.87741e-007	reflect
34	66	2.66269e-008	contract inside
35	68	1.22768e-008	contract inside
36	70	1.22768e-008	contract inside

37	72	3.39325e-009	contract inside
38	74	3.39325e-009	contract inside
39	76	6.82238e-010	contract inside
40	78	6.82238e-010	contract inside
41	82	4.77175e-011	shrink
42	84	3.1061e-011	contract outside
43	86	3.1061e-011	contract inside
44	88	3.1061e-011	contract outside
45	90	3.1061e-011	contract inside
46	94	3.51822e-012	shrink

Optimization terminated:
the current x satisfies the termination criteria using OPTIONS.TolX of 1.000000e-004
and F(X) satisfies the convergence criteria using OPTIONS.TolFun of 1.000000e-004

XY2prime = 6.4782 1.5230
H2prime = 3.9223
Best_CGXX = 4.2829
Best_CGYY = 3.4713

Iteration	Func-count	min f(x)	Procedure
0	1	0.00111262	
1	3	0.000278092	initial simplex
2	5	0.000278092	contract outside
3	7	0.0001145	contract outside
4	9	1.52552e-005	contract inside
5	11	1.52552e-005	contract inside
6	13	1.52552e-005	contract outside
7	15	1.36461e-005	contract inside

8	17	1.12925e-005	reflect
9	19	2.06186e-006	contract inside
10	21	9.62491e-007	contract inside
11	23	9.62491e-007	contract outside
12	25	5.09214e-007	contract inside
13	27	2.27928e-007	contract inside
14	29	2.1322e-007	contract inside
15	31	1.406e-007	reflect
16	33	2.62389e-008	contract inside
17	37	2.62389e-008	shrink
18	41	8.49102e-009	shrink
19	43	8.49102e-009	contract outside
20	45	8.49102e-009	contract inside
21	47	4.98942e-009	reflect
22	49	2.50881e-009	reflect
23	51	2.50881e-009	contract inside
24	53	8.21905e-010	reflect
25	55	8.21905e-010	contract outside
26	57	8.21905e-010	contract inside
27	59	8.21905e-010	contract inside
28	61	8.21905e-010	contract inside
29	63	7.7737e-010	contract inside
30	65	7.57914e-010	contract inside

Optimization terminated:

the current x satisfies the termination criteria using OPTIONS.TolX of 1.000000e-004

and F(X) satisfies the convergence criteria using OPTIONS.TolFun of 1.000000e-004

XY3 = 3.1504 4.9254

H3 = 4.5541

X3 = 3.1504

Y3 = 4.9254

x1 = 0.1504

Best_CGXX = 3.9997

Best_CGYY = 3.9998